BEACH INUNDATION AND MORPHOLOGICAL CHANGES
DURING STORMS USING VIDEO MONITORING TECHNIQUES

PROGRAMA DE DOCTORADO EN CIENCIAS DEL MAR

Memoria presentada por

Amanda Sancho García

Para optar al grado
de Doctor por la
Universidad Politécnica
de Catalunya

Director:

Jorge Guillén Aranda

Barcelona, 2012

Institut de Ciències del Mar

UNIVERSITAT POLITÈCNICA DE CATALUNYA BARCELONATECH

CSIC
CONSEJO SUPERIOR DE INVESTIGACIONES CIENTÍFICAS

Fotografías de portada:
MARC GASSER I RUBINAT

Diseño de portada:
PELOPANTÓN EQUIPO CREATIVO

Cuando todo aquello que es imposible ha sido eliminado, lo que quede, por muy improbable que parezca, es la verdad.

Arthur Conan Doyle

A mis padres,
a mi hermana y su princesa,
a ti niño,
Y por supuesto, a ti abuela.

Contents

Acknowledgements

Aunque el contenido de la tesis es lo más importante, más lo es agradecer el apoyo de toda la gente que ha estado a mi lado durante esta etapa.

La primera persona a la que tengo mucho que agradecerle es a mi director de tesis, Jorge Guillén. Mucho ha pasado desde que por allá el 2007 apareciera cual tsunami, en el Instituto para realizar una estancia de dos meses con una beca de introducción a la investigación. ¡¡Cuánto ha llovido desde entonces!! La verdad es que esa experiencia fue decisiva para que al final, sin tituvear, me animara a emprender la aventura de hacer una tesis doctoral. Jorge, me convenciste enseguida pues siempre has hecho que todo fueran facilidades, buenas palabras y sabios consejos. Gracias por creer en mí, pero sobretodo por tu infinita paciencia y tu enorme positividad.

¡¡Que hubiera sido de esta etapa sin mi Mari!! Nuestro punto de encuentro fue una vivencia personal similar, y gracias a eso hoy tengo tu amistad y tu apoyo. La palabra "crisis" significa cambio, y tras toda crisis llega un regalo. Mi regalo fue tu amistad. Gracias Maribel por tus paseos por Montjuic, por tus cenas en casa, por tus consejos, por presentarme a nuestra hada Rosetta ("vigila que no se te mueva la corona")... Porque aunque nos separan algunos años y formas de ver las cosas a veces diferentes, hay una magía especial entre nosotras. Gracias por ser tú. No puedo acabar sin mencionar a esa princesita que tienes y que tan buenos momentos me ha hecho pasar, gracias a ti también Claudia.

A Ero. Nuestros encuentros en el pasillo dieron lugar a una amistad que espero y estoy segura durará años. Darte las gracias por ser tan buenísima persona, transparente, amable y verdadera, por acogerme en tus sofás cama y por estar pendiente de mi en una ciudad tan grande que te hace sentirte muy sola. Gracias también a tu hermana y a tus padres, por mimarme con sus arroces de origen

valenciano y hacerme sentir tan querida.

A Antonio Turiel. En primer lugar, empezaré por: "1, 2, 3 yo me calmaré, 4, 5, 6 todos los veréis". Vale, ahora ya puedo empezar a escribir tu párrafo. Que decirte "Anthony", pues que infitinas gracias por tus conversaciones sobre cualquier tema, por querer que el mundo sea un poquito más justo y mejor, y por tu ayuda en los momentos de pánico porque siempre has sacado tiempo de donde no lo tenías (pues si el día tuviera más horas a ti te seguirian faltando!). No me olvido de la apuesta eh? ¡¡Volveré a saldarla!!.

A mis niñas del B-38 que tan buenos momentos hemos pasado juntas. Laura y Marta os voy a echar mucho de menos, hemos sido una piña y siempre alguna ha hecho que lo negro fuera blanco. Y recordad que cuando las fuerzas os flanqueen no olvidaros de nuestro lema: "Creus que ho pots fer millor? Yes, we can". Laura, qué será de nuestros homenajes en el Monchos a las 8, nuestros picoteos a las 12 o nuestras napolitanas de crema después de comer!!. Gracias por tu madurez, por tus consejos y por compartir la vivencia de ser madre conmigo. Marta Ribó decirte... ¿La pastilla? (jajaja), es broma!. Gracias por ponerle humor a la vida y música al silencio: *No voy a sentirme mal si algo no me sale bien, he aprendido a derrapar y a chocar con la pared, que la vida se nos va como el humo de ese tren como un beso en un portal, antes de que cuente 10!*. A Elena, por sus consejos valiosos que al principio no entendía pero que luego tomaron mucho sentido. J(X)aume! Que no me he olvidado de ti! Gracias por compartir la última etapa de la tesis, con mis agobios incluidos. Gracias por tus conocimientos de gintonics, las barbacoas y los cafés de después de comer.

A Oriol Mulet. Compañero de despacho durante un tiempo, de cortar testigos y de PUDEM. Gracias por tu dedicación, por las topografías intensivas, por estar cerca, por los desayunos y por los buenos momentos. Ets un crack!

A Oscar Chic y Sara Soto del Coastal Ocean Observatory. Gràcies Òscar per fer que gran problemes siguesin problemes xicotets, per estar sempre disposat a totes les meues recomanacions i per ser tan bona gent. Sarita! Gracias por ayudarme a hacer los mapitas de la tesis, por tus consejos sobre Santander y por tu buena disponibilidad siempre y en todo momento. Los mapas de las zonas de

estudio son obra tuya!.

A Gonzalo. Gracias por tu aportación en el último capítulo de la tesis, por tu ayuda y buen rollito. A pesar de tus pequeñas manías he aprendido mucho trabajando contigo. Porque si yo soy *Amandix* y Jorge es *George*, tu eres *Gonzalolatex*.

A la mesa redonda que tan buenos momentos y risas a montón me ha dado. Porque todavía hay sitio para uno más así que apretujaros o hacemos el ”8”: Alicia, Jordi, Mercedes, Jordi Solé, Quim, Antonio, Maribel, José Pozo, Silvia, Dolors Vaqué, Carine, Emilio, Marcos, Álvaro, Marta, Nina, Antonio García-Olivares, Roger y Justino.

A Emilio, por su ayuda para en la maquetación de la tesis.

A José A. Pozo. Gracias por tus palabras de ánimo, tu positividad, y por tu visión de futuro sobre mis postres.

A Raquel, por nuestras habitas en el mosquito, tus actuaciones de bollywood y nuestras conversaciones sobre los sobrin@s. A Eli Sañé por sus consejos sobre la tesis y los cafés de los sábados.

A Paola Castellanos por compartir nervios de tesis con un buen café y por recomendarme a PELO PANTÓN. A Verónica González, por los ánimos en la recta final y la ayuda con el latex.

A Pelo Pantón, por el diseño de la portadas. ¡¡Eres increíble Anita!!

A Marc Gasser. Gracias por tener siempre tu cámara disponible para captar las playas en temporales, con las obras, en días soleados... y así tener aun mejor monitorizadas las playas de Barcelona.

A Carmen Juan. Compañera de luchas, de pasillo, de compras en la tienda de frutos secos y de muchas risas. Gracias por tus masajes reconfortantes, por tu positividad y por esa fuerza que transmites.

A Albert Palanques y Pere Puig por invitarme a sus campañas con el García del Cid.

A la tod@s las personas del departamento de Geología Marina, con especial cariño a las chicas del laboratorio Silvia de Diago, Neus, y Mª Ángeles.

A todo el personal de la UTM en especial a Jaume Piera, Pou, Marcos, Toni, Javi y Cris.

A las chicas de la limpieza, en especial a Rosario, al personal de administración, a Conchita, Ramón, Nuria y Eva López, al personal de biblioteca, en especial a Natalia, a las chicas de recepción y los chicos de mantenimiento, a Rosa Cabanillas, y a los vigilantes. Gracias a tod@s los compañer@s/amig@s del CMIMA por todo estos maravillosos 4 años.

A la gente de la UPC que ha compartido conmigo congresos, trabajo, conversaciones, cervecitas varias y muchas risas: Daniel Calvete, Angels, Albert Falqués, José Jimenez, Herminia Valdemoro y Eva Bosom.

A Alan Lounds, por la supervisión del inglés y por su esfuerzo en el sprint final de la tesis.

I had the privilage to work under the supervision of Gerben Ruessink at the Utrech University during three months in 2010. Thanks Gerben for your warm welcome, for your knowledge on the swash and the sandbars and your advices on the modelling. Thanks also to everyone in the Institute for Marine and Atmospheric Research: my officemate Jasper, Jantin, Tim, Florin and Florence. Thanks also to the people I met: Ángeles and Mara, and my room-mates Francesca, Shima and Alex Mees.

De mi estancia en Santander no sólo me quedo con las luchas interminables con el SMC, sino también con la amistad de gente increíble. En primer lugar dar las gracias a Raúl Medina por recibirme y por todas las facilidades proporcionadas durante la estancia. Muchas gracias Vero por tus miles de minutos ayudándome con el SMC y tus "alivios sintomáticos" con los *Halls extra fuerte* para mis dolores de garganta. Gracias también a Sole, Gabriel, Cynthia y Lucía

por vuestra ayuda con el SMC y al resto de compañeros del despacho donde estuve: a Tamara, Pilar, Hala, Javier G. Alba, Javi, Svetla, y Pedro.

Como no podría ser de otra manera, no puedo olvidarme de todas mis chicas de la resi, en especial de Pilar y Merche. Pilar, et trovaré moltisim a faltar! Has sigut com una mare per mi, hem viscut molt moments, m'has vist plorar i riure però sempre t'he tingut al costat. Et vull moltisim. Gracias Merche por tus conversaciones después de volver del trabajo y por enseñar a hacer maletas a tu "rubia precaria". A mis monjitas de la Sagrada Familia: Madre Mercè, Madre Roser, Madre Presentación, Madre Miquela, Madre Pura, Madre Madgalena y con un cariño muy especial a Madre María. A todas las chicas que habeis compartido conmigo esta etapa en SAFA: Gemma, María Iglesias, Nieves, Hermi, Miren, Angela, Mercedes, Mercè, María, Angelita, Nuria, Carmen, Ana, Carmen y Maruja, Cornelia, Marisa, Josefina, Dolors, Mª José, Pepita, y Micaela.

A Marta Martínez y su ¡Arriba la Esteban!. Gracias, por entender al *atún Sancho* con solo una mirada y sonreir a los problemas.

A la gente del máster. Marina, Laia, Sergi, Marta, Jacob e Ingrid. Sergi, gracias por haber estado cerca, por tu amistad y por ser tan buena gente. Ingrid, gracias por estar ahí, por tu "brujita de la alegría" que me ha acompañado durante todo este tiempo, por tu amistad sincera y por levantarme una y otra vez.

No puedo olvidarme de toda la gente de la terreta. A Ana, Aitana y Fran. Los tres compartimos una cosa en común: el amor por la ciencia. Estudiamos juntos Ciencias del Mar y cada uno ha logrado su objetivo: Ana y su química analítica, Aitana y la oceanografía física y Fran, la microbiología marina. Os quiero muchísimo a los tres y estoy muy orgullosa de vosotros por todo lo que habeis conseguido. ¡¡Animo con vuestras tesis!!. Aniuska, gracias porque tu eres en cierta manera la causante de que hiciera el doctorado y pidiera la JAE, gracias por los emails diarios, y por las conversaciones sobre la vida. Aitana, a pesar de que tu amor a la ciencia te ha llevado a las antípodas, agradecerte que de alguna manera u otra siempre has estado cerquita, gracias por tus conversaciones que me hacen razonar y por creer en mi. Fran, nos separan unos cuantos centímetros de altura pero siempre te tengo cerca... Eres todo amor y atención; gracias por tus

visitas al despacho, por tus lunes de sueño en el tren, por tus paseos por Barna,... gracias por ser así.

A Edu y Ostara. Gracias por acompañarme en esta última etapa de la tesis, por las cenas en casa y por ser unos amigos maravillosos. Ya sabéis que os quiero mucho... y estoy muy feliz porque pronto sereis uno más!

A Emely. Investigadora de espíritu y aventurera de oficio, gracias por haber estado cerca este tiempo y por preocuparte por cómo iba evolucionando la tesis en todo momento. Eres todo corazón.

A Gema, Javi, Pablo, Elena y Arancha. Gracias por las cenas y los buenos momentos juntos, porque a pesar de la distancia y del poco tiempo del que hemos tenido estos últimos años, siempre os he tenido más que cerca. A mis amigos de Puig Val que depués de más de 15 años os sigo teniendo cerca: Carles, Fran, Dèlia, José Ramón, Jacobo y Alejandrito. A mis amigas del cole: María, Bea y Adela que después de un tiempo nos volvimos a reencontrar.

A Mar Escribano. Porque a pesar que nos separan unos cuantos kilómetros y no podemos vernos todo lo que nos gustaría, has compartido conmigo esta etapa de la tesis con mucha intensidad. Gracias por tus palabras, tus consejos, tus detalles y por tu amistad. Ya sabes que te quiero un montón.

A Germán, profesor de mates del cole y de la universidad. Siempre sabio en consejos, animándome, mimándome y creyendo en mí. Gracias por ayudarme a mantener la calma en los momentos difíciles, por darle la vuelta a los problemas y ver la parte positiva de las cosas.

A Juan y Amparo, por vuestro apoyo y mimos, por hacerme sentir como una hija más.

A mi niño. Porque *un informático y una "científica loca" decidimos compartir melancolías soledades y fantasmas a la par, miedos locos tristezas y alegrías...* Aunque a veces te cuesta entender la vida loca de la ciencia, gracias por ser mi compañero de viaje y hacer que mi vida tenga sentido. Prometo estarme quieta un tiempo.

Finalmente, dar las gracias a mi familia. A mis padres, Rafael y Mª Ángeles,

pues vosotros sois los cimientos de esta tesis, porque con vuestro esfuerzo y entrega habéis hecho que haya llegado hasta aquí. Muchas gracias por vuestra paciencia, cariño, apoyo y entrega incondicional en todo momento a pesar de los dolores de cabeza que os he dado en algún momento y mi mal humor. Ya sabéis que el amor a *la* mar viene de familia. A mi hermana Ángela, porque siempre has sido mi fan "número 1". Gracias por acompañarme desde el principio, desde Madrid hasta Las Palmas, por aguantar los interminables ensayos sobre tablas de planchar, por tu disposición y tus ánimos, pero lo más importante por hacer que creyera en mí. Pero por si no bastara, porque hoy tenga una sobrina preciosa a la que transmitir el amor hacia el mar y las playas. A ti abuela, porque aunque te fuiste a mitad del camino, sé que desde algun sitio has seguido dándome esa fuerza que me dabas. Gracias por tus enseñanzas sobre la vida, por tus consejos culinarios, y por haberte tenido como abuela. Hoy estarías muy orgullosa de mi. A ti abuelo, pues como te prometí hoy soy casi "doctora".

Finalmente, agradecer al Consejo Superior de Investigaciones Científicas la beca JAE-predoc cofinanciada por el Fondo Social Europeo y a los proyectos SEDMET (CTM2006-06919) e IMNOBE (CTM2009-11892) financiados por el Ministerio de Economía y Competitividad. Thanks also to both referees of this thesis, Paolo Ciavola and Gerben Ruessink.

Summary

Coasts are subject to erosion and inundation produced by storms, which are very frequent and can produce major damage and economic losses. Storm-induced inundation is due to the sum of astronomical tide, surge level and wave runup. The predictability of beach inundation is mainly related to wave runup and most of the formulations that have been developed focus on the hydrodynamics, disregarding the morphological changes caused during storms. For these reasons, the aim of this thesis is to provide more insight into beach inundation processes at embayed and open beaches and to determine how morphological changes can interfere with these processes. To this end, video measurements of beach inundation and the characteristic morphological changes were carried out at two stretches of coast with different wave climates: the stretch comprising La Barceloneta, Somorrostro and Nova Icaria, which are three artificial, tideless embayed beaches located in Barcelona, Spain (NW Mediterranean); and Noordwijk beach, which is an open, microtidal multibarred beach located in Noordwijk, the Netherlands (North Sea).

The effects of a submerged breakwater and a detached breakwater on the morphological and hydrodynamic changes occurring at La Barceloneta beach during storms is examined in *chapter 2*. The shoreline response before and after the beach nourishment and the construction of the protective structures was compared using a ten-year video-recorded dataset and hydrodynamics modelled using the Coastal Modelling System (SMC). As a result of the protection works, La Barceloneta was divided into two independent beaches separated by a salient. A new methodological approach to analyzing beach rotation which eliminates the morphological effect is presented. Results indicate that the previous erosive trend reported in the northeastern section is still present at the current northeastern beach and is related to the new submerged breakwater. Furthermore, the beach rotation process has been modified, with counter-clockwise beach rotation

now occurring only at the northeastern beach and clockwise beach rotation at the southwestern beach. This new behavior is caused by a change in the wave-induced current system from a single dominant alongshore current to one composed of two dominant alongshore currents with opposite directions.

In *chapter 3*, beach inundation affecting the three embayed beaches of Barcelona during the 17 strongest storm events of the period 2001-2008 is analyzed using daily time-exposure images. The shoreline variability due to storms was split into beach planform and morphological features (small beach cusps, megacusps, shoreline undulation and a salient) in order to determine its influence on beach inundation measurements. The characterization of the inundation depended on the orientation with respect to the wave direction approach and the morphological features. Beach planform changes are the foremost influence on the inundation of Barcelona beaches. Landward beach planform and salient changes accounted for almost 50% of the maximum inundation measured, whereas megacusps and shoreline undulation accounted for approximately 25%. The effect of the beach cusp on the inundation is negligible. Consequently, the variation of the shoreline during storms significantly influences the value of the inundation, especially on beaches with steep slopes. Small variations in the beach slope can substantially affect the inundation on gently sloping beaches.

The inundation at the multibarred beach of Noordwijk during the seven strongest storms in the period between 1998 and 2005 is estimated, also using video monitoring techniques in *chapter 4*. Additionally, the influence of subtidal sandbars on the inundation is analyzed using the XBeach model. To this end, seven different 1D-simulations were carried out without considering morphological changes; six simulations used barred profiles measured at Noordwijk but differing in sandbar height and location, and one simulation used a synthetic barless profile. Inundation values ranged from 22 to 105 m, with considerable alongshore variation before the peak of each storm because of the presence of the intertidal bars. The mean inundation values along the beach are well estimated using a simple inundation parameter that includes the intertidal and the supratidal beach slope, deep-water wave height and wavelength and the surge level. The XBeach model shows that the inundation is only affected by the morphology close to the shoreline, that is by the intertidal bars or by the inner bar if it is wide

and closer to shoreline. The outer bar does not seem to influence the inundation behavior.

Beach inundation prediction at Somorrostro beach is evaluated in *chapter* 5. To this end, inundation measurements using video observations are compared with estimations including the tidal variations and the wave runup formulation of Stockdon et al. (2006), introducing deep water, local wave measurements and local wave computations as inputs. Since the observations consider the mean runup and the estimations use the 2% runup exceedance ($\mathrm{R}_{2\%}$), the inundation is overestimated if any of the wave heights in the formulation are used. However, the estimations are improved if a local wave height at 10 m depth is used, in particular for waves approaching the shore obliquely. Finally, it is stated that the differences between the observations and the estimations vary along the beach, being higher in the curved zone of the embayment. The alongshore variability of the inundation is better captured if the wave runup is assumed proportional to the breaking wave height.

Resumen

Las costas están expuestas a la erosión y la inundación producida por los temporales, los cuales son muy frecuentes y pueden producir grandes daños y pérdidas económicas. La inundación producida por los temporales es debida a la marea astronómica y meteorológica y al remonte del oleaje. La predicción de la inundación de la playa está principalmente relacionada con el remonte y la mayoría de las formulaciones propuestas se centran en parámetros hidrodinámicos sin tener en cuenta los cambios morfológicos causados durante los temporales. Por todo ello, el principal objetivo de esta tesis es proporcionar un mayor conocimiento de los procesos de inundación en playas encajadas y abiertas y determinar cómo los cambios morfológicos pueden interferir con estos procesos. Para ello, se han llevado a cabo medidas de la inundación y de los cambios morfológicos característicos utilizando imágenes de video en dos tramos de costa con climas de oleaje diferente: el tramo que comprende las playas de La Barceloneta, Somorrostro and Nova Icaria, las cuales son tres playas artificiales, encajadas y sin marea localizadas en Barcelona, España (NO Mediterráneo); y la playa de Noordwijk, la cual es una playa abierta, multibarrada y micromareal localizada en Noordwijk, Holanda (Mar del Norte).

Los efectos de un dique sumergido y un dique exento en los cambios morfológicos e hidrodinámicos ocurridos en la playa de La Barceloneta durante temporales se examinan en el *capítulo 2*. La respuesta de la línea de orilla antes y después de la regeneración de la playa y de la construcción de las estructuras de protección se compara utilizando 10 años de video imágenes y la hidrodinámica modelada utilizando el Sistema de Modelado Costero (SMC). Como resultado de estas obras de protección, La Barceloneta quedó dividida en dos playas independientes separadas por un saliente. Una nueva metodología para analizar la rotación de la playa que elimina los cambios morfológicos es propuesta. Los resultados indican que la tendencia erosiva previamente observada en la zona

noreste de la playa sigue estando presente en la actual playa noreste y está relacionada con el nuevo dique sumergido. Además, el proceso de rotación de la playa se ha modificado, produciéndose solamente en sentido contrario a las agujas del reloj en la playa noreste y en sentido horario en la playa suroeste. Este nuevo comportamiento es debido al cambio en el patrón de corrientes previamente formado por una corriente longitudinal dominante, a un sistema de corrientes compuesto por dos corrientes longitudinales en direcciones opuestas.

En el *capítulo 3*, la inundación producida en las tres playas encajadas de Barcelona durante los 17 temporales más energéticos del periodo 2001-2008 es analizada utilizando imágenes diarias promediadas. La variabilidad de la línea de orilla debida a los temporales es discriminada en cambios en la forma en planta y morfologías (cúspides de playa, megacúspides, ondulaciones y saliente) para determinar su influencia en las medidas de inundación de la playa. La caracterización de la inundación dependió de la orientación respecto de la dirección de aproximación del oleaje y de las morfologías. Los cambios en la forma en planta de la playa son la máxima influencia en la inundación de las playas de Barcelona. Los cambios en la forma en planta hacia tierra y los cambios en el saliente suponen casi un 50% de la máxima inundación medida, mientras que las megacúspides y la ondulación suponen aproximadamente el 25%. El efecto de las cúspides de playa en la inundación es despreciable. Consecuentemente, la variación en la línea de orilla durante temporales influye significativamente los valores de inundación, especialmente en playas con pendientes fuertes. Pequeñas variaciones en la pendiente de la playa pueden sin embargo afectar sustancialmente la inundación en playas con pendientes suaves.

La inundación de la playa multibarrada de Noordwijk durante los 7 temporales más fuertes ocurridos en el periodo comprendido entre 1998 y 2005 es también estimada utilizando medidas de video monitorización en el *capítulo 4*. Además, la influencia de las barras submareales en la inundación es analizada utilizando el modelo XBeach. Para ello, se realizaron siete simulaciones 1-D sin considerar los cambios morfológicos; seis simulaciones utilizando perfiles barrados medidos en la playa de Noordwijk pero que difieren en altura y localización de las barras, y una simulación utilizando un perfil ideal sin barras. Los valores de inundación oscilaron entre 22 y 105 m, con variaciones considerables a lo largo de la playa

antes del pico del temporal debido a la presencia de barras intermareales. La inundación promedio a lo largo de la playa es estimada considerablemente bien utilizando un parámetro de inundación sencillo que incluye la pendiente intermareal y supramareal, la altura de ola y la longitud de onda en aguas profundas y la marea meteorológica. El modelo XBeach muestra que la inundación está solamente afectada por la morfología próxima a la línea de orilla, esto es, por las barras intermareales o por la barra interna si es ancha y próxima a la orilla. La barra externa no parece tener influencia en el comportamiento de la inundación.

La predicción de la inundación en la playa de Somorrostro es evaluada en el *capítulo 5*. Para ello, medidas de la inundación utilizando observaciones de imágenes de video se comparan con estimaciones de la inundación incluyendo las variaciones de la marea y el fórmula del remonte de Stockdon et al. (2006), introduciendo medidas locales y en aguas profundas del oleaje así como oleaje modelado. Debido a que las observaciones corresponden a un remonte medio y las estimaciones usan el remonte excedido un 2% ($\mathrm{R}_{2\%}$), la inundación es sobreestimada para cualquier altura de ola utilizada en la fórmula. Sin embargo, las estimaciones mejoran si una altura de ola medida a 10 m es utilizada en la fórmula en particular para oleajes con una aproximación oblicua a la línea de orilla. Finalmente, las diferencias entre las observaciones y las estimaciones varían a lo largo de la playa, siendo mayores en la zona de curvatura de la playa. La variabilidad de la inundación a lo largo de la playa es mejor caracterizada si el remonte se asume igual que la altura de ola en rotura.

List of Figures

List of Tables



Chapter 1

INTRODUCTION

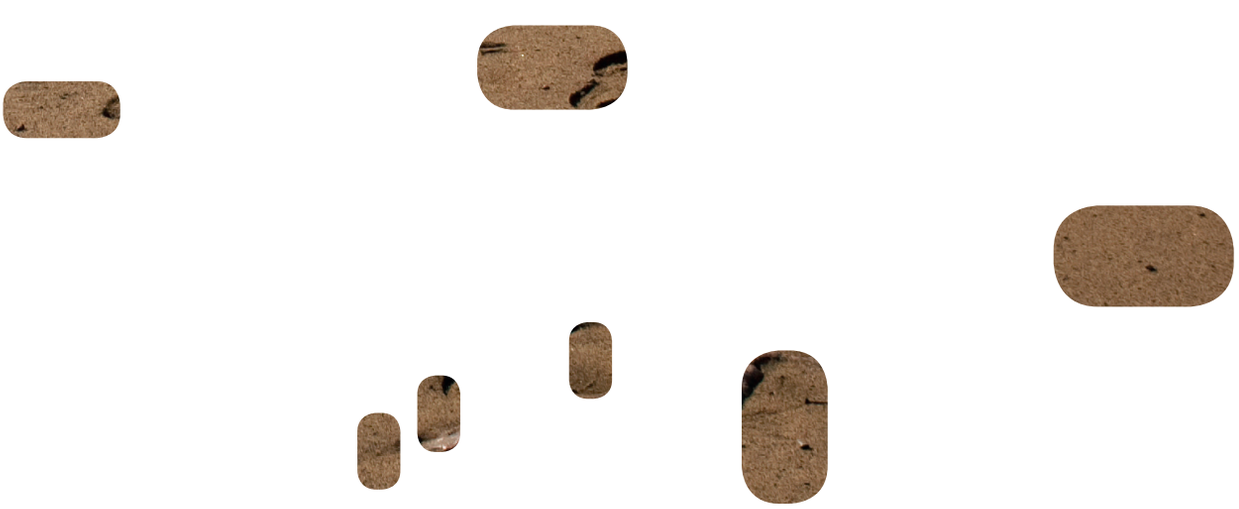

1.1 Coastal inundation

Highly populated coastal areas are exposed to a range of natural and human-induced hazards, including coastal erosion and inundation (Nicholls, 2004; Zhang et al., 2004; Ferreira et al., 2006). The global mean sea level will rise during the 21st century and consequently coastal inundation will increase in proportion to the slope of the coastal area (Zhang et al., 2004; Nicholls and Cazenave, 2010). Coupled with this, the increase in the occupation of the coastal fringe and longer storm lifetimes and greater storm intensities (Emanuel, 2005; Kron, 2008) will make the risk of inundation even greater (Condon and Sheng, 2012).

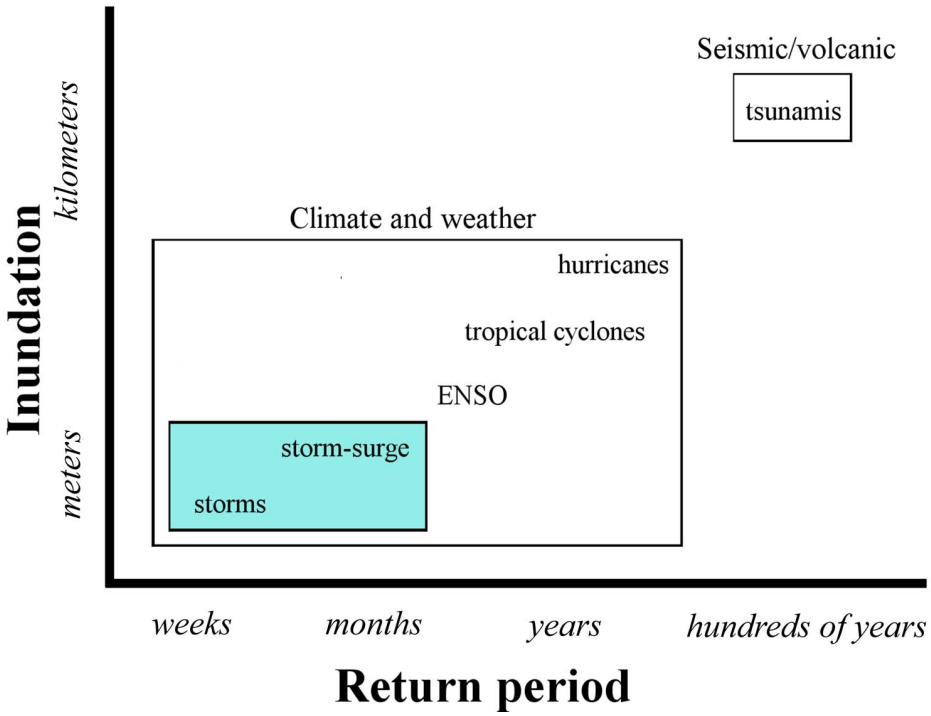

Figure 1.1: Coastal inundation operating at different temporal scales adapted from Marra et al. (2007). The inundation magnitudes are not precise but rather intended to give orientative values.

Coastal inundation (Figure 1.1) operates at different temporal and spatial scales and can be caused by seismic/volcanic processes and by climate and weather conditions (Marra et al., 2007). Undersea earthquakes, landslides, volcanic eruptions and collapses of volcanic edifices can trigger tsunamis, causing inundation of several kilometres (*e.g.*, the Japanese tsunami of 11th March 2011 caused inundation reaching 6 km inland (Mimura et al., 2011)). Fortunately, tsunamis

have large return periods (Figure 1.1) although their associated coastal damages can be catastrophic (*e.g.*, the tsunami of 26 December 2004 caused the loss of more than 220000 lives in countries around the Indian Ocean and losses of US$ 10 billion (Kron, 2008)). On the other hand, atmospheric and oceanic processes (climate and weather) can give rise to El Niño Southern Oscillation (ENSO), hurricanes, eddies and tropical cyclones whose return period ranges from one year to several years and can cause inundation reaching hundreds of meters inland.

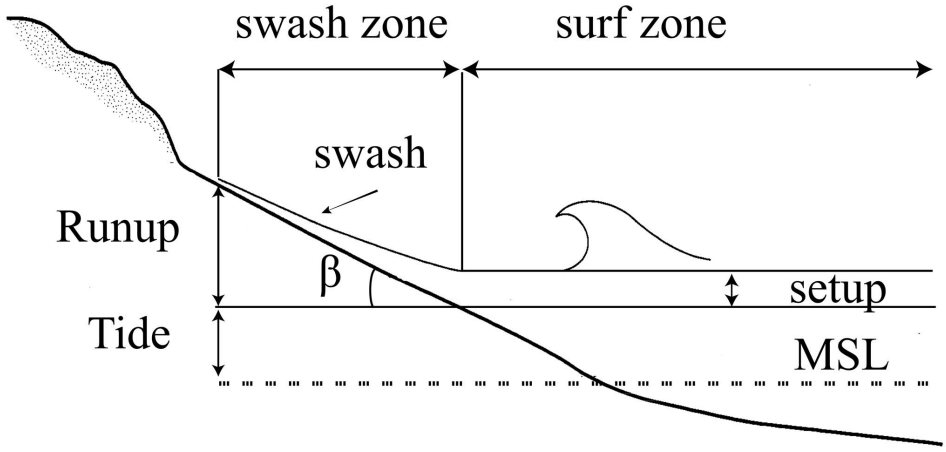

Figure 1.2: Wave runup sketch addapted from Ruggiero et al. (2001).

Coastal regions are also frequently subject to inundation produced by storms. Storm-induced inundation is caused by sea level rise resulting from the sum of astronomical tide, surge tide and wave runup. Surge level is dependent on changes in atmospheric pressure (*e.g.*, low pressure systems) (Ciavola et al., 2011) and is greatly affected by the bathymetric characteristics of the continental shelf (width and depth) (del Rio et al., 2012). Thus, the surge is higher where storms impact on narrow and shallow continental shelves (Wolf, 2009), as in the North Sea.

Wave runup (Figure 1.2) is defined as the time-varying location of the waterline around still water level (Guza and Thornton, 1982; Douglas, 1992; Gourlay, 1992) and it can be divided into *setup*, a steady super-elevation of mean water level, and *swash*, fluctuations about the set-up level (Guza and Thornton, 1982; Holman and Guza, 1984; Holman and Sallenger, 1985; Gourlay, 1992; Kobayashi, 1999; Ruggiero et al., 2004; Stockdon et al., 2006; Guedes et al., 2011; Senechal et al., 2011). The swash signal has two energy components: the

infragravity component, which dominates the swash signal on highly dissipative beaches (Ruessink et al., 1998; Ruggiero et al., 2004; Stockdon et al., 2006), and the *incident*, which dominates the swash signal on reflective beaches (Stockdon et al., 2006).

The dominance of astronomical tide, surge level and wave runup in storm inundation depends on site-specific conditions such as tidal range, storminess (exposure to surge levels and waves), the morphology of the continental shelf and the morphodynamic state of the beach. In tideless seas such as the Mediterranean, wave runup can be the main process controlling coastal inundation during storms because surge levels as a whole are likely to be much lower owing to the much deeper water depth (Wolf, 2009; Bosom and Jimenez, 2011).

1.2 Runup formulations

The prediction of beach inundation during storms involves the accurate prediction of wave runup. Many runup formulations can be found in the literature, most of them including deep water significant wave height (H_0) and wavelength (L_0), which is related to the peak period (T_p) and the beach slope (β):

$$\mathrm{L}_0 = \frac{g{T_p}^2}{2\pi} \tag{1.1}$$

Hunt (1959) proposed the above runup (R) equation after doing tests aimed at improving the design of seawall and breakwaters after flooding in the Netherlands and England caused by the storm surge of 1953 breached dikes and seawalls.

$$\mathrm{R} = \mathrm{H}_0 \xi \tag{1.2}$$

where ξ is the Iribarren number (Battjes, 1974) given by:

$$\xi = \frac{\beta}{\sqrt{\frac{\mathrm{H}_0}{\mathrm{L}_0}}} \tag{1.3}$$

The beach slope (β) used in the Iribarren number (ξ) is the foreshore beach slope. After Hunt, other authors have also proposed formulations based on the

Iribarren number and they have highlighted the difficulty of defining *beach slope*. For example, Holman and Sallenger (1985) calculated the mean slope over the range $\pm$2.5 m from the mean runup, while Ruessink et al. (1998) calculated the beach slope within the region of minimum run-down and maximum runup. Nielsen and Hanslow (1991) pointed out that for dissipative beaches this problem may not be as pronounced because the difference between the foreshore beach slope and the slope of the surf zone is fairly small: quite the opposite to intermediate to reflective beaches. For this reason, they suggested that an ideal measure of beach slope in relation to the runup processes should account for the foreshore and the surf zone. However, as the foreshore beach slope (β_f) is easier to measure during storm conditions, they considered this beach slope to be representative.

Guza and Thornton (1982) carried out for the first time runup measurements using dual resistance wires on a sandy oceanic beach with a gentle slope (β comprised between 0.03 and 0.05). They concluded that the significant runup (R_s) was about 70% of the significant wave height at 10 m depth (H_s):

$$\mathrm{R}_s(cm) = 3.48(cm) + 0.71\mathrm{H}_s(cm) \tag{1.4}$$

On the other hand, Holman and Sallenger (1985) found a strong dependence of the runup on ξ. The runup time series was collected using video images for the first time.

Holman (1986) measured extreme runup using video techniques and gave a new relationship for the 2% exceedance runup level based on ξ:

$$\mathrm{R}_{2\%} = (0.83\xi + 0.2)\mathrm{H}_0 \tag{1.5}$$

After experiments in a wave flume, Mase (1989) proposed a new relationship between the runup and the Iribarren number (ξ) for gentle, smooth and impermeable slopes ($\frac{1}{30} \leq \beta \leq \frac{1}{5}$), :

$$\frac{\mathrm{R}}{\mathrm{H}_0} = a\xi^b, for \frac{\mathrm{H}_0}{\mathrm{L}_0} \geq 0.007 \tag{1.6}$$

The coefficients a and b take different values depending on the statistical runup expression:

- The 2% exceedance runup, $\mathrm{R}_{2\%}$:

$$\frac{\mathrm{R}_{2\%}}{\mathrm{H}_0} = 1.86\xi^{0.71} \tag{1.7}$$

- The maximum runup, R_{max}:

$$\frac{\mathrm{R}_{max}}{\mathrm{H}_0} = 2.32\xi^{0.77} \tag{1.8}$$

- The mean runup, $\overline{\mathrm{R}}$:

$$\frac{\overline{\mathrm{R}}}{\mathrm{H}_0} = 0.88\xi^{0.69} \tag{1.9}$$

Nielsen and Hanslow (1991) presented a new runup equation distinguishing between dissipative and reflective beaches, using a data set from a wide range of natural beach types. Under the assumption of Rayleigh distribution, several representative runups are obtained:

- The significant runup (R_s):

  $\mathrm{R}_s = \mathrm{L}_{zwm}$

- The 2% exceedance runup, ($\mathrm{R}_{2\%}$):

  $\mathrm{R}_{2\%} = 1.98\mathrm{L}_{zwm}$

- The mean runup ($\overline{\mathrm{R}}$):

  $\overline{\mathrm{R}} = 0.98\mathrm{L}_{zwm}$

$$\mathrm{L}_{zwm} = \begin{cases} \cdot 0.05\sqrt{\mathrm{H}_{\mathrm{rms}}\mathrm{L}_0} & \text{if } \beta_f < 0.1, \\ \cdot 0.6\beta_f\sqrt{\mathrm{H}_{rms}\mathrm{L}_0} & \text{if } \beta_f \geqslant 0.1. \end{cases} \tag{1.10}$$

where L_{zwm} is the vertical scale for Rayleigh-distributed wave runup values and H_{rms} is the offshore root mean square wave height.

Douglas (1992), using the dataset of Holman (1986), proposed an independent beach slope relationship for the maximum runup (R_{max}):

$$\frac{\mathrm{R}_{max}}{\mathrm{H}_0} = \frac{C}{\sqrt{\frac{\mathrm{H}_0}{\mathrm{L}_0}}}, \tag{1.11}$$

where C is an empirical coefficient which for Holmans's data is C = 0.12. Walton (1992) re-analysed the database of Mase, giving a new equation for mean runup ($\overline{\mathrm{R}}$) based on a modified dimensionless form of the fourmula of Hunt (1959) with a linear intercept term:

$$\overline{\mathrm{R}} = 0.77\xi + 0.2, \tag{1.12}$$

Ahrens and Seelig (1996) used runup measurements on sandy beaches carried out among others by Holman (1986) and by Nielsen and Hanslow (1991) and runup data collected in the laboratory on gravel beaches. They developed a formula to estimate the upper limit of wave runup including the sediment grain size and showed a connection between runup and beach morphology, highlighting the importance of submerged morphology and alongshore variability in runup.

$$\frac{\mathrm{R}_{2\%}}{\mathrm{H}_0} = 10.4\sqrt{d_{sw}/d_{sr}}\left[w_{sr}/\sqrt{gH_0}\right]/\sqrt{\mathrm{H}_0/\mathrm{L}_0} \tag{1.13}$$

where $\frac{\mathrm{d_{sw}}}{\mathrm{d_{sr}}}$ is the beach diversity defined as the ratio of median sediment size in the swash zone, $\mathrm{d_{sw}}$, to median size in the surf zone, $\mathrm{d_{sr}}$, $\mathrm{w_{sr}}$ is the sediment fall velocity in the surf zone and $\mathrm{w_{sr}}/\sqrt{\mathrm{gH_0}}$ is a surf zone Froude-type number.

Ruessink et al. (1998) carried out video measurements of swash in highly dissipative conditions (a low-sloping beach), concluding that *infragravity waves* dominated the swash. A linear relationship between the significant infragravity runup ($\mathrm{R_s}^{ig}$) and the Iribarren number (ξ) was also found:

$$\frac{\mathrm{R_s}^{ig}}{\mathrm{H}_0} = 0.53\xi + 0.09 \tag{1.14}$$

Ruggiero et al. (2001), using wave runup video measurements made at different beaches and the wave runup dataset of Holman (1986), proposed a model to evaluate the susceptibility of coastal properties to erosion during extreme storms events. This model included a new runup expression (see Equation (1.15)) based

on the video measurements and the tide. Here, the foreshore beach slope (β_f) was defined in the region between plus and minus two standard deviations from the mean runup elevation.

$$\mathrm{R}_{2\%} = 0.27\sqrt{\beta_f \mathrm{H}_0 \mathrm{L}_0} \tag{1.15}$$

The most complete study on wave runup is that done by Stockdon et al. (2006), using an extensive dataset of video measurements from open and oceanic beaches (ranging from dissipative to reflective). The general parameterization proposed on all natural beaches for the 2% exceedance runup, $\mathrm{R}_{2\%}$, includes the terms for the setup and discriminates between the incidence and the infragravity swash:

$$\mathrm{R}_{2\%} = 1.10\left(\mathrm{H}_0\mathrm{L}_0\right)^{0.5}\left(0.35\beta_f + \frac{\left(0.563{\beta_f}^2 + 0.004\right)^{0.5}}{2}\right) \tag{1.16}$$

β_f was defined as the average slope over a region $\pm 2\sigma$ around the set-up at the shoreline and σ was the standard deviation of the continuous water level record.

This expression can be simplified as follows for highly dissipative beaches:

$$\mathrm{R}_{2\%} = 0.043\left(\mathrm{H}_0\mathrm{L}_0\right)^{0.5} \tag{1.17}$$

and for reflective beaches:

$$\mathrm{R}_{2\%} = 0.73\beta_f\left(\mathrm{H}_0\mathrm{L}_0\right)^{0.5} \tag{1.18}$$

More recently, Roberts et al. (2010) examined runup measurements from movable-bed laboratory studies and suggested that the total wave runup for non-scarped beaches is directly related to the significant breaking wave height (H_b). Roberts et al. (2010) did not include the beach slope in this analysis, arguing that it is difficult to measure and depends on the wave properties.

$$\mathrm{R}_{max} = \mathrm{H}_b \tag{1.19}$$

Whereas Roberts et al. (2010) did not include the beach slope, in a study of the runup on beaches affected by long wave periods Mather et al. (2011) concluded that wave runup varies not only with the beach slope but also with the bathymetric

profile and presented a new runup expression:

$$\mathrm{R}_{max} = \mathrm{CH}_0\mathrm{S}^{2\backslash 3} \tag{1.20}$$

where C is a dimensionless coefficient whose value depends on the beach characteristics (open beaches, C = 10, large embayments, C = 9 and small embayments, C = 6) and S is a representative nearshore slope.

The two most recent runup equations were proposed by Vousdoukas et al. (2012) and Guza and Feddersen (2012). Vousdoukas et al. (2012), using video observations, proposed a new equation including some additional terms that had not been previously found, such as the shore-normal wind speed component, $\mathrm{U_{w,x}}$, and the tidal water-level variations relative to mean sea level, η_{tide}:

$$\mathrm{R}_{2\%} = 0.503\beta_\mathrm{f}\left(\mathrm{H}_0\mathrm{L}_0\right)^{0.5} + 0.878\xi\sqrt{\frac{\mathrm{H}_0^3}{\mathrm{L}_0}} - 0.016U_{w,x} + 0.188\eta_\mathrm{tide} + 0.457 \tag{1.21}$$

Guza and Feddersen (2012) computed numerical simulations with the Boussinesq wave model *funwaveC* and suggested that the infragravity significant wave runup ($\mathrm{R}_s{}^{ig}$), which dominates on dissipative beaches, depends on frequency (f_s) and directional (σ_θ) spread of the incident wave spectrum:

$$\frac{\mathrm{R}_s{}^{ig}}{\sqrt{\mathrm{H}_0\mathrm{L}_0}} = -0.013ln\left[\frac{f_p}{f_s}\sigma_{\theta,0}\right] + 0.058 \tag{1.22}$$

where f_s is the frequency spread, f_p is the peak frequency, $\frac{\mathrm{f}_p}{\mathrm{f}_s}$ is the dimensionless spreading parameter and $\sigma_{\theta,0}$ is the deep water directional spread.

All the aforementioned runup equations consider the wave hydrodynamics (wave height, wavelength and peak period) and a morphological parameter (beach slope). Moreover, most of the equations are based on runup studies focusing on the hydrodynamics of the wave runup, with little discussion on how the morphological changes could interfere. For instance, Ahrens and Seelig (1996) pointed out the importance of the coordination between beach runup and beach morphology, Holman and Sallenger (1985) and Stockdon et al. (2006) found alongshore variability in the runup related to the rhythmic topography. Vousdoukas et al. (2009) compared runup observations with predicted runup using the formulations of Holman (1986) and Stockdon et al. (2006) but the results did not match, sug-

gesting that the wave runup was influenced by the nearshore bed morphology. Additionally, Roberts et al. (2010) found that the formulations of Holman (1986) and Stockdon et al. (2006) underpredict (overpredict) the runup considerably if erosion (accretion) takes place.
To date no study has quantified the variability due to shoreline changes and morphological features and its influence on runup prediction and therefore on beach inundation prediction.

1.3 Video monitoring techniques

As noted above, the proposed runup formulations have been based on several approaches, including model computations, laboratory studies and field measurements by means of resistance wires, most of them using video measurements.

In 1980, the Coastal Imaging Lab (CIL) at Oregon State University accomplished the first time-lapse video measurements of wave runup as a diagnostic method for sampling infragravity edge waves (Holman, 1981). This technique was validated years later by Holman and Guza (1984) and Holland et al. (1995), who compared wave runup measurements using video and resistance wires. Since that time a large number of wave runup studies have been done using video measurements (Holman and Guza, 1984; Holman, 1986; Aagaard and Holm, 1989; Ruessink et al., 1998; Ruggiero et al., 2001, 2004; Salmon et al., 2007; Bryan et al., 2009; Bryan and Coco, 2010; Guedes et al., 2011; Senechal et al., 2011; Vousdoukas et al., 2012).

The most well-known video monitoring system is the Argus station. Normally, an Argus video system is composed of a number of video cameras placed at a certain height above sea level and pointing towards the coast. This system routinely collects three types of image every daylight hour: a single snapshot, a 10-minute time-exposure (or timex) and a 10-minute variance image (Holman and Stanley, 2007). In order to obtain real-world coordinates from these oblique images, each camera must be calibrated and the image must go through some geometrical transformation to find the relation between the image coordinates and the real-world locations (Holland et al., 1997).

One approach to obtaining observations of beach inundation would be to measure the wave runup using video observations and the astronomical and surge tide and then transform the data into horizontal excursion. The common methodology for measuring wave runup is a *timestack* (Aagaard and Holm, 1989; Bailey and Shand, 1994; Holman and Stanley, 2007), which consists of time series of pixel intensity sampled at 1 or 2 Hz along a cross-shore transect defined on the image. This timestack of pixel intensities shows runup and rundown as a white edge moving back and forth in the swash zone. The leading edge of the runup is digitized automatically and it can be converted to a time series of water level elevation using photogrammetric relationships (Holland et al., 1997). Despite the higher pixel resolution (centimeters), this technique has some disadvantages: the beach profile must be surveyed at the location where the timestack lies for good accuracy of the runup magnitudes, and several timestacks must be defined to study the alongshore variability of the wave runup. In addition, during storm conditions, it is not always possible to do topographic surveys and morphological changes may take place, altering the beach profile and therefore the magnitude of the runup. An alternative methodology is to extract the waterline from the timex images (Kroon et al., 2007) during a storm, which allows the morphological patterns to be identified and the beach inundation alongshore to be quantified without depending on topographic surveys.

1.4 Embayed beaches

Most runup studies are carried out on open, macrotidal and oceanic sandy beaches where the waves are characterized by large periods, so the formulations are based on this beach type. However, few runup studies have been carried out on embayed beaches (Salmon et al., 2007; Bryan et al., 2009; Vousdoukas et al., 2009; Guedes et al., 2011). Further, no runup study has been done on artificial and tideless embayed beaches characterized by large protection structures (*e.g.*, dikes and breakwaters) where wave transformation processes such as diffraction can be important. Inaccuracies in inundation prediction could therefore arise when these formulas are used for such beaches.

Embayed beaches are cited in the literature in several ways: *zetabays*,

crenulate-shaped bays, *headland bay beaches*, *hook beaches*, *spiral beaches*, *curved beaches*, *half-heart bays*, *pocket beaches*, *structurally controlled beaches* and *topographycally-bound beaches* (Hsu et al., 2010). These beaches are affected by headland bypassing, rip formations and *beach rotation*. The most important agent in the shoreline changes of embayed beaches is the beach rotation process (Ranasinghe et al., 2004; Ojeda and Guillen, 2008; Martins et al., 2010; Ojeda et al., 2010; Archetti and Romagnoli, 2011). According to Short and Masselink (1999), this process refers to a shift in the alongshore sediment transport between opposite ends of the beach, causing shoreline accretion and erosion at either end with no net change in the sediment budget. Beach rotation is caused by variation in the wave direction, which can be related to storm events, seasonal changes in the wave climate (Klein et al., 2002; Martins et al., 2010; Archetti and Romagnoli, 2011), alongshore mud bank migration (Anthony et al., 2002), El Niño Southern Oscillation (Ranasinghe et al., 2004) and North Atlantic Oscillation (Thomas et al., 2011).

A common feature of these beaches is the asymmetric beach planform shape, characterized typically by a curved zone, a gentle transition and/or a relatively straight tangential segment. Their planform has a close correspondence to the refraction pattern associated with the prevailing waves. For this reason, the study of embayed beaches is usually based on the concept of their planform stability and geometry. Three empirical formulas have been proposed to fit part or whole of the embayment: *logarithmic spiral* (Krumbein, 1944; Yasso, 1965), *hyperbolic tangent*, (Moreno and Kraus, 1999) and *parabolic* (Hsu and Evans, 1989). The first two formulas consider only the fitting of geometry to the shoreline rather than the stability and ignore wave direction and relative position of the headland to a beach while the third relates the shoreline change to the tip of an updrift headland or wave diffraction point.

1.5 Study sites

This thesis focuses on three embayed beaches located in Barcelona, Spain (NW Mediterranean) and an open beach in Noordwijk, the Netherlands (North Sea), both of which are monitored by an Argus video system. The hydrodynamic conditions governing the beach inundation process and the morphological

characteristics of these field sites are different.

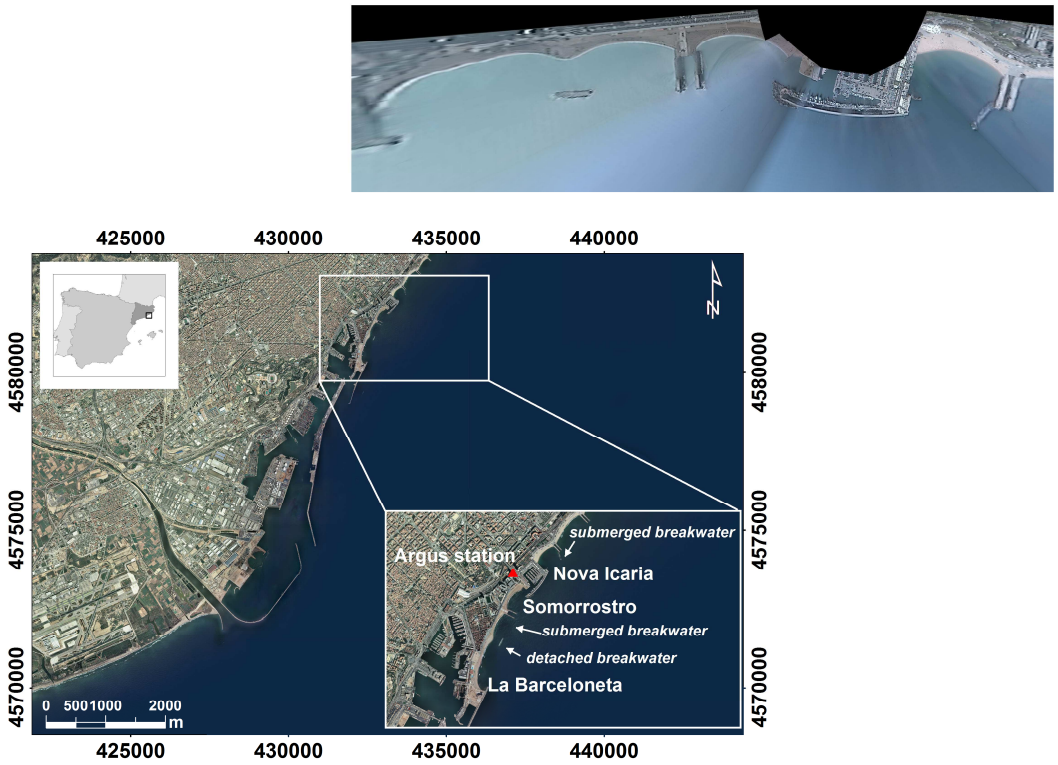

Figure 1.3: Location of the study area of Barcelona, indicating the coastal structures and the Argus station location. Top, a plan view obtained from the Argus station showing the three embayed beaches studied. The orthophotos are copyright of the ICC, and are available at www.icc.cat.

Barcelona is located on the central Catalan coast, facing the semi-enclosed Mediterranean Sea. It has 13 km of coastline containing the city harbour in the southernmost part, three marinas and 3 km of beaches. The beaches of Barcelona were created as part of the urban renewal plan for the 1992 Olympic Games. Waves are the main natural mechanism controlling coastal evolution (Ojeda and Guillen, 2008) and the tidal range is less than 20 cm. This thesis focuses only on three beaches of Barcelona: Nova Icaria, Somorrostro and La Barceloneta (Figure 1.3). Nova Icaria is a non-barred beach protected by two submerged breakwaters above sea level and separated from the next beach by two double dikes; sometimes a shoreline undulation is observed. Somorrostro is a non-barred beach at the south of the Olympic Marina and beach cusps can be distinguished under certain hydrodynamics conditions. Finally, during the study period, between 2001 and 2008, La Barceloneta changed from a single barred

beach bounded by Barcelona harbor in the south and Somorrostro dike in the north (hereinafter called La Barcelona I) to a two embayed beaches separated by a salient (hereinafter called La Barcelona II). La Barceloneta I was a barred beach in which megacusps formed under storm conditions because of the attachment of the sandbar to the beach (Ojeda and Guillen, 2008).

Noordwijk beach is located on the central Dutch coast facing the semi-enclosed North Sea. It is a sandy, wave-dominated coast with a beach and nearshore zone that consists of a single intertidal slip-face ridge and two subtidal bars (Figure 1.4). Occasionally, a second intertidal bar may form on a pre-existing bar during low-energy wave conditions (Quartel et al., 2007). The tide at Noordwijk is semi-diurnal and microtidal. The mean tidal range is 1.8 m and 1.4 m during spring and neap tide, respectively. During the study period, Noordwijk beach underwent one shoreface nourishment. A total of 1.7 Mm^3 of sand was placed 5 to 8 m over an approximately 3-km-wide (alongshore) area, roughly 900 m from the shore. This shoreface nourishment was implemented as a hump over the seaward side of the outer subtidal bar (Ojeda et al., 2008; Quera, 2010).

1.6 Aims and outline of the thesis

The general objective of the research presented in this thesis is *to provide more insight into beach inundation at embayed and open beaches and to consider how beach inundation can be affected by morphological changes.* This broad aim can be divided into the detailed research questions that are addressed in this thesis:

1. What are the shoreline changes at tideless embayed beaches during storms?
2. How do protection works affect shoreline reshaping and hydrodynamics during storms at embayed beaches?
3. What are the differences in beach inundation behavior between embayed beaches and open multibarred beaches?
4. How do morphological features and the beach planform modify beach inundation?
5. Should shoreline changes be included in inundation prediction?

6. Are the wave runup formulations suitable for predicting beach inundation at embayed beaches?

The rest of the thesis is divided into four chapters (Chapters 2 to 5), which are edited versions of scientific publications, including the results obtained and their interpretation. A final chapter (Chapter 6) contains the overall conclusions of this thesis and some suggestions for further research on the topics studied.

Chapter 2 examines the effects of a submerged breakwater and a detached breakwater on the morphological and hydrodynamic changes occurring during storms at La Barceloneta. Research questions 1 and 2 are addressed using video observations, the Coastal Modelling System (SMC) model, and a new methodological approach to analyzing beach rotation that eliminates the morphological effect.

Chapter 3 characterizes the beach inundation using video observations during storms at the three embayed beaches of Barcelona (research question 3) and quantifies the influence of the shoreline changes (research question 5). Research question 4 is addressed by splitting the shoreline variability into beach planform and morphological features (small beach cusps, megacusps, shoreline undulation and a salient).

Chapter 4 characterizes the beach inundation during storms at the open beach of Noordwijk (research question 3) and investigates the influence of intertidal sandbars (research questions 4 and 5) using video observations. Furthermore, using the XBeach model, this chapter addresses the influence of submerged morphologies (*i.e.*, sandbars) on inundation (research questions 4 and 5).

Chapter 5 answers research question 6 by evaluating the runup paramerization of Stockdon et al. (2006) and Roberts et al. (2010) at Somorrostro beach. To this end, inundation measurements using video observations are compared with estimations, including tidal variations and the wave runup formulation of Stockdon et al. (2006) introducing deep water and local wave measurements and computations and the runup formulation of Roberts et al. (2010) using wave computations.

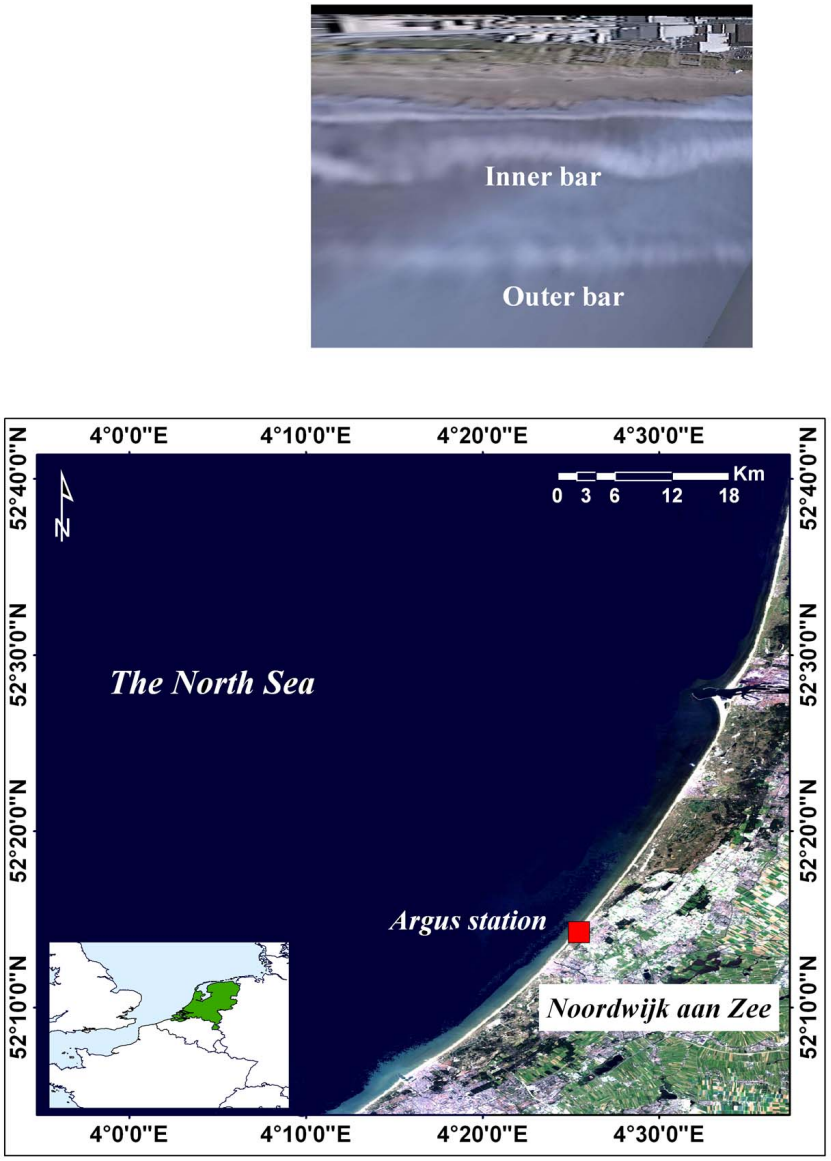

Figure 1.4: Location of the study area of Noordwijk (the Netherlands) indicating the Argus station location (red square). Top, a plan view obtained from the Argus station showing the inner and the outer bars of Noordwijk beach. The image used is a product of IMAGE2000. Intellectual property rights IMAGE2000 of JRC, based on Landsat 7 ETM+ © ESA, distributed by Eurimage; ortho-correction EU15 © Metria, ortho-correction other countries GISAT; mosaic production GISAT.

Chapter 2

SHORELINE RESHAPING OF AN EMBAYED BEACH DURING STORMS AFTER PROTECTIONS WORKS

Edited version of A. Sancho-García, J. Guillén and E. Ojeda. Shoreline reshaping of an embayed beach during storms after protections works. *Submitted to Geo-Marine Letters.*

2.1 Introduction

Storm events are responsible for major changes in the configuration of sandy embayed beaches (Cooper et al., 2004; Ojeda and Guillen, 2008; Martins et al., 2010; Ojeda et al., 2010). In particular, the most important agent in the shoreline changes of embayed beaches is the beach rotation process (Ranasinghe et al., 2004; Ojeda and Guillen, 2008; Martins et al., 2010; Ojeda et al., 2010; Archetti and Romagnoli, 2011). According to Short and Masselink (1999), this process refers to a shift in the alongshore sediment transport between opposite ends of the beach, causing shoreline accretion and erosion at either end with no net change in the sediment budget. Beach rotation is caused by variation in the wave direction, which can be related to storm events, seasonal changes in the wave climate (Klein et al., 2002; Martins et al., 2010; Archetti and Romagnoli, 2011), alongshore mud bank migration (Anthony et al., 2002), El Niño southern oscillation (Ranasinghe et al., 2004) or North Atlantic Oscillation (Thomas et al., 2011).

The approaches applied in order to increase shoreline stability can be divided into hard engineering solutions (*e.g.*, groins, seawalls and offshore structures), and soft engineering solutions (beach nourishment). A common approach is to apply combination of the two. Shore-parallel breakwaters are structures built at a certain distance from the shore and totally unconnected to it, protecting a particular shoreline area from wave action (Bricio et al., 2008). Their primary function is to protect the coast from flooding or erosion but they have also been used to create artificial beaches (Ilic et al., 2005). These structures decrease the wave energy in the area immediately behind the breakwater and modify the nearshore currents to initiate sediment deposition at the shoreline (Ranasinghe and Turner, 2006; Turner, 2006; Ilic et al., 2007), resulting in the development of tombolos and salients. However, their performance depends on the effect of the breakwater on the littoral sediment transport and the results obtained after their construction have not always been as desired (Bricio et al., 2008). This fact reveals an insufficient knowledge of the sedimentary processes governing morphological changes. Emerged shore-parallel breakwaters are called detached breakwaters and their characteristics and the processes governing shoreline response are fundamentally different from those of submerged breakwaters (Ranasinghe and Turner, 2006). Although submerged structures offer a low aesthetic impact, unlike detached breakwaters they can result in shoreline erosion

on their lee side (Ranasinghe and Turner, 2006).

On the Mediterranean coast beach erosion is attributed to wave action, large-scale residential development, interruption of the sand transport by harbour installations, extraction of sand and gravel from rivers and beaches, and reduction of fluvial sediment inputs to the beach due to the building of dams and the destruction of littoral dunes (Hanson et al., 2002; Sanjaume and Pardo-Pascual, 2005; Bricio et al., 2008). The practical consequences of this erosion are that beaches are narrow and the subaerial surface is not wide enough to fulfil usual beach functions, such as protection and/or recreation (Ariza et al., 2008).

Shoreline changes at La Barceloneta, a Mediterranean beach located in Barcelona (Spain), have been well documented (Ojeda et al., 2006; Ojeda and Guillen, 2008; Ojeda et al., 2011). This is an artificial urban beach that is occupied during most of the year by tourists and inhabitants (Guillen et al., 2008). To date La Barceloneta has been the focus of numerous counter-erosion and stabilization projects, the most important of which was carried out between 2006 and 2007 when the beach was nourished and a detached and a submerged breakwater were built. After these protection works the morphological configuration and the response of La Barceloneta to storms changed.

In this chapter, the changes in the sedimentary processes induced by the presence of the new breakwaters are investigated in order to analyze the different response of the beach to storms. To attain this, the morphological behaviour of La Barceloneta under storms conditions using ten years of video images and wave hydrodynamics modelled are compared before and after these protection works.

2.1.1 Study area

Barcelona city is located on the south Catalan coast, facing the Mediterranean Sea. It has 13 km of coastline containing the city harbour in the southernmost part, three marinas and 3 km of beaches (Figure 2.1). The beaches of Barcelona were created as part of the renewal plan that took place in the zone for the 1992 Olympic Games. This study focuses on La Barceloneta, the longest artificial embayed beach of Barcelona, which has an orientation of approximately 20^{o} from the north and a length of 1100 m.

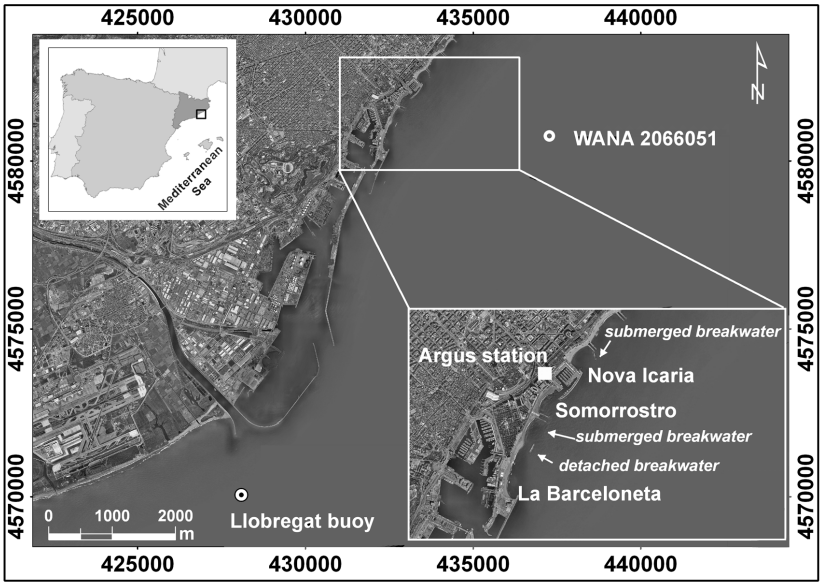

Figure 2.1: Localization of La Barceloneta beach. The beach shows the morphological configuration after the construction of the detached breakwater. The Argus station and the Llobregat buoy and WANA (node 206601) locations are indicated by a square and a double-circle, respectively. The orthophotos are copyright of the ICC, and are available at www.icc.cat.

Human activity has continuously affected La Barceloneta. Between 1992 and 2005 (Figure 2.2a), the emerged area of La Barceloneta displayed an erosive trend (Ojeda and Guillen, 2008) alleviated by a sporadic artificial nourishment (40000 m^3 of sand) in summer 2002 and a sand relocation of about 30000 m^3 from the southwest to the northeast in summer 2004. The authorities carried out a number of protection works between 2006 and 2007 in order to prevent this erosion. First, La Barceloneta was nourished with 80000 and 46000 m^3 of sand in March and June 2006, respectively. Second, a detached breakwater of 140 m length, located at 7.5 m depth and standing approximately 1 m above sea level, was built between November 2006 and May 2007 and a submerged breakwater of 120 m length, standing 2 m below sea level, was built between December 2006 and March 2007

Beach	Length (m)	Beach orientation	Average beach slope	D_{50} (μm)
La Barceloneta I	1100	N20E	0.13	900
La Barceloneta II	1100	N20E	0.07	614

Table 2.1: Morphological characteristics of La Barceloneta

(Figure 2.2b). These protection works gave rise to a change in the morphological configuration of the beach and in the beach profile, which is now gentler than before (see Table 2.1). Despite these protections works, La Barceloneta continued to erode and two sporadic nourishments were carried out in June 2009 and May 2010 in the northeastern section of La Barceloneta, considerably increasing the beach area.

In order to analyze the shoreline response to storms, the first configuration (La Barceloneta I, Figure 2.2a) and the latest configuration (La Barceloneta II, Figure 2.2b) are considered separately. La Barceloneta I had a submerged sandbar located 80 m from the shoreline, with the bar crest at 2 m water depth (Ojeda et al., 2011) and megacusps formed under storm conditions owing to surf processes which transformed the submerged bar into a crescentic bar and caused it to become attached to the beach (Ojeda and Guillen, 2008). The most significant morphological features at La Barceloneta II were megacusps that were only observed in the southwestern section.

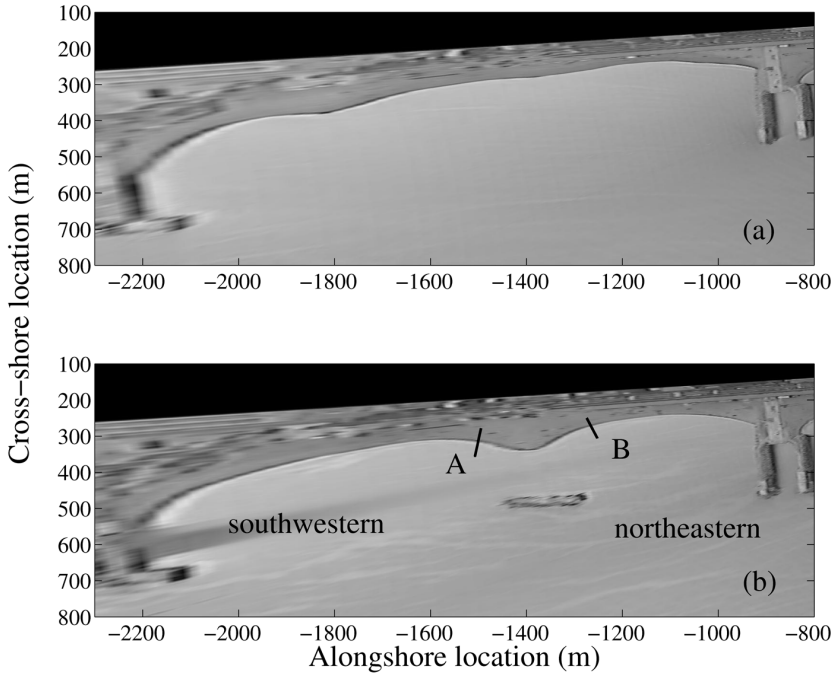

Figure 2.2: Morphological configuration of La Barceloneta beach before (a) and after (b) the construction of the detached breakwater. Coordinates are given in Argus coordinates.

2.2 Material and methods

2.2.1 Wave data

Wave measurements of the Llobregat buoy (XIOM, www.xiom.cat) located at a depth of 45 m (Figure 2.1) were used to characterize storm events. This buoy has been directional since 2004, recording data every hour. Interruptions in the buoy time series and the lack of wave direction before 2004 were filled in with data from the WANA model (node 2066051, Figure 2.1), which provides directional wave information every three hours. The WANA data has been computed by the Spanish National Institute of Meteorology using the HIRLAM and WAM numerical model since 1991 (Spanish Port Authority, www.puertos.es). Wave height and period data from the WANA model were calibrated through linear regression using the buoy observations from October 2001 to December 2008 (R^2 = 0.70). When the buoy was not directional (before 2004), the wave peak period (T_p) was obtained using a calibration between the wave significant period ($\mathrm{T}_{1/3}$) and the wave peak period for the period 2004-2008 (R^2 = 0.62). The wave direction data were not calibrated because a very poor relationship was found.

From 2001 to 2011 storm events with a significant wave height higher than 2.5 m during the peak of the storm and a minimum duration of 12 hours were selected following the methodology of Ojeda and Guillen (2008) (Table 2.2). The threshold wave height used to estimate the storm duration was 1.5 m so the initial day occurred when the wave height started to exceed 1.5 m and the final day when the wave height started to be less than or equal to 1.5 m, although the wave height was allowed to be below the threshold for 6 h.

2.2.2 Video images

An Argus Video system (Holman and Stanley, 2007) located atop a building close to the Olympic Marina at a height of around 142 m has been deployed since 2001 (Coastal Ocean Observatory, http://coo.icm.csic.es/). The Argus station is composed of five cameras pointing at the Barcelona beaches and offering a 180$^{\mathrm{o}}$ view of the coast. Images are in the visible range of light and sampling is done every daylight hour during a ten-minute period (1 picture per second).

Event	Initial date	$H_{o_{mean}}$ (m)	$H_{o_{\max}}$ (m)	$T_{p_{\text{mean}}}$ (s)	Wave direction_{mean} (^{o})	Duration (hours)
La Barceloneta I						
1	11/10/2001	2.27	8.52	9.17	69	163
2	12/14/2001	2.55	3.16	10.09	68	49
3	01/03/2002	2.37	3.34	8.39	108	33
4	05/07/2002	2.67	3.79	9.18	93	48
5	11/14/2002	2.10	2.68	8.77	199	13
6	02/24/2003	2.18	2.90	8.57	118	73
7	10/15/2003	2.95	4.11	10.00	80	89
8	10/30/2003	2.95	4.09	9.33	201	37
9	12/03/2003	1.98	3.89	10.26	94	26
10	12/08/2003	2.44	3.15	9.79	83	22
11	02/20/2004	2.34	3.25	9.45	91	51
12	03/29/2004	2.28	3.39	8.87	103	58
13	04/15/2004	2.24	3.27	9.41	109	45
14	05/03/2004	2.25	3.07	8.67	105	25
15	02/12/2005	2.57	3.81	9.26	202	38
16	01/30/2006	2.43	3.01	10.17	94	39
17	02/19/2006	2.11	2.57	7.77	201	19
La Barceloneta II						
18	10/20/2007	2.26	3.09	8.82	77	32
19	10/25/2007	2.01	2.54	9.56	78	32
20	12/15/2007	2.10	3.50	8.88	89	45
21	05/09/2008	2.12	2.77	7.90	124	41
22	12/26/2008	2.79	4.65	10.29	88	65
23	01/23/2009	2.08	3.66	8.48	204	33
24	12/24/2009	2.03	2.97	7.88	197	28
25	12/31/2009	2.22	2.85	8.27	198	26
26	03/03/2010	2.51	3.52	9.71	100	37
27	03/08/2010	2.37	4.76	10.84	105	51
28	03/08/2011	2.15	2.80	8.67	95	34
29	03/14/2011	1.86	2.57	8.01	122	54

Table 2.2: Characterization of storm events

Beach	$\mathrm{Mean}_{\mathrm{error}}$	Standard $\mathrm{deviation}_{\mathrm{error}}$
La Barceloneta I	4.70	2.98
La Barceloneta II	4.54	1.99

Table 2.3: Alongshore differences between dGPS surveys and Argus-derived shorelines in metres.

The shorelines before and after each storm event were obtained from the ten-minute time exposure images. Shorelines were mapped using the Intertidal Beach Mapper software (included in the Argus Runtime Environment) by the automated alongshore tracking of the intensity maxima across the shoreline. In order to minimize errors, three shoreline positions were obtained for each sampled day and then they were alongshore averaged. Some problems were found for the shoreline detection due to bad visibility caused by the presence of fog or clouds. Therefore, in these moments and when there was a lack of contrast between sand and water, the shoreline positions were mapped manually from the images. The 2D image coordinates were transformed to real coordinates (Holland et al., 1997). The accuracy of the photogrammetric transformation from image to ground coordinates is 1 pixel and the pixel size ranges from 1 to 1.5 m in the cross-shore direction and from 1 to 20 m in the alongshore direction (Ojeda et al., 2011). The worst resolution is found in the southwestern section of La Barceloneta, where 1 pixel corresponds to 20 m.

Video-derived shorelines were compared with the ones obtained from differential global positioning system (dGPS) surveys performed at La Barceloneta (three at La Barceloneta I and one at La Barceloneta II). Differences were evaluated on a grid with 2 m spacing in the y-direction and results are given in Table 2.3, where $\mathrm{mean}_{\mathrm{error}}$ represents the average of the differences found for each point along the beach for all the dGPS surveys performed at the beach. For every comparison the Argus-derived shoreline was offshore of the dGPS surveyed shorelines.

A reference shoreline was defined for each beach as the result of the averaged position from all available shorelines fitted to a polynomial curve. The shoreline response at La Barceloneta I was measured as the difference between the final and the initial shoreline of each storm event following profiles along the reference

shoreline every 4 metres. The same approach was used to analyze the shoreline response of La Barceloneta II, although some previous considerations were taken into account. It was assumed that La Barceloneta II was composed of two independent embayed beaches, hereinafter referred to as La Barceloneta II-N and La Barceloneta II-S, separated by the salient. This methodological approach was selected following previous studies on embayed beaches with similar morphological characteristics (Klein et al., 2002, 2010). In order to mark out the boundaries of the salient and to establish the limits of these two beaches, a curvature parameter was applied to the reference shoreline of La Barceloneta II. The two relative maximums of this parameter curvature, lines A and B in Figure 2.2b, marked the extension of the salient and the limits of these two new beaches. Afterwards, the procedure explained at the beginning of the paragraph for La Barceloneta I was applied to each beach.

To facilitate the observation and analysis of the changes in the planform of the beaches, excluding the effects of other morphologies (*e.g.*, megacusps), each shoreline was fitted to a shoreline hyperbolic tangent shape characteristic of embayed beaches (Moreno and Kraus, 1999) for analyzing the beach planform changes. Although the logarithmic spiral shape fits better for embayed beaches with two headlands (Martino et al., 2005; Oliveira and Barreiro, 2010), this shoreline shape was selected because the fitting considered only the geometry of the shoreline rather than the stability, and the fitting procedure was simpler (Lausman et al., 2006; Hsu et al., 2010). Thus, beach planform changes were calculated as the difference between the shorelines fitted before and after each storm event following the same beach profiles as those previously defined.

The final and the initial emerged beach area of La Barceloneta I was calculated for each storm event as the area delimited by the shoreline, the beach promenade at the landward limit of the beach and the dikes in the northern area, and the first beach profile localized in the southwestern section. For storm events in which the beach planform changes suggested changes in the beach orientation of La Barceloneta I, the northeastern and southwestern sections of La Barceloneta I were analyzed independently and separated by a pivotal point. This pivotal point varied from one storm event to another and was selected after comparison of the fitted shorelines. Following Ojeda and Guillen (2008), beach rotation occurred

when there was an opposite behaviour (erosion/accretion) of similar magnitude in the two sections of the beach separated by a pivotal point. The variation in the emerged beach area of each section of La Barceloneta I was also calculated, but in this case the emerged area was calculated using the fitted shoreline. The same procedure was applied to the two beaches of La Barceloneta II.

2.2.3 Hydrodynamics

The wave processes and the wave-induced currents of Events 11 and 22, with similar wave direction (Table 2.2) and affecting La Barceloneta I and II, respectively, were modelled using the Coastal Modelling System (SMC) (Gonzalez et al., 2007). The simulations were carried out with the Oluca-SP wave transformation model using spectral analysis for propagating waves from offshore to La Barceloneta. This model includes the effect of shoaling, refraction, energy dissipation (bottom friction and wave breaking), diffraction and wave-current interaction (Gonzalez et al., 2007). Wave-induced currents were modelled with the 2DH Copla-SP module using the wave-breaking formulation of Rattanapitikon and Shibayama (1998). Copla-SP solves the vertically integrated equations of conservation of mass and momentum in two horizontal dimensions. The wave gradient of radiation stresses obtained from the Oluca-SP model is used as input forcing for Copla-SP (see Gonzalez et al. (2007) for more details).

2.3 Results

2.3.1 La Barceloneta I (before breakwaters)

Beach morphodynamics

The emerged beach area of La Barceloneta I evolved from approximately 60000 m^2 at the beginning of the study period (October 2001) to 50000 m^2 before the protection works (Figure 2.3a). The most significant losses of sediment occurred during storms 10, 11, 16 and 17. On the other hand, gains of the emerged area took place during Events 3, 4 and 8. The emerged beach area remained almost unchanged during the other events, some of them showing a differential behaviour in the northeastern and southwestern sections according with a rotation

of the beach in response to the storm (*e.g.*, Events 1 and 2).

The nourishment carried out in summer 2002 and the sand relocation from the southern to the northeastern section of La Barceloneta carried out in June 2004 caused increases in the total emerged beach area of 6000 m^2 and 2000 m^2, respectively. However, these increases are not appreciated in Figure 2.3a because of the time elapsed between Events 4 and 5 in the case of the sand nourishment and between Events 14 and 15 in the case of the sand relocation, during which several minor storms occurred. In particular, on the days prior to Event 5 some minor storm events caused a temporary decrease in the area but, when the complete time series of the beach area (not only the pre- and post-storm events series) is analysed, the effect of the beach nourishment is clearly visible until February 2003.

The shoreline response to storms at La Barceloneta I can be grouped into three categories: general erosion or accretion, beach rotation, and differential erosion/accretion alongshore. General erosion was only observed in Event 11 (February 2004, eastern direction) and resulted in a shoreline retreat that varied alongshore between 2 and 12 m. A general non-uniform alongshore accretion from 2 to 9 m was observed in Events 3 and 4. Counter-clockwise beach rotation was observed during Events 1 and 2, with maximum values of accretion and retreat of 12 and 15 m, respectively (Figure 2.4a). The beach rotated clockwise only during Event 15, with maximum erosion/accretion values of 6 and 7 m, respectively (Figure 2.4b). Finally, the remaining events displayed a differential erosion/accretion pattern alongshore the beach, where the accretion was related to the formation of the megacusps in the southwestern section (maximum values of 11 m).

The beach planform changes were calculated as the difference between the fits of each shoreline before and after the storm. A general cross-shore displacement of the beach planform of between 1 and 7 m occurred landward (Events 10, 11, 13 and 16) or seaward (Events 4, 3, 8, and 14). In particular, these beach planform changes were homogeneous alongshore in some events (Events 8, 11, 13, 14). No beach planform change was observed in Events 9 and 12. Finally, counter-clockwise (Events 1, 2 and 16) and clockwise (Events 5, 6, 15 and 17) beach planform changes were also observed.

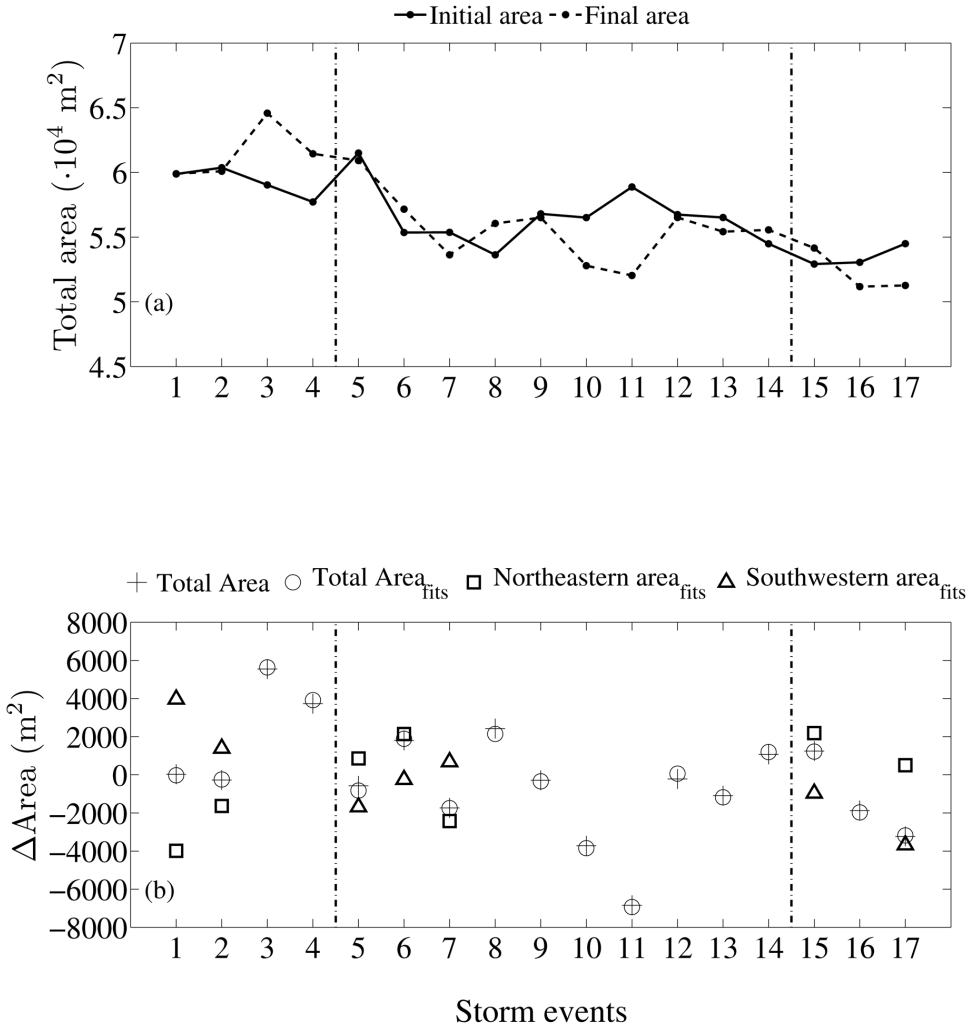

Figure 2.3: Temporal evolution of the beach area at La Barceloneta I. (a) Initial and Final beach area for each storm event. (b) Changes in the total emerged beach area after each storm event calculated using the shoreline extracted from the images (crosses) and the fitted shoreline (circles). Also shown is the variation in the beach area calculated using the shoreline fitted in the northeastern section (squares) and the southwestern section (triangles) of La Barceloneta I in those events in which the pivotal point was defined. The vertical dashed lines indicate human interventions.

Figure 2.3b shows the variation in the emerged beach area (calculated using the shorelines fitted) in the northeastern and southwestern sections of La Barceloneta I, separated by the pivotal point, in those events in which the beach planform changes were counter-clockwise and clockwise. In Events 1 and 2, the northeastern section decreased while the southwestern area increased; quite the opposite occurred in Events 5 and 15, in which the northeastern section

increased and the southwestern section decreased. During these four events the total emerged area remained stable. For the remaining events, the total emerged area did not remain constant, increasing in Event 6 and decreasing in Events 7 and 17.

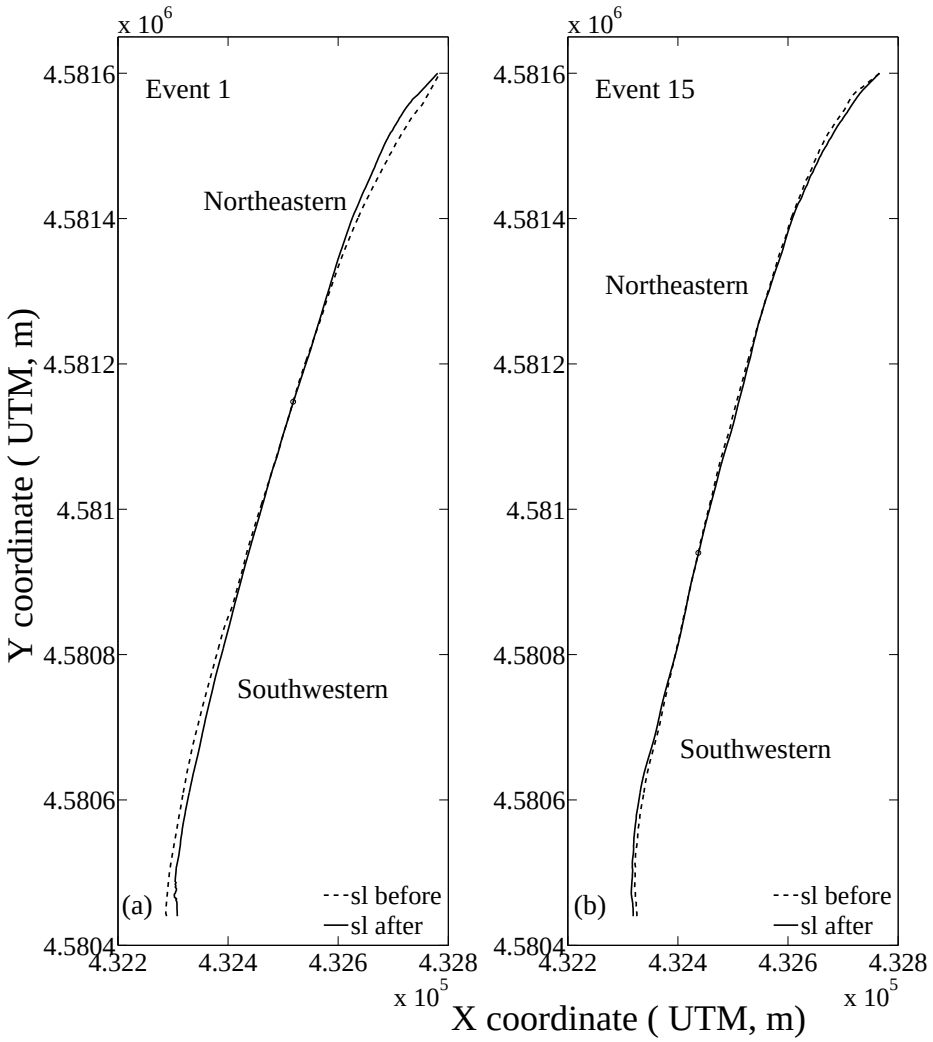

Figure 2.4: Beach rotation observed at La Barceloneta I. The dashed and solid lines represent the shoreline position before and after each storm, respectively. The circles represent the location of the pivotal point. (a) Counter-clockwise beach rotation in Event 1. (b) Clockwise beach rotation in Event 15.

Beach hydrodynamics

The maximum wave height of Event 11 (February 2004, eastern direction) is the input parameter of the wave-current model used to illustrate hydrodynamics at

La Barceloneta beach before the construction of the detached breakwater. Waves at La Barceloneta I were affected by the double dike in the north and the L-dike in the south, which produced diffraction in these areas, but in general the wave fronts approached almost parallel to the beach (Figure 2.5). When moderate wave periods are introduced in the model (T_p <10.5 s) the current system is shown to be mainly composed of an alongshore homogeneous current towards the southwestern end and two closed circulation cells (C1 and C2, the second located in the lee of the L-dike) at the southwestern end (Figure 2.6). The alongshore current was stronger in the northeastern area close to the dikes but its intensity decreased and, because of the bathymetric effects, it returned seaward when it reached the southwestern end of La Barceloneta I.

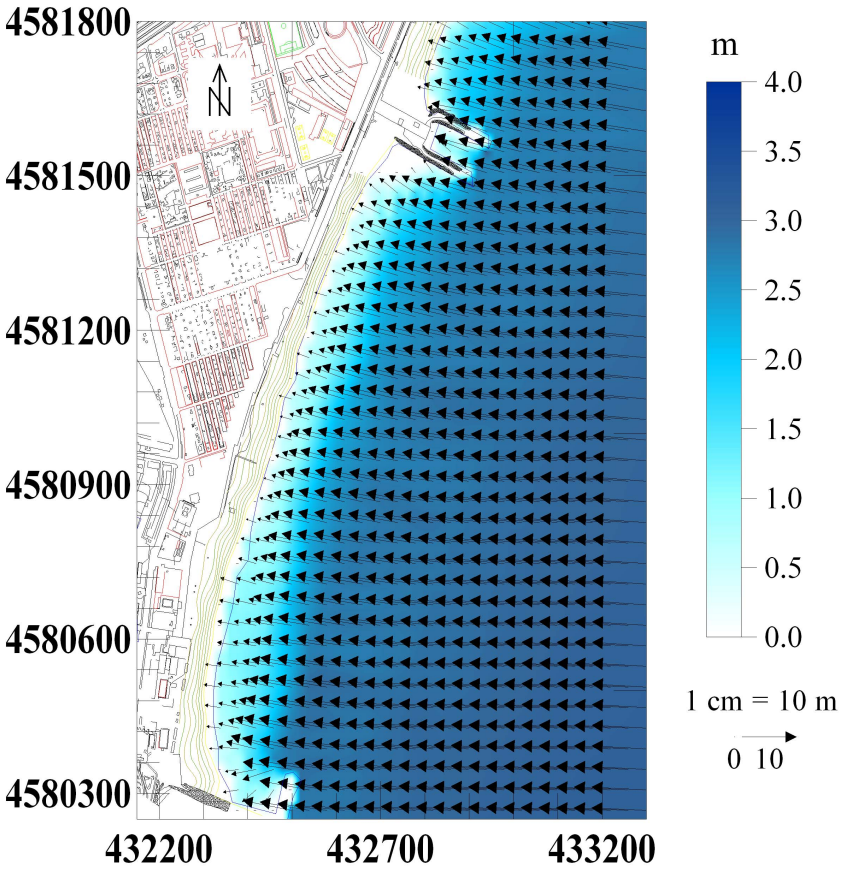

Figure 2.5: Wave propagation for the maximum wave height of Event 11 at La Barceloneta I. H_0 = 3.25 m; T_p = 7.7 s; $\theta = 90^o$

When longer wave periods (T_p >10.5 s) are considered, the current pattern is modified. The system is still dominated by an alongshore current towards the southwest but in the middle of the beach this current diverges into two minor cur-

rents, one returning seaward and one moving towards the south. Additionally, a minor longshore current flows from the southwestern section towards the northeast, converging with the minor longshore current coming from the northeast, both returning seaward.

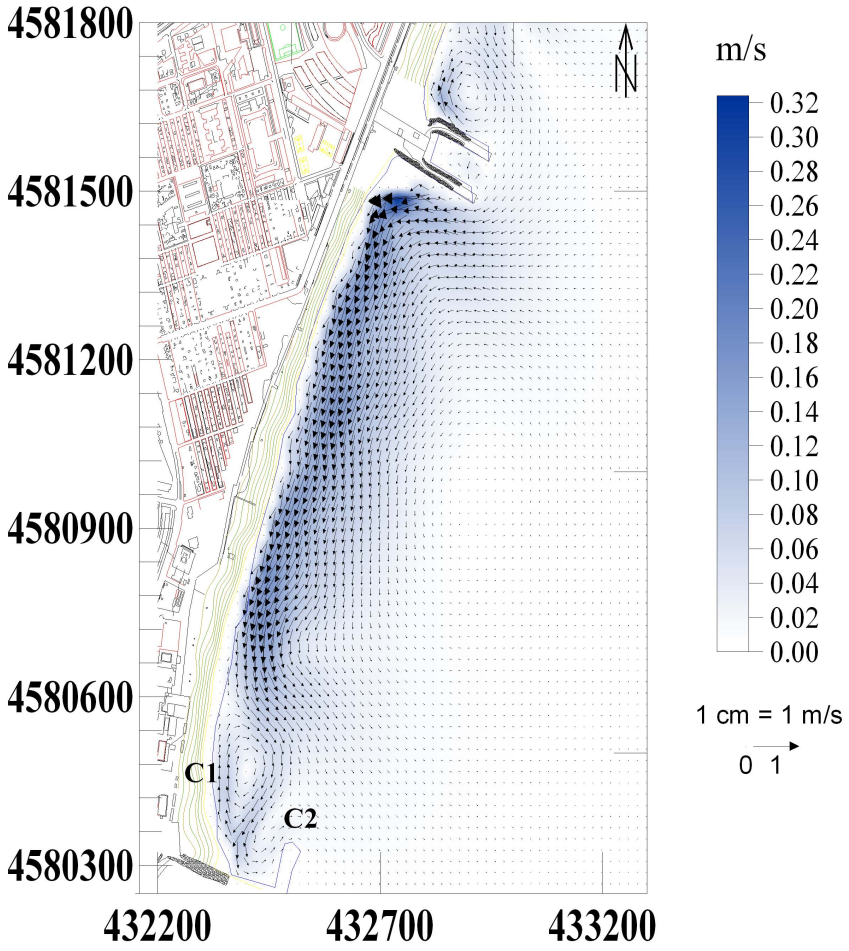

Figure 2.6: Wave-induced currents for the maximum wave height of Event 11 at La Barceloneta I. H_0 = 3.25 m; T_p = 7.7 s; $\theta = 90^o$

The current pattern at La Barceloneta I is very sensitive to the wave approach direction. Although the main wave direction of Event 11 was east, at the beginning of the storm there were some hours during which waves approached from the ESE (θ = 107º) and at the end they approached from the ENE (θ = 77º). The current system created by waves approaching from the ENE was similar to the current pattern for waves from the east with low wave periods, but the alongshore current towards the southwest was stronger. When the waves approached from the ESE, the current system was dominated by an alongshore current towards the northeast. This wave-induced current was diverted by the northern double dike

and a vortex system was generated.

2.3.2 La Barceloneta II (after breakwaters)

Beach morphodynamics

It can be considered that the construction of the detached breakwater at La Barceloneta II divided the beach into two beaches separated by a salient. The initial emerged beach area of La Barceloneta II was 71100 m^2, which represented an increase of approximately 21000 m^2 in comparison with the configuration of La Barceloneta I. The initial beach areas of La Barceloneta II-N and La Barceloneta II-S were 23260 m^2 and 27850 m^2, respectively (Figure 2.7a and Figure 2.8a), whereas the remaining beach area (approximately 20000 m^2) corresponded to the salient.

The majority of the storms caused decreases in the emerged beach area, with sand losses that were higher at La Barceloneta II-N. In particular, Event 22 (December 2008) reduced the beach area by around 6500 and 2000 m^2 at La Barceloneta II-N and La Barceloneta II-S, respectively. In summer 2009, a sand relocation at La Barceloneta II-N increased the beach area by about 10000 m^2 (Figure 2.7a). Afterwards, the two consecutive storm events, Events 26 and 27 (March 2010), still decreased the beach area of La Barceloneta II-N (2300 m^2). Due to the erosional trend of the beach, La Barceloneta II-N was nourished in May 2010, increasing the beach area by 19000 m^2. The only event occurring after the nourishment that caused a visible effect on the beach area was Event 28, which reduced the beach area of La Barceloneta II-N by about 2800 m^2.

The most frequent shoreline response to storms at both beaches was general erosion, which was higher at La Barceloneta II-N than at La Barceloneta II-S (Events 20, 21, 22 and 26). For instance, Event 22 (eastern direction) produced a shoreline retreat that varied alongshore from 12 to 25 m at La Barceloneta II-N, while at La Barceloneta II-S the retreat varied from 5 to 15 m. Differential erosion accretion alongshore was also observed at both beaches (Event 25). The other storm events caused different shoreline responses at the two beaches. Hence, the shoreline response at La Barceloneta II-S was differential erosion/accretion along-

shore and clockwise beach rotation (Event 23), that is, the shoreline retreated in its southwestern section and advanced in its northeastern section (Figure 2.9a). On the other hand, the shoreline response at La Barceloneta II-N was general erosion (Events 18, 27 and 28), general accretion (Event 24), differential erosion/accretion alongshore (Event 23) and counter-clockwise beach rotation (Event 19, Figure 2.9 b), that is, the shoreline advanced in its southwestern section and retreated in its northeastern section.

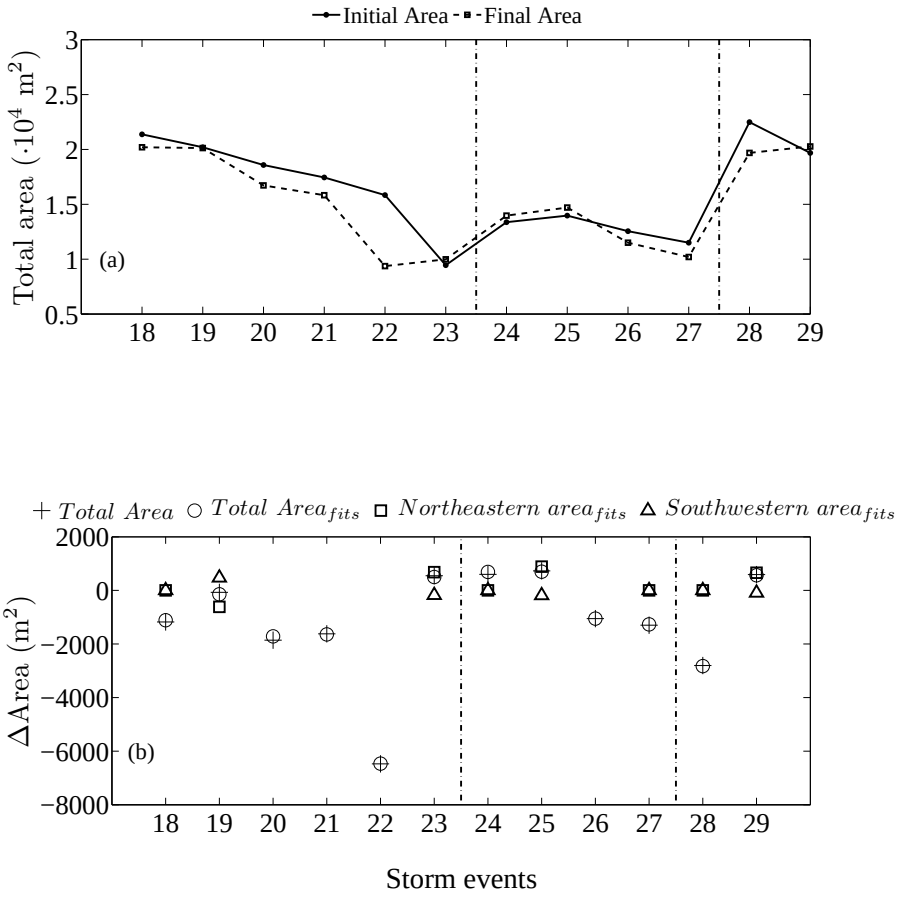

Figure 2.7: Temporal evolution of the beach area of La Barceloneta II-N. (a) Initial and final beach area for each storm event. (b) Changes in the total emerged beach area after each storm event calculated using the shoreline extracted from the images (crosses) and the fitted shoreline (circles). Also shown is the variation of the beach area calculated using the shoreline fitted in the northeastern section (squares) and the southwestern section (triangles) for events in which the pivotal point was defined. The vertical dashed lines indicate human interventions.

The evolution of the beach planform during storms follows similar patterns to that of the shoreline. The two new beaches of La Barceloneta II showed general landward displacements of the beach planform that were heterogeneous

alongshore and usually of higher magnitude at La Barceloneta II-N than at La Barceloneta II-S (*e.g.*, Event 22, landward displacement of 10 to 27 m at La Barceloneta II-N and 3 to 10 m at La Barceloneta II-S). In addition, beach planform changes that were landward/seaward in the southwestern section and seaward/landward in the northeastern section of each beach were observed in Events 23, 25, 29 and Event 19, respectively. The beach planform changes differed between these two beaches for Events 18 and 24: at La Barceloneta II-S they were seaward in the southwestern section and landward in the northeastern section in both events, whereas at La Barceloneta II-N they were landward in Event 18 and seaward in Event 24.

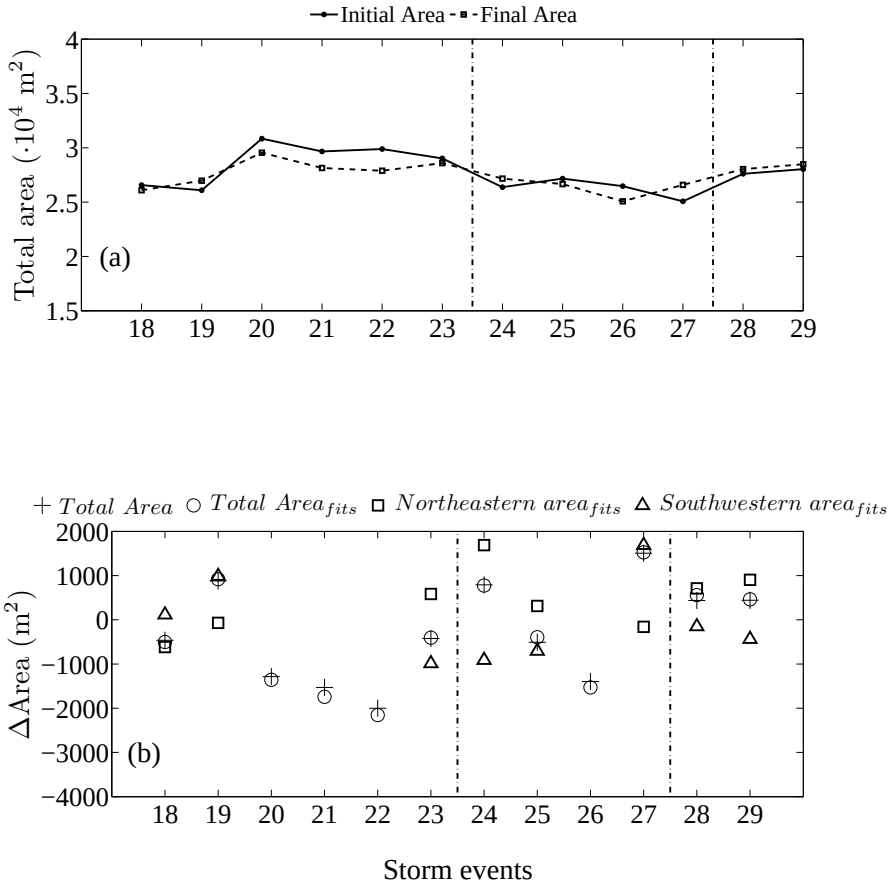

Figure 2.8: Temporal evolution of the beach area of La Barceloneta II-S. (a) Initial and final beach area for each storm event. (b) Changes in the total emerged beach area after each storm event calculated using the shoreline extracted from the images (crosses) and the fitted shoreline (circles). Also shown is the variation of the beach area calculated using the shoreline fitted at the northwestern section (squares) and the southwestern section (triangles) for events in which the pivotal point was defined. The vertical dashed lines indicate human interventions. The vertical dashed lines indicate human interventions.

Following the same methodology as that applied to La Barceloneta I, the beach orientation changes of La Barceloneta II were calculated using fitted shorelines for each of the beach sections (Figure 2.7b and Figure 2.8b). At La Barceloneta II-N, only Event 19 produced beach rotation, *i.e.*, the northeastern and the southwestern section decreased and increased respectively, while the beach area remained stable (Figure 2.7b). For the remaining events (23, 25 and 29) at the same beach, the northeastern and southwestern sections showed opposite behaviours but both related to an increase in the total area (Figure 2.7b).

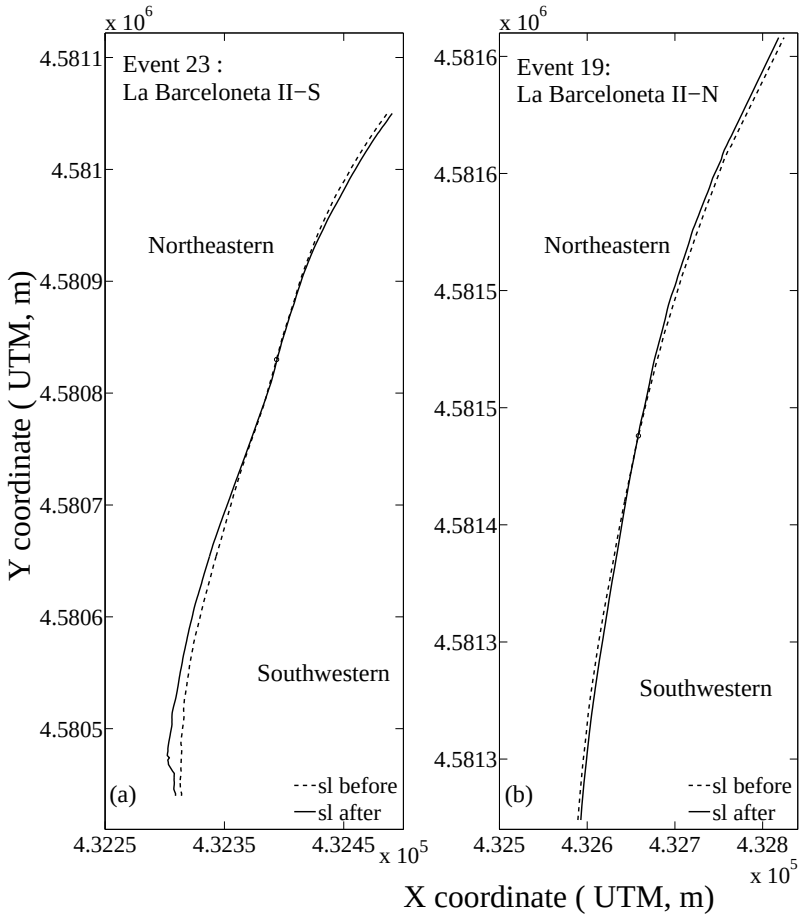

Figure 2.9: Beach rotation observed at La Barceloneta II. The dashed and solid lines represent the shoreline position before and after each storm event, respectively, and the circles represent the location of the pivotal point. (a) Clockwise beach rotation of La Barceloneta II-S in Event 23. (b) Counter-clockwise beach rotation of La Barceloneta II N in Event 19.

At La Barceloneta II-S (Figure 2.8 b), in Events 23, 24, 25, 28 and 29 the northeastern section increased and the southwestern section decreased, while in Events 18, 19 and 27 the northeastern and the southwestern sections behaved in

the opposite manner. During Events 23 and 29 the emerged beach area remained unchanged (*i.e.*, beach rotation), whereas in Events 19, 24, 27 and 28 the beach area increased and in Events 18 and 25 it showed a minor decrease.

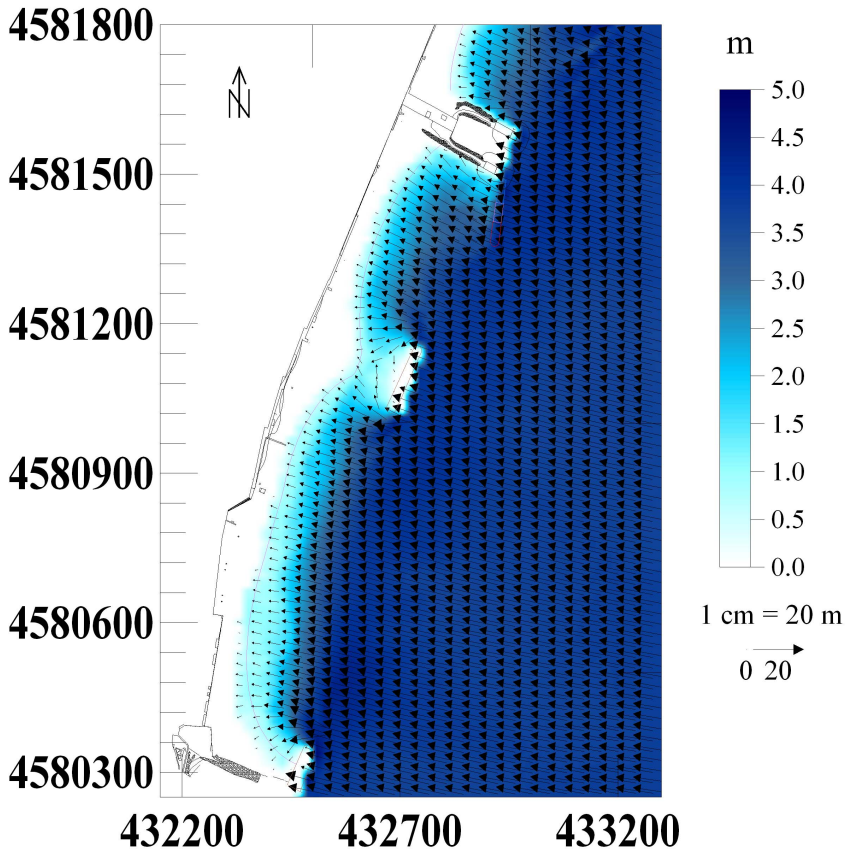

Figure 2.10: Wave propagation for the maximum wave height of the storm of Event 22 at La Barceloneta II. $H_0 = 4.65m$; $T_p = 12.5s$; $\theta = 83^o$.

Beach hydrodynamics

Wave propagation for each hour of Event 22 (December 2008, eastern direction) showed that beach hydrodynamics at La Barceloneta II was highly affected by the submerged and the detached breakwater and the L-dike (Figure 2.10). The detached breakwater reduced the wave energy in its lee and its limits produced a rotation of the wave fronts reaching each beach due to the diffraction effects. On the other hand, the submerged breakwater produced a concentration of the wave energy and rotation of the wave front (diffraction) reaching La Barceloneta II-N. It should be noted that waves overtopped the detached breakwater and flooded the salient during a few hours of this event (ob-

served in video images) but the wave propagation did not model this phenomenon.

The wave-induced current system for waves coming from the east were composed of two main currents (Figure 2.11): (1) a strong current that originated at the submerged breakwater, flowing towards the southwest and splitting into two currents near the detached breakwater, one seaward and one moving towards the southwest parallel to the detached breakwater; and (2) an alongshore current at La Barceloneta II-S towards the north that converged with the longshore current coming from La Barceloneta II-N, both flowing seaward.

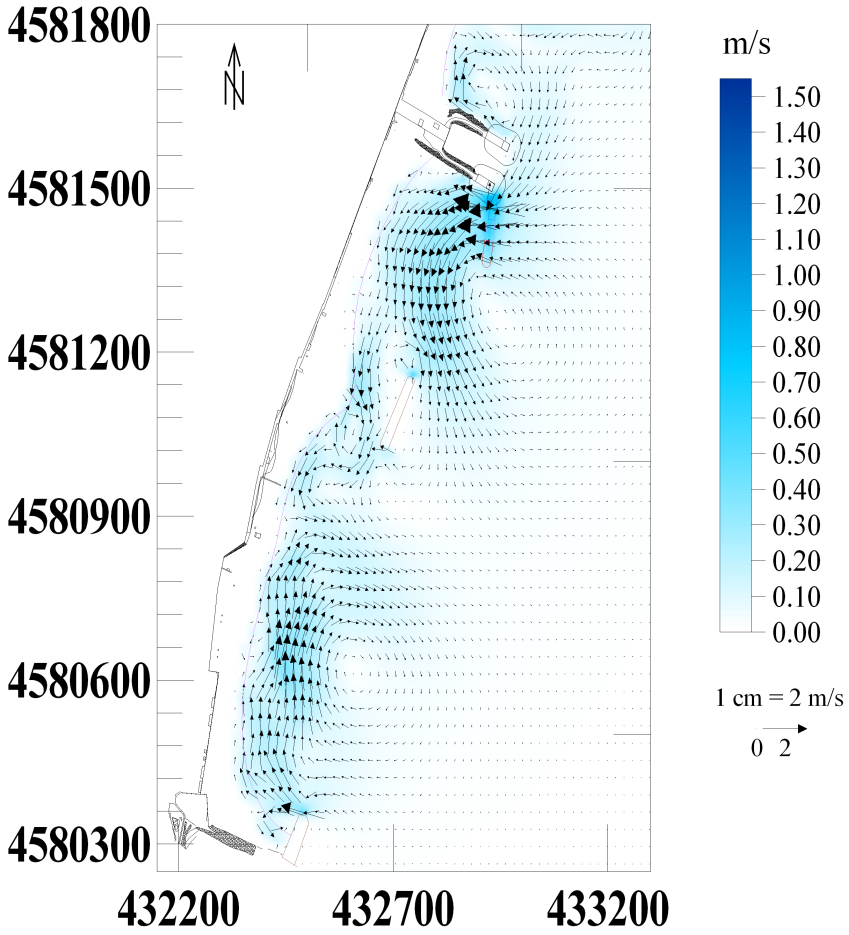

Figure 2.11: Wave-induced currents for the maximum wave height of Event 22 at La Barceloneta II. $\mathrm{H}_0 = 4.65m$; $\mathrm{T}_p = 12.5s$; $\theta = 83^{\mathrm{o}}$.

For waves approaching from the ENE ($\theta = 77^{\mathrm{o}}$) the wave-induced current system was similar to the east current system although with the difference that the southwest current that originated at the submerged breakwater was stronger, particularly at the end of La Barceloneta II-N (at beginning of the salient). Finally,

the wave-induced current system for waves coming from the ESE ($\theta = 107^{o}$) were also composed of two main currents (Figure 2.12): (1) a divergent current over the submerged breakwater that returned seaward without reaching the beach; and (2) a stronger current along La Barceloneta II-S towards La Barceloneta II-N. This alongshore current diverged into two minor currents close to the detached breakwater: one returned offshore and other reached La Barceloneta II-N.

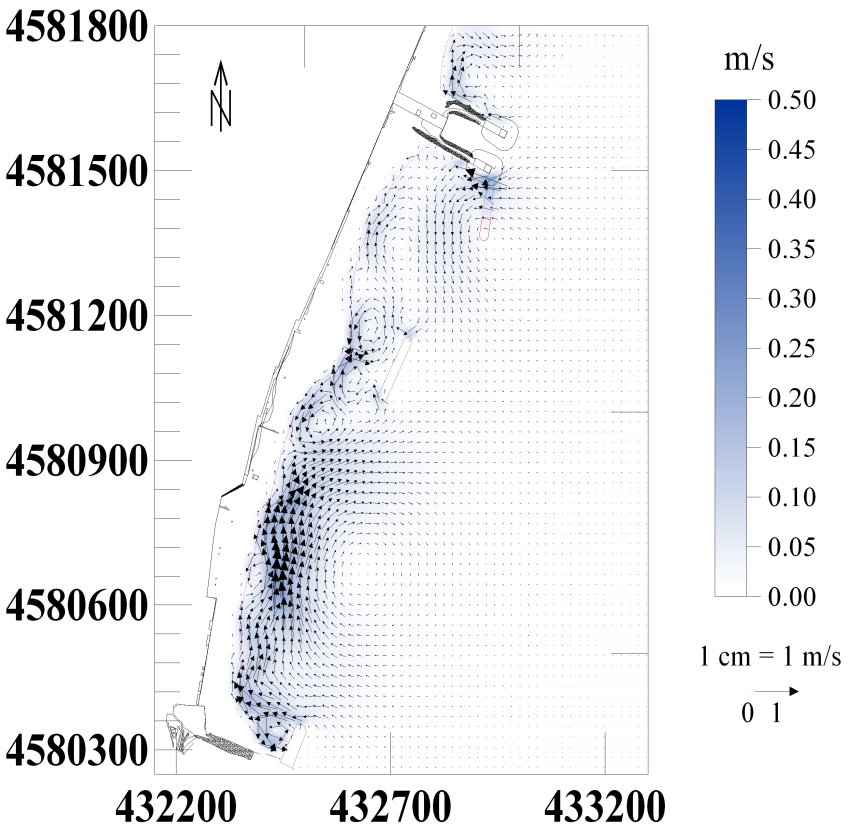

Figure 2.12: Wave-induced currents for waves approaching from the ESE ($\theta = 107^{o}$) in Event 22 at La Barceloneta II. H_0 = 2.25 m; T_p = 6.7 s.

2.4 Discussion

La Barceloneta beach is an artificial embayed beach that has been highly affected by stabilization and counter-erosion projects since it was created as a part of the renewal plan for the Barcelona Olympic Games in 1992. Because of its erosive trend and instability (Ojeda and Guillen, 2008), between 2006 and 2007 both soft and hard engineering solutions were applied, including beach nourishment and the construction of two breakwaters (one submerged and one detached) that completely changed the morphological configuration of the beach.

The objective of these protection works was to reduce the wave energy in the beach and therefore to modify the wave-induced current system, in order reduce the erosion tendency of La Barceloneta and stabilize the beach, particularly in the northeastern section.

The breakwaters have completely altered the beach hydrodynamics and sedimentary processes of La Barceloneta. At La Barceloneta I the approach of the wave fronts was homogeneous alongshore, whereas at La Barceloneta II the wave fronts were affected by the detached and submerged breakwaters, causing diffraction of the wave fronts and changes in the distribution of the energy dissipation. As a result the wave-induced current system was modified and became more complex.

For instance, for waves coming from the ENE, the alongshore current towards the southwest of La Barceloneta I changed at La Barceloneta II to a current system composed of two alongshore currents: one originating at the submerged breakwater, reaching the coast and running towards the southwest; and one originating at La Barceloneta II-S and running towards the northeast. Also, in the case of waves coming from the ESE, the main changes caused by the new beach configuration were an increase in the intensity of the longshore current originating at La Barceloneta II-S and flowing towards the northeast, and the return offshore of the alongshore current originating over the submerged breakwater before it reaches the coast of La Barceloneta II-N (Figure 2.12).

Therefore, the protection works carried out at La Barceloneta beach transformed a beach system dominated by an alongshore current whose direction was determined by the wave angle approach into a more complex system in which each section of the beach has a differential current pattern and alongshore and cross-shore currents coexist. Interestingly, the dominant alongshore currents at both beaches of La Barceloneta II are in opposite directions, both running towards the salient.

These changes in the hydrodynamic system induced changes in the shoreline response to storms and, more specifically, in beach rotation. To analyze the differential response of the beach against storms before and after the protection works, the shoreline was extracted from video images. Previous studies reported pro-

Coefficients	Moreno and Krauss (1999)	La Barceloneta I	La Barceloneta II- N	La Barceloneta II-S
a (m)	320.9	3903.4	221.5	309.4
b (m)	0.0045	0.00015	0.0047	0.0013
m	0.533	0.76	0.89	0.77

Table 2.4: Fitting parameters that solve the hyperbolic tangent model (Moreno and Kraus, 1999) at La Barceloneta. The coefficients a, b, and m of La Barceloneta I and II are the mean values of these coefficients after application of the hyperbolic tangent model for all the shorelines analyzed.

blems in the detection of short-term beach rotation processes in embayed beaches related to the formation and migration of different morphologies such as megacusps or submerged sandbars (Ojeda and Guillen, 2008; Klein et al., 2010). In this thesis therefore it is used a new approach in which the shoreline was fitted to a hyperbolic tangent shape before and after each storm to study the short-term beach rotation.

The best-fit coefficients were obtained following the procedure of Moreno and Kraus (1999). The hyperbolic tangent shape shows a good fit except for the higher curvature zone adjacent to the headland, in accordance with the results of Oliveira and Barreiro (2010). The fitting coefficients estimated by Moreno and Kraus (1999) were compared with the coefficients of La Barceloneta I, La Barceloneta II-N and La Barceloneta II-S (Table 2.4). Differences in the coefficients of the hyperbolic fit between Moreno and Krauss (1999) and La Barceloneta I may be related to the extension of the beach considered (415 and 1100 m length, respectively) and to the presence of the sedimentary structures (megacusps). On the other hand, for the two beaches of La Barceloneta II, the coefficients were more similar to those of Moreno and Kraus (1999), except for the slope (see Table 2.4).

The difference between the shorelines fitted before and after each storm event was used to analyze the beach planform changes and especially the beach rotation process. This represents an advantage from previous studies, in which the shoreline changes (Ojeda and Guillen, 2008; Archetti and Romagnoli, 2011) or the beach width (Ranasinghe et al., 2004) were used directly to identify beach rotation, because the proposed methodology allows a clear identification of the pivotal point. For instance, using the shoreline changes, the pivotal point was only identified in 5 events in which the beach rotation was patent at La Barceloneta. The proposed methodological approach allowed the pivotal point to be identified

in 8 additional events in which morphological features were present and prevented identification using only the shoreline location. Thus, the pivotal point was clearly identified for 13 of the 29 analyzed events; for the remaining events the beach response was not associated with beach rotation. Beach rotation associated with 7 events was observed, while the remainder represented changes in the shoreline orientation but with losses or gains in the emerged beach area (Tables 2.5 and 2.6). For instance, there were two events in which this methodology clearly helped to eliminate the effect of changes in certain morphologies: Event 5 at La Barceloneta I and Event 29 at La Barceloneta II-N. In both cases megacusps were present at the beach and accreted after the storm. During Event 5, two megacusps were found at La Barceloneta I, one at the southwestern section (MC1) and one in the middle of the beach (MC2) (Figure 2.13). The shoreline response to both 5 and Event 29 was differential erosion and accretion alongshore, with 4 m accretion in MC1 and 2 m accretion in MC2. However, following calculation of the beach planform changes the results showed an apparent clockwise beach rotation that was confirmed by the variations in area of each beach section (-1518 and 939 m^2 in the northeastern and southwestern sections, respectively).

The beach rotation (clockwise and counter-clockwise) observed at La Barceloneta I is attributed to the alongshore current generated by the oblique wave approach coming from the ENE and S. This does not mean that waves coming from these directions must result in beach rotation (*e.g.*, Event 8, southern event), because this process also depends on the morphological state of the beach before the storm (Ojeda and Guillen, 2008; de Alegria-Arzaburu and Masselink, 2010; Archetti and Romagnoli, 2011). Clockwise beach rotations associated with S events were also observed at La Barceloneta II-S and an episode of counter-clockwise rotation associated with an ENE event was observed at La Barceloneta II-N. However, the configuration of La Barceloneta II-S prevents counter-clockwise rotation because several modelled situations showed that there is almost no alongshore current towards the south in this section of the beach.

La Barceloneta II was analyzed as two independent beaches separated by the salient formed by the detached breakwater. This approach has been used previously in the study of embayed beaches (Klein et al., 2010), and although several factors must be taken into account, it has proven to facilitate the study of beach

behaviour. However, beaches are not isolated cells and this approach may lead to an underestimation of beach rotation, because when the sand moving alongshore exceeds the artificial limit proposed for a beach, it will disappear from the system, being equivalent to a cross-shore transport of the sand. On the particular occasions when sediment transport between the salient and the beach was appreciated, a more in-depth evaluation was accomplished. During these events (18, 19, 23, 24 and 25) the analysis of the shoreline response prompted the authors to re-analyze the event, considering the entire beach (including the salient). Afterwards, La Barceloneta-II-N and La Barceloneta-II-S were divided using the absolute maximum obtained from the curvature parameter applied to the shoreline prior to the occurrence of the event (instead of using the reference shoreline, as described in the Methodology section and Figure 2.2b). Using this new division, the variation of the emerged beach area in each section of La Barceloneta II was recalculated, confirming only a clockwise beach rotation process in Event 23.

La Barceloneta I		
Event	Wave $\mathrm{direction}_{mean}$ (º)	Beach planform change
1	69	BR
2	68	BR
3	108	S
4	93	S
5	199	BR
6	118	CBO
7	80	CBO
8	201	S
9	94	NC
10	83	L
11	91	L
12	103	NC
13	109	L
14	105	S
15	202	BR
16	94	CBO
17	201	CBO

Table 2.5: Summary of the beach planform changes at La Barceloneta I: *L* landward; *S* Seaward; *NC* no changes; *CBO* change in the beach orientation; *BR* beach rotation.

La Barceloneta II			
Event	Wave direction_{mean} (º)	Beach planform change	
		La Barceloneta II-N	La Barceloneta II-S
18	77	L	CBO
19	78	BR	CBO
20	89	L	L
21	124	L	L
22	88	L	L
23	204	CBO	BR
24	197	S	CBO
25	198	CBO	CBO
26	100	L	L
27	105	L	CBO
28	95	L	CBO
29	122	CBO	BR

Table 2.6: Summary of the beach planform changes at La Barceloneta II: *L* landward; *S* Seaward; *NC* no changes; *CBO* change in the beach orientation; *BR* beach rotation.

The shoreline response of La Barceloneta I was characterized by a higher erosion in the northeastern section of the beach and by responses to storms varying between general erosion or accretion, differential erosion/accretion alongshore, and beach rotation. Under the new configuration (La Barceloneta II) the most common shoreline response to storms was erosion and, furthermore, the shoreline retreat increased drastically in the northern section (La Barceloneta II-N) during some events. This was an unexpected situation at La Barceloneta II-N taking into account that it is supposed to be the most protected section of the beach located on the lee side of the submerged breakwater. However, it has been previously observed that submerged breakwaters may produce erosion in their lee (Ranasinghe and Turner, 2006). The mechanisms responsible for this erosion remain unclear; in the case of submerged detached breakwaters, the wave direction approach in combination with other factors such as the breakwater orientation and its distance from the shoreline have been put forward as potential reasons for the erosion (Ranasinghe et al., 2010). Ranasinghe and Turner (2006) suggest that, while shoreline accretion is linked to oblique waves, the shoreline erosion is caused by strong divergent wave-induced currents under shore-normal waves near the shoreline (behind the structure) moving the sediment away from the area. This is

in agreement with the modelled results, which showed a strong divergent wave-induced current (which may be responsible for the shoreline erosion) under waves approaching shore-normal to the submerged breakwater (ENE-E). Under oblique incidence waves (*e.g.*, ESE), the model showed a lower divergent current that did not reach La Barceloneta II-N (Figure 2.12).

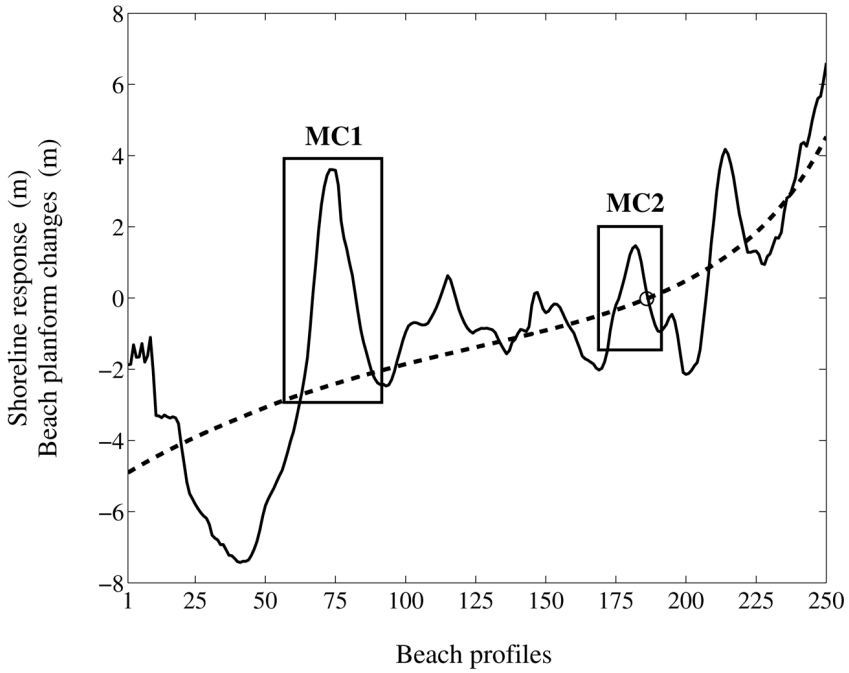

Figure 2.13: Shoreline response and beach planform change in Event 5. The solid line represents the shoreline change and the dashed line the beach planform change. The circle indicates the pivotal point and the two rectangles the location of each megacusp (MC1 and MC2)

The prediction of the impacts of submerged structures on shoreline evolution remains largely unknown because our experience is quite limited and a better understanding of the shoreline response is required (Ranasinghe et al., 2010). Observations and modelling from La Barceloneta II show an undesired erosion in the lee of the submerged breakwater, generation of seaward currents because of the combined effect of the detached and submerged breakwaters and the salient, limitation of the beach rotation at La Barceloneta II-S, and the existence of differential nearshore circulation patterns at both beaches separated by the salient. In addition, some observed processes, such as the overtopping of the detached breakwater during the highest storms, are quite difficult to include in models. Hence, coastal protection works can cause drastic changes in sediment redistribution processes that are complex and cannot yet be predicted with much certainty.

2.5 Conclusions

The shoreline response and the beach planform changes of La Barceloneta beach were analysed before and after the construction of a detached breakwater and a submerged breakwater using ten years of video images. This human intervention has given rise to a new morphological configuration of La Barceloneta, dividing it into two different beaches. Previous to the construction of the detached breakwater, storms were responsible for changes in the emerged beach area that ranged between +5600 and 6500 m^2. After the counter-erosion works, most of the storms caused decreases in the emerged beach area at both beaches. Changes in the emerged beach area ranged from +700 to -6500 m^2 and from +1500 m^2 to -2000 m^2 at La Barceloneta II-N and La Barceloneta II-S, respectively, while changes in the total emerged beach area ranged from +2600 to -12000 m^2.

In this chapter a new methodological approach has been developed to analyze the beach rotation process by eliminating morphological effects (*e.g.*, those related to the formation, changes in shape or migration of megacusps) and for improving the choice of the pivotal point. Following this new methodology, at La Barceloneta I counter-clockwise beach rotation was observed during E and NE wave conditions and clockwise beach rotation during S and S-SW wave conditions. With the new configuration beach rotation was also observed under the same wave conditions, but the counter-clockwise beach rotation was only observed at La Barceloneta II-N and clockwise beach rotation only at La Barceloneta II-S.

La Barceloneta I was characterized by a simple current system composed of a longshore current flowing northward or southward depending on the wave conditions. The new coastal structures have given rise to a new, complex wave-induced current system which, in general, is composed of two opposite alongshore currents. The first one originates at the submerged breakwater, approaches the northernmost section of the beach and runs along La Barceloneta II-N, before returning offshore or moving towards La Barceloneta II-S (depending on the wave conditions). The second alongshore current comes from the southern section of La Barceloneta II-S, moves toward the northeast and can reach La Barceloneta II-N when waves come from the S.

Finally, the new submerged and detached breakwaters have not completely solved the erosion problems of La Barceloneta. Indeed, the submerged breakwater has even enhanced shoreline erosion at La Barceloneta II-N under specific wave conditions.

Chapter 3

BEACH INUNDATION AND SHORELINE VARIABILITY DURING STORMS

Edited version of A. Sancho-García and J. Guillén. Beach inundation and shoreline variability during storms. Submitted to Marine Geology.

3.1 Introduction

Coastal flooding by seawater is a worldwide process governed by forcing mechanisms that operates at different temporal scales ranging from hours (tsunamis and storm events) to thousands of years (sea-level rise). In particular, the inundation occurring during storms modifies sediment dynamics and impacts on inland activities, coastal structures and protections works (Nielsen and Hanslow, 1991).

The need to assess the risk associated with coastal flooding has led to the development of several approaches to prediction. Most of these methods are based on semi-empirical equations taking into account the hydrodynamics conditions (run-up and water level) and some morphological parameters (Battjes, 1971; Holman, 1986; Nielsen and Hanslow, 1991; Stockdon et al., 2006). More sophisticated approaches, which include the morphological evolution of the beach during storms, have also been applied for specific sites using 2DH models such as XBeach (McCall et al., 2010), MIKE 21 (Archetti and Zanuttigh, 2010) and MIKE FLOOD (Patro et al., 2009). However, the bathymetry and topography data before the storm are not always available. Therefore, most of vulnerability maps of coastal inundation during storms are based on approximations in which the morphological changes during the storm are unrealistic or poorly considered.

Systematic observations of beach inundation and morphological changes during storms tend to be scarce, although several previous studies suggest that morphological changes affect beach inundation. For instance, Vousdoukas et al. (2009) compared the observed run-up with predicted run-up using formulations of Stockdon et al. (2006) but the results were unmatched, suggesting that morphology could interfere. The shoreline displacement or the development/destruction of morphologies (e.g. beach cusps or intertidal bars) during the storm will modify the inundation along the beach (Masselink and Pattiaratchi, 1998). Video observations provide an appropriate tool for achieving a better understanding of wave run-up processes (Holman, 1986; Ruggiero et al., 2001; Stockdon et al., 2006; Salmon et al., 2007; Vousdoukas et al., 2009) and beach inundation (Sancho-Garcia et al., 2008; Archetti and Zanuttigh, 2010).

The aim of this chapter is to consider how and to what extent beach inundation

is affected by shoreline variability occurring during storms. This knowledge will determine whether beach inundation prediction models should include modules for reproducing morphological changes during storms or, on the contrary, simpler models can give adequate predictions. First, it is characterized and quantified the inundation occurring on three embayed beaches located in the city of Barcelona (Spain) under the most energetic storm conditions from 2001 to 2008 using video monitoring techniques. Second, it is analyzed how beach planform changes and the presence of different morphologies modify beach inundation. Finally, a quantitative assessment of the importance of shoreline changes on beach inundation is presented.

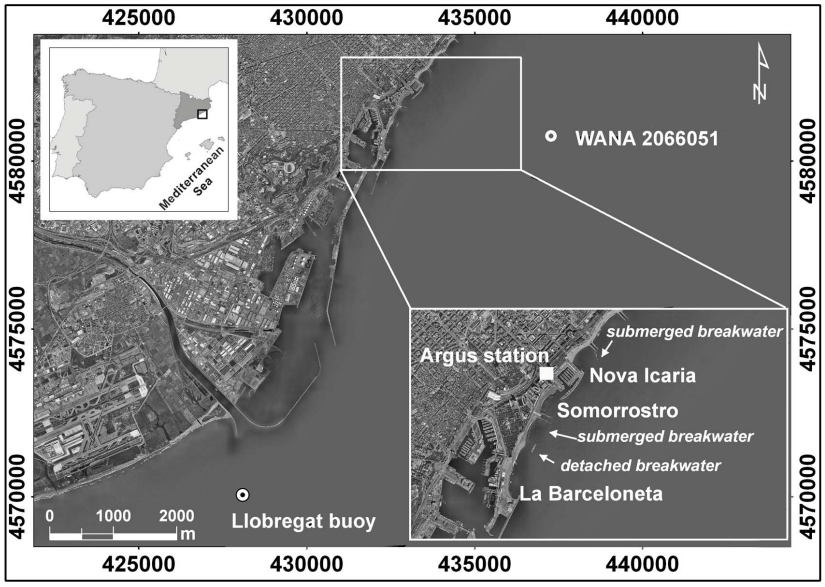

Figure 3.1: Location of Barcelona beaches (Spain). The Argus station and the Llobregat buoy and WANA (node 206601) locations are indicated by a square and a double-circle, respectively. The orthophotos are copyright of the ICC, and are available at www.icc.cat.

3.2 Study area

Barcelona, which is located on the south Catalan coast, facing the semi-enclosed Mediterranean Sea, has 13 km of coastline containing the city harbour in the southernmost part, three marinas and 3 km of beaches (Figure 3.1). The beaches of Barcelona were created as part of the renewal plan that took place in

Beach	Average Beach Width m	Length m	Beach Orientation	Average beach slope	D_{50} (μ m)
La Barceloneta I	40	1100	N20E	0.13	900
La Barceloneta II	55	1100	N20E	0.07	900
Somorrostro	52	400	N32E	0.08	450
Nova Icaria	53	400	N47E	0.09	660

Table 3.1: Morphological characteristics of the three studied beaches.

the zone for the 1992 Olympic Games. This study focuses on three beaches of the city of Barcelona (Figure 3.1), from the north to the south: (i) Nova Icaria, a non-barred beach protected by two submerged breakwaters above sea level and separated from the next beach by two double dikes; (ii) Somorrostro, a non-barred beach at the south of the Olympic Marina; and (iii) La Barceloneta, a barred beach bounded by Barcelona harbour in the south and Somorrostro dike in the north (3.1). These beaches are microtidal (range <0.2 m) and waves are the main natural mechanism controlling coastal evolution (Ojeda and Guillen, 2008). The most energetic storms approach from the east and have a typical duration of a few days.

Human activity is continuously affecting these beaches, especially at La Barceloneta. During the study period, La Barceloneta was nourished with approximately 40000 m^3 of sand during the summer of 2002 and a sand relocation of about 30000 m^3 from the southwest to the northeast was carried out in summer 2004. The major intervention at La Barceloneta took place between 2006 and 2007. First, a submerged and a detached breakwater were built between November 2006 and May 2007, and then the beach was nourished in March and June 2007 with 80000 m^3 and 46000 m^3 of sand, respectively, creating a salient in the middle of the beach. These protection works led to a change in the morphological configuration of the beach and in the beach profile, which is now gentler than before (see Table 3.1). Therefore, it is considered separately the first configuration (La Barceloneta I) and the latest configuration (La Barceloneta II).

It should be noted that the distribution of the beach slope at these beaches is non-uniform alongshore, with the exception of that of Somorrostro. There is an increasing trend, from southwest to northeast, reaching to 0.2, 0.12 and 0.21 at La Barceloneta I, La Barceloneta II and Nova Icaria, respectively. The beach slope of the salient is on average 0.04. Finally, according to the morphodynamic

state classification of Wright and Short (1984), Nova Icaria and Somorrostro are usually in the Reflective state, and exceptionally in the Low Tide Terrace state, whereas La Barceloneta can be in one of the four intermediate morphodynamic states, depending on the wave energy (Ojeda et al., 2011).

3.3 Material and methods

3.3.1 Wave data

Storm events were characterized using wave measurements of the Llobregat buoy (XIOM, www.xiom.cat) located at a depth of 45 m (Figure 3.1). This buoy has been directional since 2004, recording data every hour. Interruptions in the buoy time series and the lack of wave direction before 2004 were filled in with data from the WANA model (node 2066051, 3.1), which provides directional wave information every three hours. The WANA data has been computed by the Spanish National Institute of Meteorology using the HIRLAM and WAM numerical model since 1991 (Spanish Port Authority, www.puertos.es). Data from the WANA model were calibrated using the buoy observations from October 2001 to December 2008 through a linear regression. When the buoy was not directional, the wave peak period (T_p) was obtained using a calibration between the wave significant period ($\mathrm{T}_1/3$) and the wave peak period for the period 2004-2008. The characterization of the mean water level (η) was obtained from the tide gauge located at Barcelona harbour.

Storm events with a significant wave height higher than 3 m during the peak of the storm between 2001 and 2008 were selected (Table 3.2). The threshold for each storm event was the initial day when the wave height started to exceed 1 m and the final day when the wave height started to be less than or equal to 1 m. In order to analyze in detail the behaviour of La Barceloneta II, two events (Event 14 and Event 16) with a significant wave height of more than 2.5 m during the peak of the storm were included in the analysis.

Event	Initial date	$H_{o_{max}}$ (m)	$T_{p_{H_{max}}}$ (s)	Wave $direction_{H_{max}}$ (º)	Wave $direction_{mean}$ (º)	Duration (hours)
1	13/11/2001	8.5	13.3	114	110	127
2	13/12/2001	3.2	9.8	111	104	97
3	03/01/2002	3.3	10.2	124	128	49
4	06/05/2002	3.2	10.4	116	127	51
5	06/05/2002	3.8	11	125	130	88
6	13/10/2003	4.1	10	111	125	183
7	28/10/2003	4.1	9.7	177	164	114
8	07/12/2003	3.2	9	113	118	40
9	20/02/2004	3.3	7.7	91	123	77
10	27/03/2004	3.4	9.1	98	113	110
11	15/04/2004	3.3	10	120	119	93
12	01/12/2005	3.8	10	195	201	64
13	27/03/2007	3.3	7.7	96	94	63
14	20/10/2007	3.1	8.3	68	79	73
15	15/12/2007	3.5	10	86	88	93
16	08/05/2008	2.8	8.3	139	136	86
17	26/12/2008	4.7	12.5	83	96	81

Table 3.2: Characterization of storm events

3.3.2 Beach inundation

An Argus Video system (Holman and Stanley, 2007) located atop a building close to the Olympic Marina at a height of around 142 m has been deployed since 2001 (Coastal Ocean Observatory, http://coo.icm.csic.es/). The Argus station is composed of five cameras pointing at the Barcelona beaches and offering a 180º view of the coast. Images are in the visible range of light and the sampling is done every daylight hour during a ten-minute period (1 picture per second).

The hourly waterline position was obtained from the ten-minute time-exposure images using the IBM Intertidal Beach Mapper software (included in the Argus Runtime Environment) by the automated alongshore tracking of the intensity maxima across the waterline. During the peak of the storm, some problems were found for the waterline detection due to bad visibility caused by the presence of fog, clouds and rain. Therefore, in these moments and when there was a lack of contrast between sand and water, the waterline positions were mapped manually from the images. The 2D image coordinates were transformed to real coordinates (Holland et al., 1997). In total, the dataset comprise 445 waterlines for La Barceloneta I and 151 for La Barceloneta II, 630 waterlines for Somorrostro and 606 waterlines for Nova Icaria. Because the images used are averaged images, the

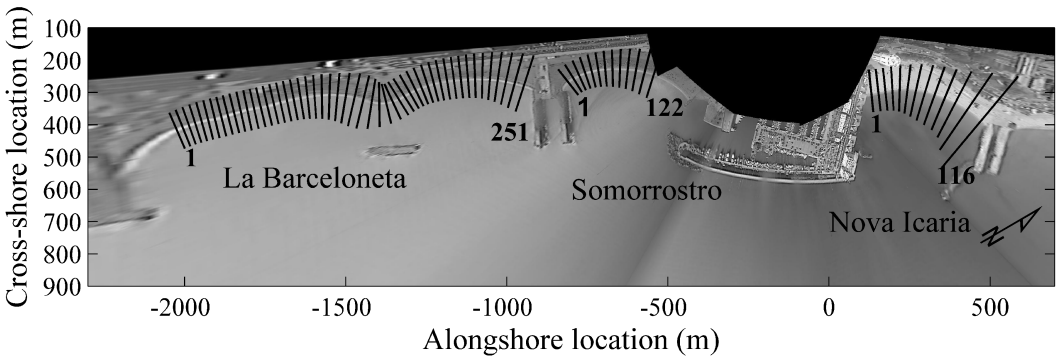

Figure 3.2: Argus plan view with the locations and the numbering of the profiles for each beach (for design reasons not all beach profiles are shown). Axes are given in Argus coordinates (in metres).

waterline position obtained should have captured the effects of sea level (storm surge and astronomical tide), setup and the mean position of the fluctuations associated with the swash.

The inundation is defined as the horizontal distance between the waterline position and the initial reference shoreline (IRS) in each event. Every IRS corresponds to a few days before each storm event when the wave height was less than 0.5 m and the water level was approximately zero. The temporal evolution of the inundation was measured following profiles along the beach every 4 metres at La Barceloneta and every 2 metres at Nova Icaria and Somorrostro (Figure 3.2). The profile direction at each point was defined as perpendicular to a reference shoreline (the average of the overall IRS).

3.3.3 Shoreline changes: beach planform changes and morphological features

The shoreline and beach morphologies were characterized from video observations. Shoreline modifications during the storm were calculated as the difference between the initial and final shorelines. This variation includes the effects of the morphological features and the changes in the beach planform.

Four different morphological features were studied and analyzed the shape of each waterline (Figure 3.3): (a) beach cusps at Somorrostro; (b) megacusps at La Barceloneta; (c) a salient at La Barceloneta II with a new configuration; and (d)

an undulation at Nova Icaria.

The beach cusps that developed at Somorrostro (Figure 3.3a) were characterized by an embayment consisting of finer sand and horns with coarser material, which included natural gravel and other similar-sized unnatural material such as glass fragments and building rubble. These subaereal features are supposed to form by swash zone processes (*swash cups*) (Garnier et al., 2010) and are usually associated with reflective wave conditions, relatively steep beach gradients and normally incident waves (Dodd et al., 2008).

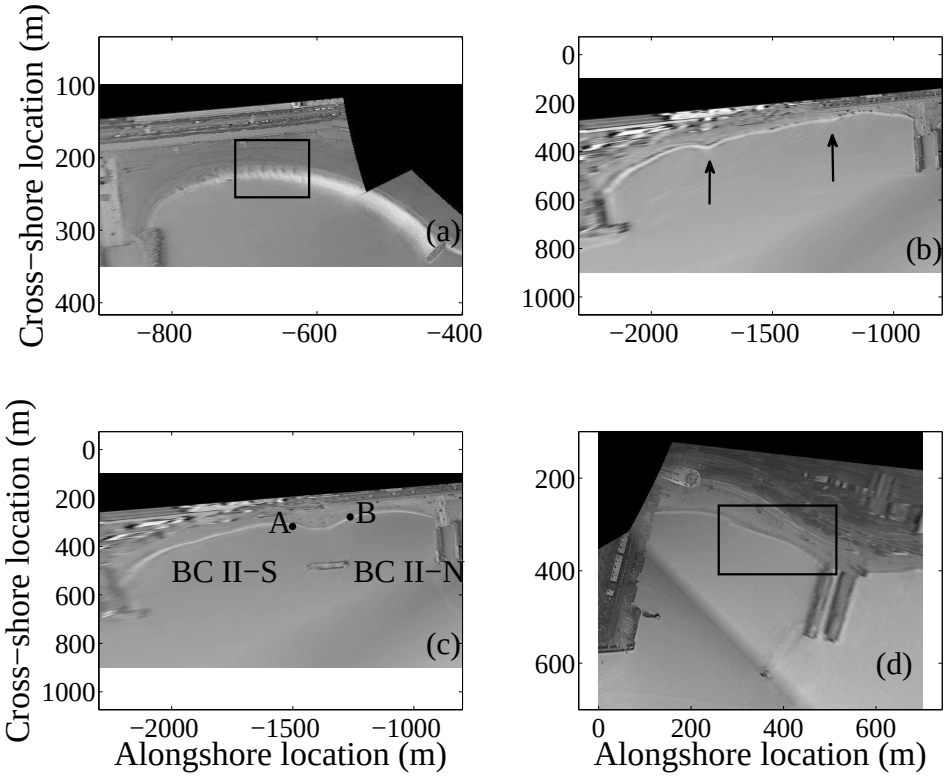

Figure 3.3: Morphological features analyzed. (a) Beach cusps at Somorrostro; (b) Megacusp at La Barceloneta I; (c) Salient created artificially at La Barceloneta II; (d) Shoreline undulation at Nova Icaria. Axes are given in Argus coordinates (in metres).

Megacusps at La Barceloneta (Figure 3.3b) are formed under storm conditions due to surf processes which transformed the submerged bar into crescentic bar and caused them to become attached to the beach (Ojeda and Guillen, 2008). The salient was generated artificially at La Barceloneta after a detached breakwater was built in May 2007 (Figure 3.3c). Finally, a shoreline undulation (Figure 3.3d)

unrelated to a submerged sandbar localized in the northeastern zone of Nova Icaria was also analyzed. The shape of this feature varied between events, but in general it was characterized by one bay and a cusp (Figure3.4).

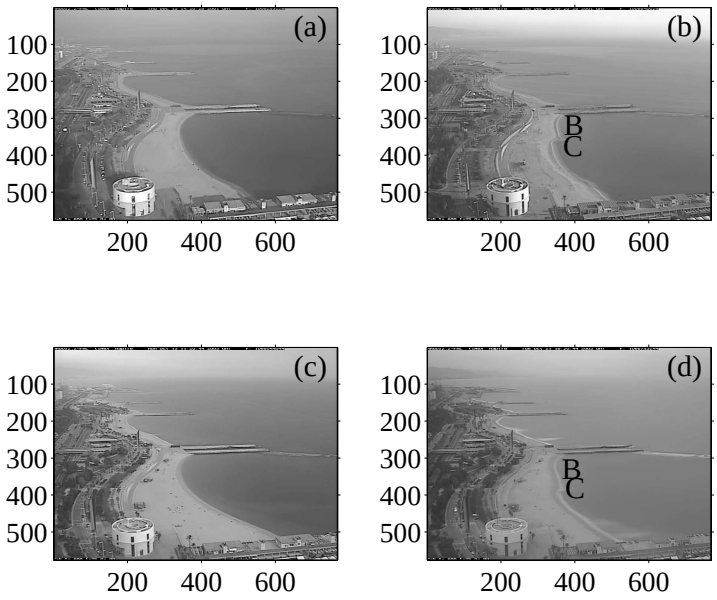

Figure 3.4: Shape of the shoreline of Nova Icaria. (a) Before Event 2. (b) After Event 2. (c) Before Event 6; After Event 6.

The shoreline variability related to morphological features and beach planform changes was discriminated by the following procedure:

- The shoreline response was calculated as the difference (D) between the final and the initial shoreline along the beach for each storm event.
- The initial and the final shoreline for each storm event were fitted to a shoreline hyperbolic tangent shape characteristic of embayed beaches (Moreno and Kraus, 1999). This shoreline shape was selected because this fitting considered only the geometry of the shoreline rather than the stability (Hsu et al., 2010) and the fitting procedure was simple. The deviations from this hyperbolic tangent shape must be caused by other morphological shapes.
- The beach planform changes were obtained as the difference (F) between the fits of the final (F2) and the initial shoreline (F1). It is considered that

this value represents changes in the equilibrium planform shape of the beach as well as crosshore shoreline displacements. The difference (R) between the deviation of the final (R2) and initial shoreline (R1) from its hyperbolic tangent shape was considered as characteristic of the morphological features.

All the differences were calculated using the same beach profiles as those defined in the inundation measurements.

At La Barceloneta II the shoreline variability was analyzed using a different approach. It was assumed that La Barceloneta II was composed of two independent embayed beaches, hereinafter referred to as La Barceloneta II-N and La Barceloneta II-S, separated by a salient. A curvature parameter was applied to the reference shoreline of La Barceloneta II in order to mark out the boundaries of the salient and to establish these two beaches. The two relative maximums of this parameter curvature, points A and B in Figure 3.3c, marked the extension of the salient and the beginning of these two new beaches. Afterwards, the procedure explained in the previous paragraph for La Barceloneta I was applied to each beach of La Barceloneta II. As a result, the shoreline variability observed between points A and B is related only to the salient.

Quantification of the influence of shoreline changes on beach inundation

The magnitude of the shoreline change due to the presence of morphological features and changes in the beach planform was compared with the magnitude of the inundation in order to quantify the potential influence of the morphology on the inundation. It should be noted that the shoreline changes are estimated by comparing the shoreline at the beginning and the end of the storm, and it is obtained the information of the resulting morphological configuration regardless of the exact moment at which these changes occurred. Therefore, it was not able to compare simultaneous measurements of inundation and morphological changes during the storm, but the variability of the morphological parameters (R and F) is evaluated in relation to the maximum inundation during the storm (MIs) with the aim of including a quantitative evaluation of the potential influence of morphology on the inundation.

3.4 Results

3.4.1 Beach inundation

Values of maximum and minimum beach inundation and the alongshore average of the maximum inundation for the storms analyzed at the Barcelona beaches are displayed in Table III. In general, the results showed that the magnitude of the beach inundation was higher at La Barceloneta and Nova Icaria than at Somorrostro. The maximum beach inundation, 71 m, was observed at La Barceloneta II, followed by 54 m at Nova Icaria, and 38 m at Somorrostro. The mean maximum values of the inundation were lower for La Barceloneta II (4-12 m, excluding Event 17) than for La Barceloneta I (6-23 m).

Figure 3.5 shows the maximum values of the inundation (MI) and the average maximum inundation (AMI) along the beach during the period 2001-2008. The alongshore distribution of the inundation at these beaches followed a non-uniform pattern. The northeastern area of Barcelona beaches, except for La Barceloneta II, was less inundated, because it is more protected from the most frequent and energetic storms (E-NE) and because of the increasing trend of the beach slope towards the north. The maximum inundation at La Barceloneta I (Figure 3.5a) displayed a decreasing alongshore trend from the southwestern zone (38 m) to the northeastern zone (12 m). With the new morphological configuration, the inundation behaviour along La Barceloneta II changed, increasing from the southwestern to the central section, where it reached maximum values, and then decreasing from the central to the northeastern section (Figure 3.5b). Somorrostro and Nova Icaria displayed a similar inundation pattern (decreasing from southwest to northeast), though it was more uniform at Somorrostro (maximum values 38-12 m) than at Nova Icaria (maximum values 54-10 m) (Figure 3.5c, d).

The temporal evolution of the inundation during a storm followed a similar pattern at these three beaches and was consistent with wave conditions: the inundation values increased until the peak of the storm and decreased subsequently. In absence of shoreline changes, the waterline at the beginning and the end of the storm coincided. However, morphological shoreline changes occurred during most storms, affecting the observed beach inundation.

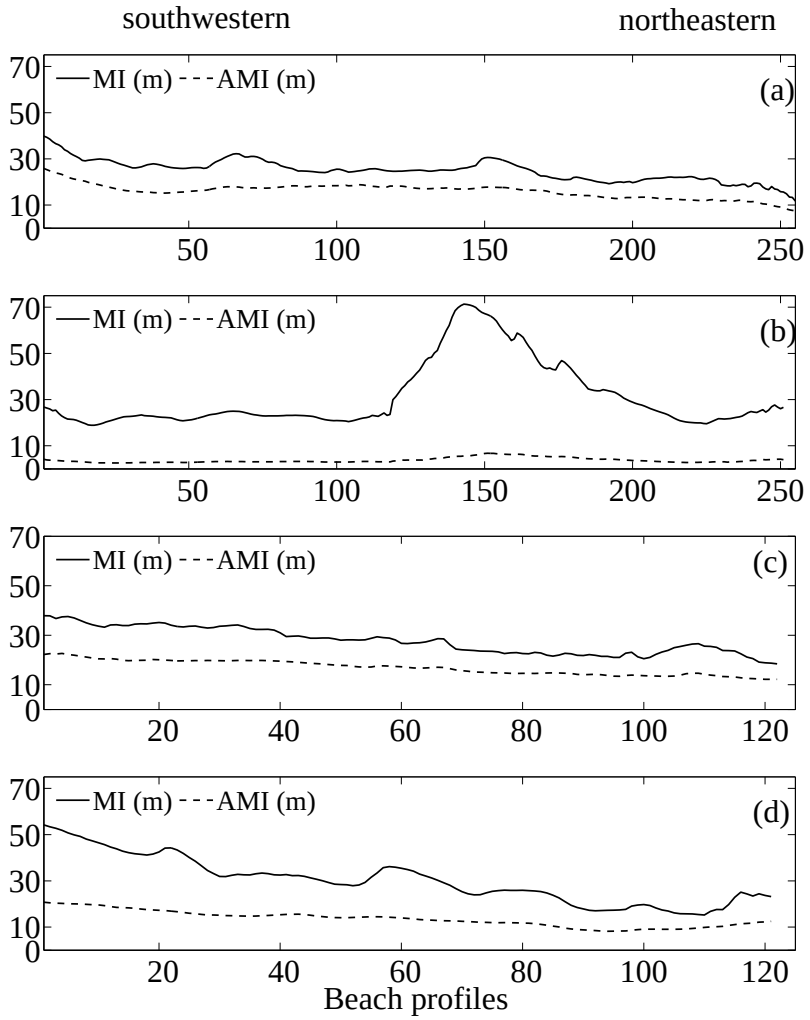

Figure 3.5: Alongshore distribution of the inundation at Barcelona beaches. The solid line shows the maximum inundation (MI) observed for each beach profile and the dashed line the average maximum inundation (AMI) for each beach profile. (a) La Barceloneta I; (b) La Barceloneta II; (c) Somorrostro; (d) Nova Icaria.

3.4.2 Shoreline changes

The shoreline change at Barcelona beaches was characterized by landward displacement during most storms. The most striking onshore displacements were observed at Somorrostro and at La Barceloneta II-N (13 m and 26 m, respectively, for Event 17) and at Nova Icaria (29 m for Event 6). A general seaward displacement of the shoreline was observed during Events 1 and 7, with a maximum seawards shoreline displacement of 13 m at Somorrostro, 7 m at La Barceloneta I and 8 m at Nova Icaria. Finally, Event 14 produced hardly any

shoreline response in the Barcelona beaches.

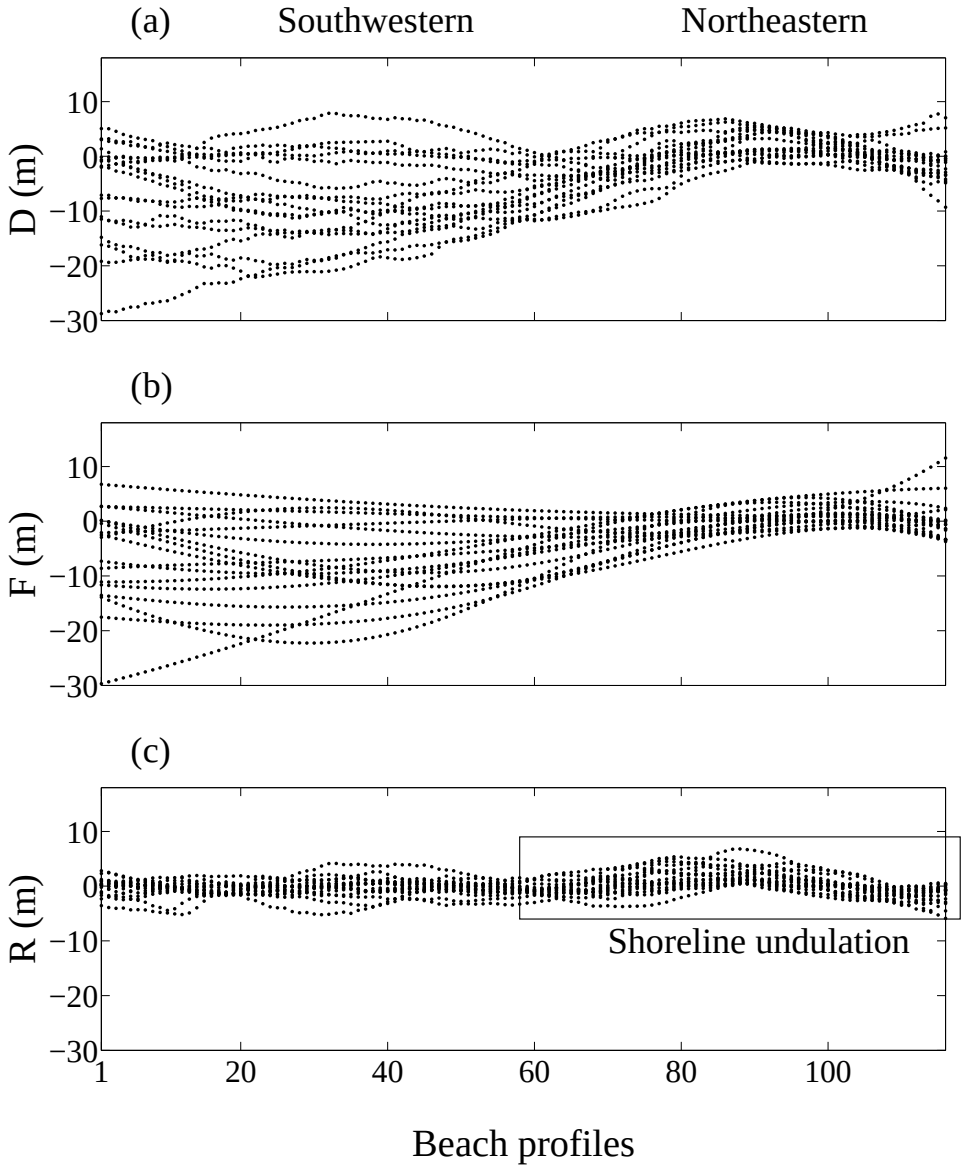

Figure 3.6: Shoreline variability at Nova Icaria. (a) Shoreline changes (D), (b) beach planform changes (F) and (c) morphological feature variability (R) for each beach profile in all the storms. The rectangle indicates the location of the shoreline undulation.

The shoreline response of Nova Icaria and La Barceloneta I varied alongshore, but Nova Icaria showed a noticeable shoreline variability in the southwestern zone, where erosion was the common shoreline response (Figure 3.6 a and Figure 3.7a). On the other hand, the two new beaches of La Barceloneta II displayed shoreline retreat, although the shoreline variability was higher in La Barceloneta II-N, es-

pecially for Event 17, in which the erosion was twice as high in this zone (Figure 3.8a). Finally, Somorrostro exhibited more uniform alongshore shoreline changes (Figure 3.9a), except in Event 17, when the shoreline was displaced further shoreward (on average 10 m) in the southwestern zone than in the northeastern zone.

These shoreline changes can be broken down into beach planform and morphological feature variability.

Beach planform

The shoreline changes related to the beach planform were analyzed by comparing the differences between the fit of the measured shoreline before and after the storm event, using the approach of Moreno and Kraus (1999). The squared correlation, R^2, between the fit and the shoreline was almost 1 and the goodness of the fit measured using the root mean square error (rmse) in metres for the Barcelona beaches is presented in Table 3.3. In general, the shoreline after the storm exhibited greater differences from the hyperbolic tangent fitting than the initial shoreline. Somorrostro showed the best correlation and the lowest rmse. Most shoreline variability was related to beach planform changes.

Normally, the beach planform changes were landward (negative values) during storm events, although the magnitude of the change and the alongshore behaviour differed according to the beach. Nova Icaria displayed the highest beach planform changes of all three beaches. The alongshore distribution of the changes had a marked differential pattern between the southwestern and northeastern zones (Figure 3.6b). Abrupt changes in the beach planform were observed in the southwestern zone (from -29 m to 7 m) while in the northeastern zone the changes were moderate and mainly landward (from -7 m to 6 m).

The beach planform changes of La Barceloneta I were non-uniform alongshore (Figure 3.7b). The changes were higher in the northeastern profiles (180-251), where they ranged from -10 to +10 m, than in the other profiles, where they ranged from -6.5 to 7.5 m. Beach rotation (displacement seaward in the southwestern zone and landward in the northeastern zone) was observed in some events at La Barceloneta I (Figure 3.7b). La Barceloneta II was analyzed as two different beaches, the northeastern one (La Barceloneta II-N) and the southwestern one (La

Barceloneta II-S). The beach planform changes were mostly landward and heterogeneous along the beach at these beaches, but higher in La Barceloneta II-N (between -25 and 1 m) than in La Barceloneta II-S (between -10 and 1 m) (Figure 3.8b). In Event 17, a different behaviour of these beaches was observed because the beach planform changes increased gradually alongshore from approximately -5 to -7 m in La Barceloneta II-S, while in La Barceloneta II-N the beach planform changes decreased sharply from -24 to -8 m.

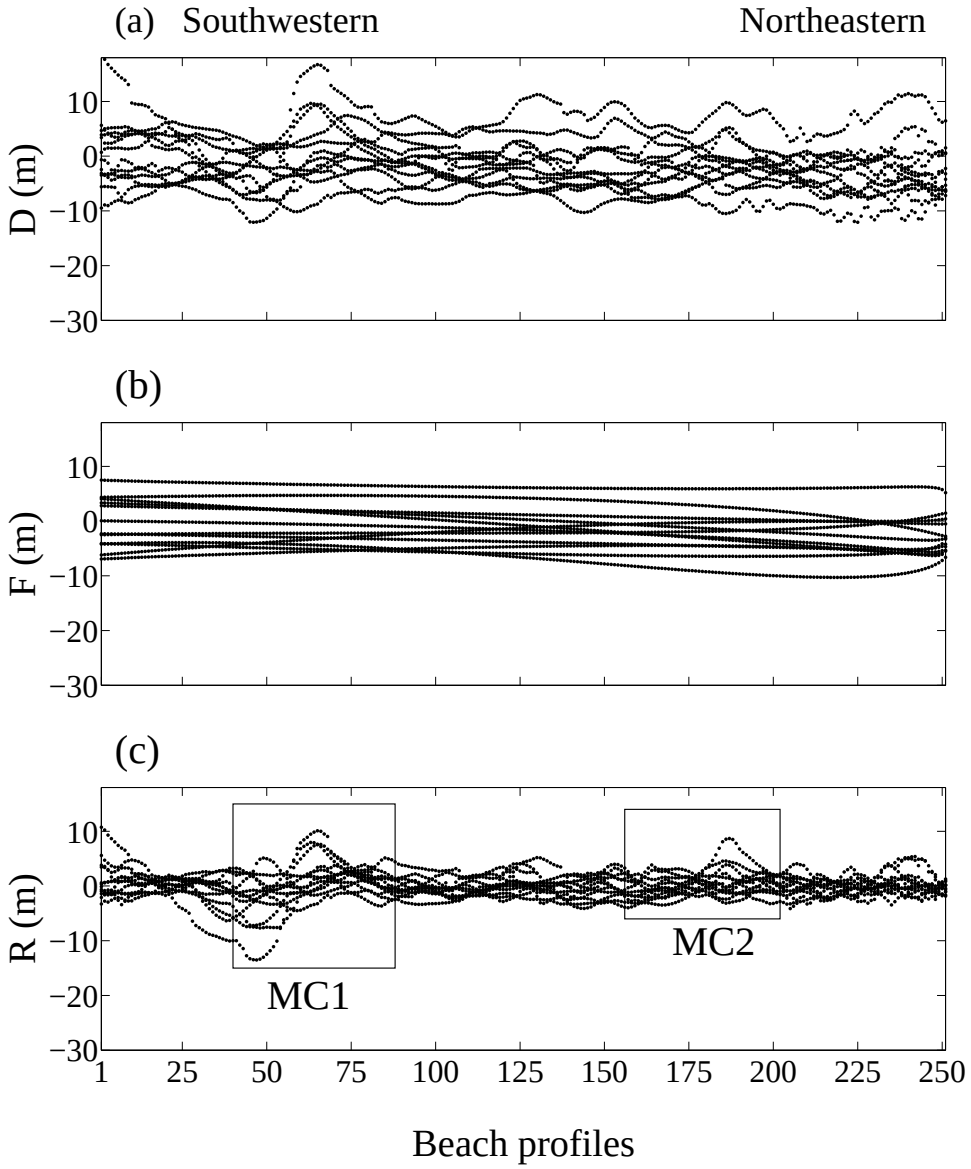

Figure 3.7: Shoreline variability at La Barceloneta I. (a) Shoreline changes (D), (b) beach planform changes (F) and (c) morphological feature variability (R) for each beach profile in all the storms. The boxes indicate the location of the salient and the megacusps MC1 and MC2.

Event	La Barceloneta				Somorrostro		Nova Icaria	
	Initial shoreline RMSE (m)		Final shoreline RMSE (m)		Initial shoreline RMSE (m)	Final shoreline RMSE (m)	Initial shoreline RMSE (m)	Final shoreline RMSE (m)
1	1.74		1.93		1.57	1.71	1.42	2.44
2	2.41		2.91		1.36	2.5	3.11	3.25
3	2.59		1.78		2.04	1.48	3.09	3.58
4	2.71		2.60		1.62	1.19	2.22	2.38
5	2.44		2.87		1.48	1.74	1.26	1.46
6	3.58		3.75		0.81	1.06	1.26	4.04
7	3.17		5.70		1.94	2.43	1.88	2.62
8	3.77		4.36		1.01	1.53	1.17	1.91
9	5.87		5.56		1.17	1.61	1.32	4.52
10	5.75		4.86		1.25	2.34	2.13	2.62
11	5.53		4.32		1.16	2.55	1.51	2.92
12	1.67		2.68		0.81	1.67	1.31	2.19
13	Northeast	Southwest	Northeast	Southeast	0.45	0.98	1.91	2.36
14	0.47	1.76	2.10	1.68	0.46	0.87	1.25	1.25
15	1.25	1.21	3.18	1.57	0.63	1.79	1.01	3.54
16	0.68	1.01	3.73	2.81	0.83	1.57	1.71	2.38
17	1.42	1.32	2.91	1.80	0.87	2.59	1.61	1.56

Table 3.3: Root mean square error (RMSE) of the hiperbolic tangent fitting (Moreno and Kraus, 1999) at La Barceloneta, Somorrostro and Nova Icaria.

Finally, the beach planform changes of Somorrostro (Figure 3.9b) fluctuated gently alongshore (<5 m). The main changes occurred in Events 7 and 17, with variations ranging from 5 to 10 m in the southwestern zone, and from 1 to 4 m in the middle and northeastern zone. These displacements were seaward and landward in Events 7 and 17, respectively.

Morphological features

(a) Beach cusps

Beach cusps (2-4 beach cusps) were observed at Somorrostro in the southwestern and central zone of the beach in Events 3, 5, 6 and 12. The beach cusp wavelength was about 12 to 18 m and the cross-shore distance between horn and bay was 2 to 3 m. These features were observed before, during or at the end of each event. The shoreline variability produced by the beach cusps during these storm events was 1 to 2 m (Figure 3.9c). The methodology for discriminating the variability considered the initial and final shorelines, so the variability associated with the beach cusps of Event 6 was not evidenced because they were formed and destroyed during the storm. Furthermore, the variability associated with the beach cusps was not evidenced directly because the error between the fit and the shoreline was of the same magnitude as the variability of the beach cusps.

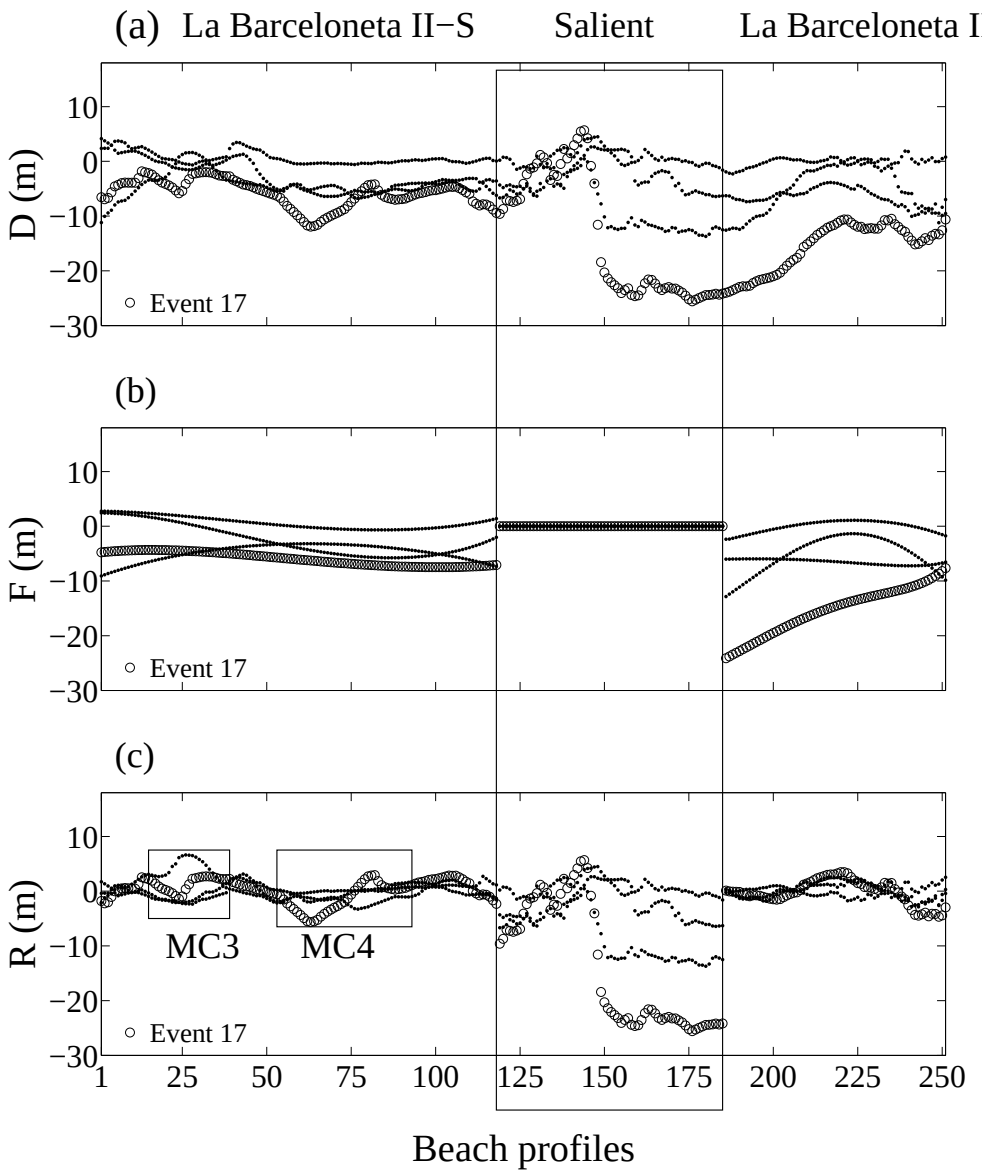

Figure 3.8: Shoreline variability at La Barceloneta II. (a) Shoreline changes (D), (b) beach planform changes (F) and (c) morphological feature variability (R) for each beach profile in all the storms. The boxes indicate the location of the megacusps MC3 and MC4 and the rectangle indicates the location of the salient.

(b) Megacusps

The first megacusp was observed in May 2002 in the southwestern zone of La Barceloneta I, but it disappeared several weeks later. Three megacusps developed after Event 6, from the southwest to northeast, with a cross-shore amplitude of 5, 7 and 3 m and an alongshore length of 120, 80 and 124 m, respectively. Only two of them remained on the shoreline from October 2003 to April 2004 (during

six consecutive storm events), one in the southwestern zone (megacusp MC1) between profiles 40 and 90 (an extension from 120 to 260 m) and the other in the northeastern zone (megacusp MC2) between profiles 157 and 200 (an extension from 80 to 160 m). The cross-shore amplitude of these two megacusps ranged between 5 and 15.5 m at MC1 and from 4 to 6 m at MC2.

Soon after the morphological change occurred at La Barceloneta, megacusps were only observed at La Barceloneta II-S. The first megacusp was observed at the beginning of Event 14, with an amplitude and extension of 4 and 86 m, respectively. Later, a megacusp of 5 m height and 176 m length was observed before Event 16. Finally, two megacusps (MC3 and MC4), which were 72 m apart and had a different amplitude (2.2 and 3.7 m) and extension (40 and 128 m) were formed before Event 17, but disappeared almost completely at the end of this event.

The presence of the megacusps produced shoreline variability that was negative or positive depending on when they were formed (before or during the event), the migration from the south to north along the shoreline and whether the amplitude and extension of the megacusp increased or decreased (Figure 3.7c). Megacusp MC1 in the first period caused the maximum shoreline variability (10 m) after Event 7. This megacusp not only increased its amplitude but also migrated alongshore 48 m, causing a negative shoreline variability of 13.5 m during this event. In general, the variability observed at megacusp MC1 and MC2 was, in absolute terms, 3 to 13.5 m and 2 to 8.7 m, respectively. On the other hand, the shoreline variability of the megacusps formed before Events 14 and 17 in La Barceloneta II-S caused a shoreline variability of 2.5 and 6.6 m, respectively and a shoreline variation of 2 and 3.2 m, respectively, because of its migration from southwest to northeast (Figure 3.8c). Finally, the megacusps MC3 and MC4 formed before Event 17 gave rise to a shoreline variability of -1 and -5.6 m, respectively.

(c) Shoreline undulation

Nova Icaria displayed a shoreline undulation that developed at the end of Events 1, 2, 4, 6, 8, 9, 11 and 15. This feature was localized around profiles 60 and 116; its alongshore length was approximately 120 m and the cross-shore

distance between cusp and bay ranged from 2.5 to 8.5 m. The shoreline variability related to the shoreline undulation (R) ranged from -1.5 to -4.5 m in the bay and from 6.8 to 2.5 m in the cusp (Figure 3.6c).

(d) Salient

The protection works carried out at La Barceloneta produced a different configuration of the beach and led to a salient. This morphological feature is located behind a detached breakwater. In order to analyze the extension variability after each event, a line between points A and B was defined in each initial shoreline (Figure 3.3c). Thus, the initial extension at the beginning of the storm was steady (264 m) and the final extension was calculated as the distance between the intersection of this line and the final shoreline. The amplitude of the salient was calculated as the maximum distance between this line and the initial and final shoreline. Points A and B corresponded to beach profiles 118 and 185, respectively (Figure 3.8). The amplitude of the salient increased from 38 to 57 m and the extension decreased from 258 to 164 m. The shoreline variability related to the salient for beach profiles from point A to 150 (section 1) was different to that for beach profiles from 151 to point B (section 2). In section 1, the variability was lower, from -6 to 4 m, than in section 2, where it was -25 to 2 m (Figure 3.8c).

3.4.3 Shoreline changes versus beach inundation

The beach inundation measured on Barcelona beaches corresponds to the cumulative effects of hydrodynamics (mainly run-up, but also storm surge and astronomical tide), initial morphology and morphological changes during the storm. As the inundation was measured considering a reference shoreline position before the storm (IRS), the presence of morphological features on the shoreline influenced the inundation. For example, the cuspate topography of the morphological features shaped the inundation, causing alongshore non-uniformity. The inundation values were higher in the bay than in the horn of the beach cusps (see Figure 3.10, although the differences were small (around 2-3 m). On the other hand, the differences between the cusp and the bay of the shoreline undulation were abrupt: approximately 10 m. Furthermore, megacusps reduced the inundation when they were present before the beginning of the storm. The amplitude and extension of these features was also important because the greater the amplitude and extension,

the more the inundation is altered. During the peak of the storm of Event 7, inundation reached 1.5 m and 4 m at the most seaward position of the southwestern (MC1) and northeastern (MC2) megacusps, respectively, while the inundation in the other areas was around 15 to 20 m (Figure 3.11).

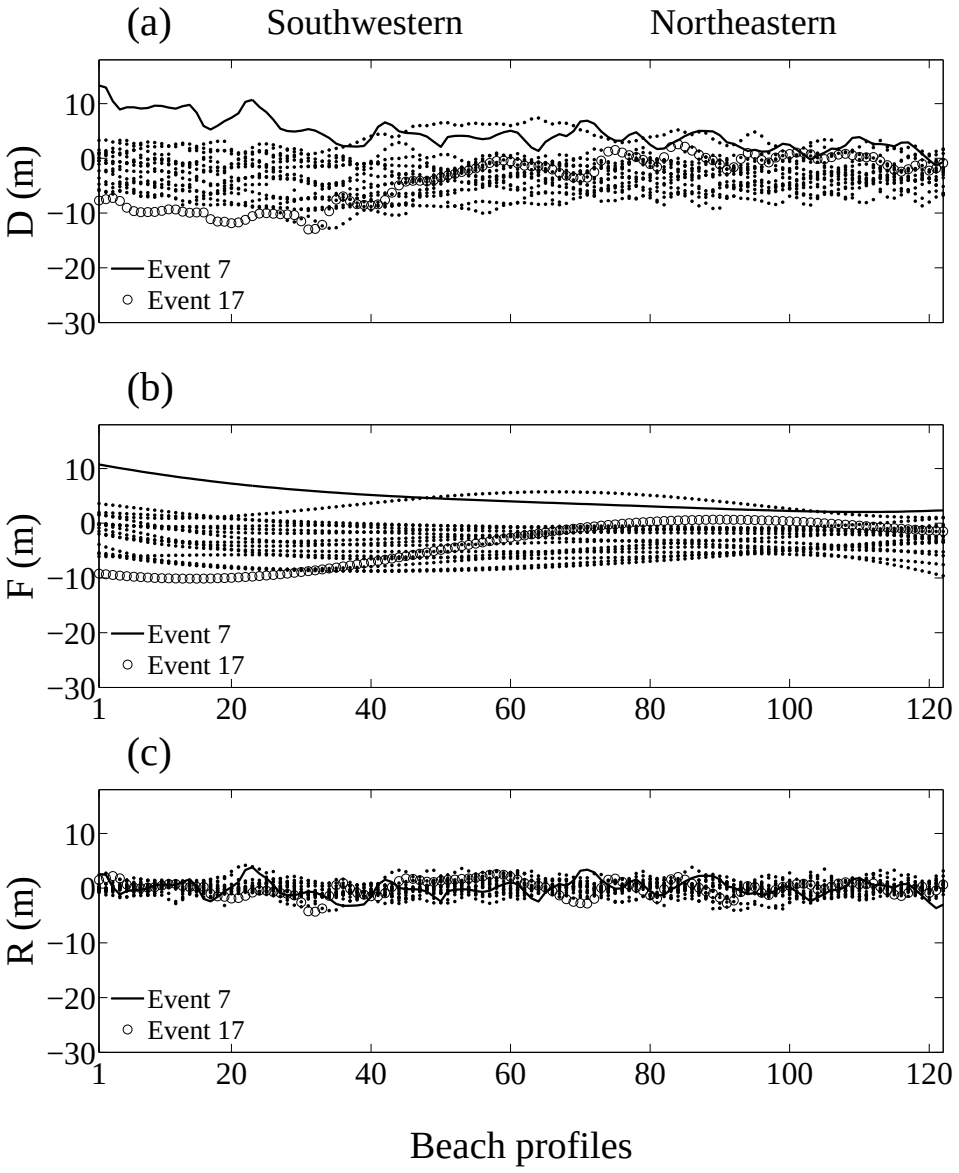

Figure 3.9: Shoreline variability at Somorrostro. (a) Shoreline change (D), (b) beach planform changes (F) and (c) morphological feature variability (R) for each beach profile in all the storms.

The inundation was also modified when morphological features were formed or evolved during the storm event. The alongshore migration of megacusps caused increases/decreases in the expected inundation along the beach. Hence,

the southwestern megacusp MC1 migrated and the inundation during the peak of the storm at the previous location of the megacusp MC1 was 6 m higher than the inundation at the new location (Figure 3.11). Finally, the influence of the salient on the inundation was totally different from one storm event to another. For instance, the inundation in Event 14 was negligible, whereas the inundation in Event 17 was 45 to 71 m at the salient.

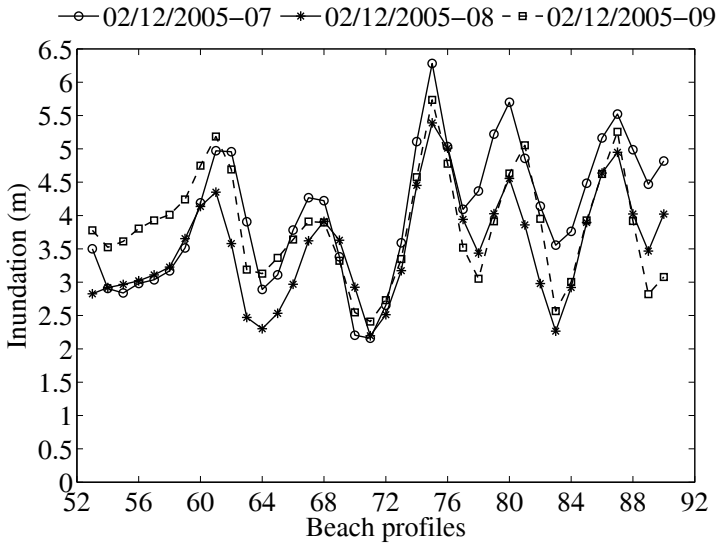

Figure 3.10: Inundation at the beach cusps of Somorrostro on 2 December 2005 (Event 12).

In general, the influence on the inundation of the morphological features located along the shoreline at the beginning of the storm was directly proportional to the magnitude of these morphologies. Shoreline displacements during the storm add a new factor to be considered: when the shoreline displacement was landward, the waterlines came inland more than expected. On the other hand, when shoreline displacement was seaward, the inundation was lower or there was no inundation. For example, in La Barceloneta II-N a severe inundation (30 m) nearly reaching the promenade was observed during Event 17. Results of the beach planform changes here show a shoreline retreat of 20 m, causing a higher inundation than expected. On the other hand, during Event 7 at the southwestern end of Nova Icaria no inundation was observed because of a seaward displacement of the shoreline.

The relative influence of a shoreline change (SC) on the inundation (I)

can be expressed as the SC/I ratio and it is possible to differentiate between changes in the planform (F) and in morphological features (R). Since from the data it does not know the exact instant when the shoreline change took place, the maximum inundation (IMs) is considered in the SC/IMs ratio in order to define a minimum potential influence of the shoreline change on the inundation.

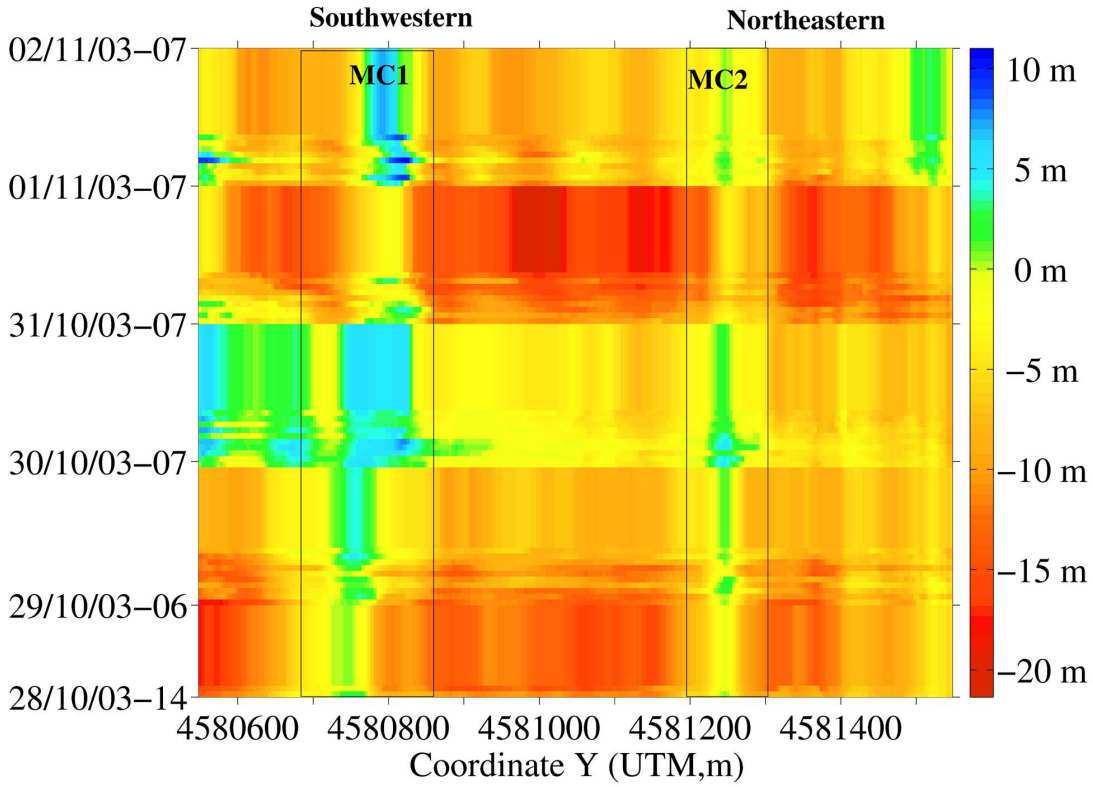

Figure 3.11: Temporal evolution of the waterline during Event 7 at La Barceloneta I. MC1 and MC2 refer to the location of the megacusps. Negative values mean landward position with respect to the IRS.

Influence of beach planform changes

The F/IMs ratio (in absolute terms) for beach planform changes was higher than 0.25, in 63.8%, 77.3%, 45.9%, 46.3% and 56.3% of the measurements at La Barceloneta II-N and La Barceloneta II-S, La Barceloneta I, Somorrostro and Nova Icaria, respectively. It is noteworthy that in 12.5%of the cases at La Barceloneta I, 44.9% at Barceloneta II-N and 30.5% at Nova Icaria, the magnitude of the beach planform changes was at least half the maximum inundation measured. Landward beach planform displacements were more intense than

seaward displacements, but also had a major influence on the inundation of Barcelona beaches.

On the other hand, seaward beach planform changes had a slight effect on the inundation at La Barceloneta I and Nova Icaria because 2.8% and 3.2% of the values were higher than 0.5, respectively, while at the two new beaches of La Barceloneta II and Somorrostro the effect was negligible, with fewer than 1% of the values higher than 0.5.

Influence of the morphological features

Morphological changes higher than 4 m with R/IMs values higher than 0.25 occurred at La Barceloneta I related to megacusp variability. On the other hand, megacusps at La Barceloneta II-S led to maximum morphological changes of 6 m (Figure 3.12). The percentage of cases in which the ratio of megacusp variability to IMs was higher than 0.25 was 11% and 15.4 % at La Barceloneta I and II, respectively. It should be borne in mind that these features were observed in only half the storm events and at some beach profiles. Therefore, megacusps are dynamic features that modify the beach inundation.

The greatest morphological changes (28 m) and the maximum inundation (71 m) were related to the salient variability at La Barceloneta II beach (Figure 3.12). Morphological changes ranged between 10 and 25 m, whereas inundation values ranged between 15 and 45 m. In 62.5% of cases the ratio of morphological change of the salient to maximum inundation was higher than 0.25, and in particular, in 34.3% of the cases the influence accounted for half the maximum inundation.

Most of the R/IMs values of shoreline changes related to morphological features of Somorrostro (96.5%) were lower than 0.25. All shoreline changes were below 5 m, whereas the morphological change caused by the beach cusps was 1 to 2 m. Therefore, the presence and morphological variability of the beach cusp at Somorrostro barely influenced the inundation. Additionally, beach cusps are expected to be destroyed during the peak of the storm (Masselink et al., 1997), so the potential influence of beach cusps on the inundation is limited to low or medium wave conditions. The shoreline changes related to morphological

features higher than 3 m correspond to other artificial features formed after the storms at Somorrostro (not considered here) but the influence was also negligible (R/IMs lower than 0.1).

Most of the morphological variability at the Nova Icaria was caused by shoreline undulation. Morphological changes related to the undulation were up to 7 m and in 13.3% of measurements the relation between the undulation variability and the maximum inundation was between 0.25 and 0.5. Only 1% of the R/IMs values were higher than 0.5.

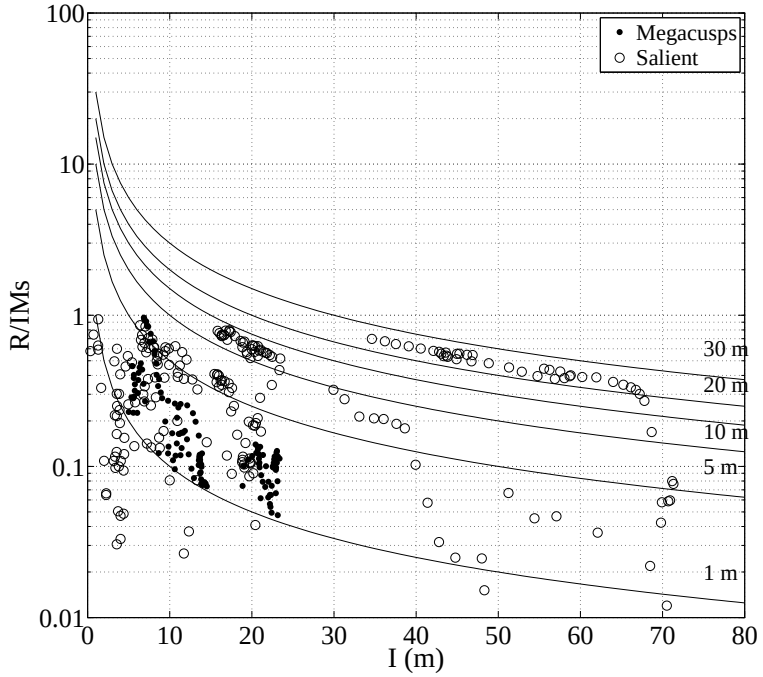

Figure 3.12: Abacus of the megacusps and salient influence on the inundation (R/IMs) at La Barceloneta II. Isolines represent the influence of a morphological change of 1, 5, 10, 15, 20 and 30 m on the inundation.

3.5 Discussion

The influence of shoreline evolution trends in the quantification of the potential beach inundation during storms is an important factor considered in long-term coastal management to predict the location of set-back lines (Ferreira et al., 2006) and coastal flooding hazards (Benavente et al., 2006), and to map coastal vulnerability (Bosom and Jimenez, 2011). In a short-term perspective,

the intensity of the inundation is also affected by morphological changes during storm conditions, although they are not systematically considered. Stockdon et al. (2006) analyzed the influence of beach morphology on vertical run-up, stating that if the beach slope becomes steeper (gentler) the prediction of the run-up will be underestimated (overestimated). In addition, the presence of morphological features along the beach shapes the inundation and this effect cause alongshore non-uniformity (Masselink et al., 1997; Masselink and Pattiaratchi, 1998; Bryan and Coco, 2010). For instance, Masselink et al. (1997) found that horizontal run-up was higher in the embayment than in the horn of beach cusps, owing to the flatter beachface slope of these features. Changes in the beach slope associated with the presence of megacusps caused the maximum alongshore variability in run-up measurements (Stockdon et al., 2006).

Observations at the Barcelona beaches are consistent with previous findings: the alongshore variability of the inundation is related to the presence of morphological features or changes in the beach slope along the beach. Of more interest to the aim of this thesis is a comparison of the scale of the shoreline change during the storm and the magnitude of inundation. The observed inundation mainly results from the combined action of run-up and shoreline change. Under this perspective, it is assumed that if a morphological feature does not change during the storm, it has no influence on the inundation value. In the case of Barcelona beaches, the influence of changes in the planform shape or morphological features on beach inundation was strong. When the potential contribution of the shoreline change to the observed inundation is higher than 25%, it is considered it a noteworthy influence. The shoreline variation associated with beach planform changes (BPC) is the main influence on beach inundation. The BPC/I ratio is higher than 0.25 for 63.8%, 77.3%, 45.9%, 46.3% and 56.3% of the measurements at La Barceloneta II-N and La Barceloneta II-S, La Barceloneta I, Somorrostro and Nova Icaria, respectively, and most of them are related to the retreat of the beach planform. From the morphological features studied, the salient has the greatest influence on the inundation values. In 34.3% of the measurements at the salient, the contribution of shoreline changes accounted for more than 50% of the inundation. The remaining morphologies displayed a decreasing influence on beach inundation from megacusps to beach cusps, whose influence was almost negligible.

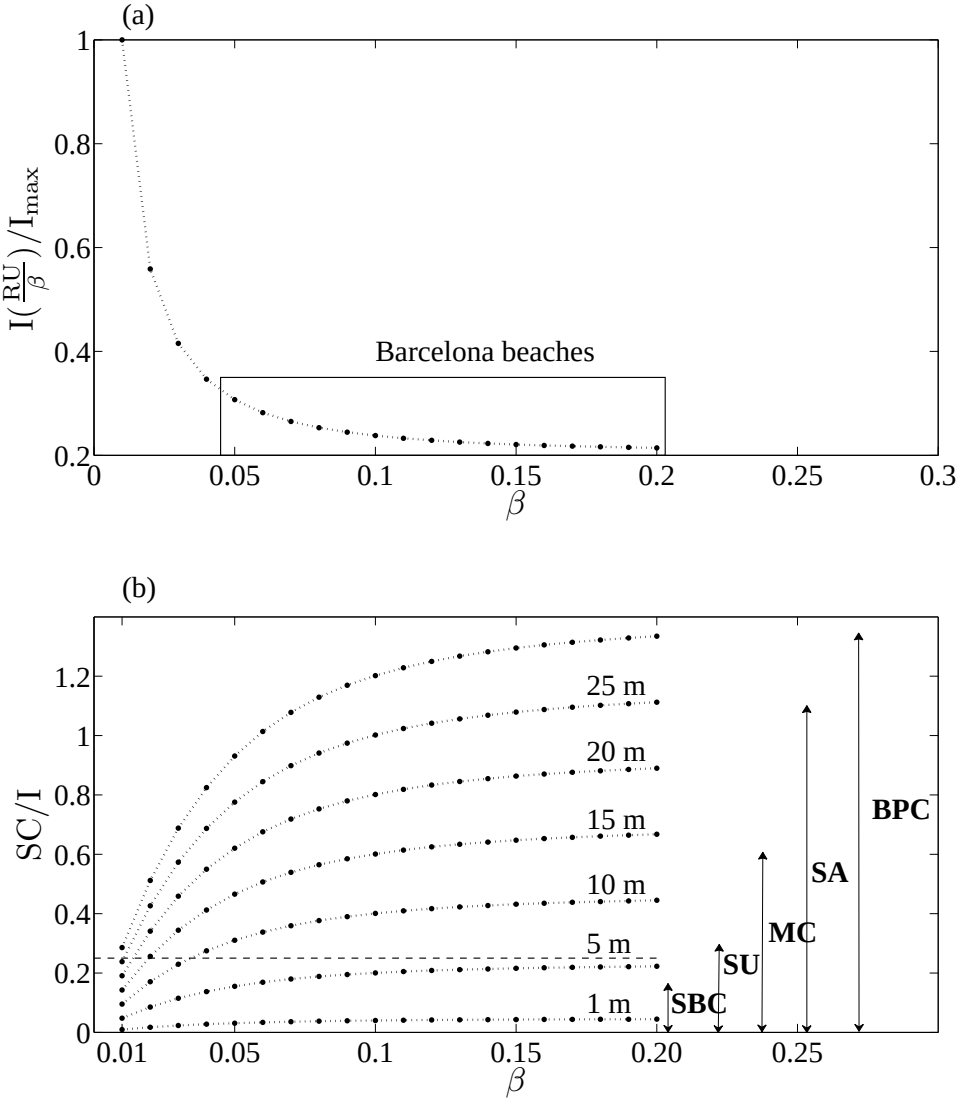

Figure 3.13: (a) The relation between the inundation (I), normalized by the maximum inundation (I_{max}), and the beach slope (β). (b) Relationship between the shoreline change influence on the inundation (SC/I) and the beach slope. Isolines represent different shoreline changes (1, 5, 10, 15, 20 and 25 m). The dashed line represents the limit for considering the influence of shoreline change on the inundation as noteworthy. Also shown is the range of variability of small beach cusps (SBC), shoreline undulation (SU), megacusps (MC), salient (SA) and beach planform changes (BPC).

The influence of shoreline change on inundation depends on the magnitude of the beach change and the intensity of the inundation in relation to wave conditions and beach slope. Whereas the shoreline variability observed during storms at

Barcelona beaches is expected to be of the same order of magnitude (metres to tens of metres) for all beaches, the magnitude of the inundation (the horizontal displacement of the waterline) largely depends on the beach slope. Because Barcelona beaches are characterized by steep beach slopes (see Table 3.1), the relative influence of the morphological variability is only illustrative for beaches with similar slopes. In order to extend the analysis to beaches with different slopes, the relationship between inundation and beach slope is shown in Figure 3.13a. The inundation (I) and the beach slope (β) have an inverse relationship. It should be pointed out that the magnitude of the inundation is very sensitive to the change of slope for gently sloping beaches ($\beta < 0.04$), but this influence decreases drastically for steep beaches (Figure 3.13a). Consequently, beach slope variability should be considered in the prediction or understanding of inundation processes in gently sloping beaches but it is not a decisive factor in steep beaches.

The inundation (waterline displacement) during storms on tideless beaches mainly corresponds to the horizontal extension of the run-up, because the magnitude of the storm surge and the astronomical tide is much lower than the wave-induced run-up (Bosom and Jimenez, 2011). Differences between inundations as defined in this chapter and the vertical excursion of the run-up should be taken into account. It was demonstrated by Stockdon et al. (2006) that the beach slope does not affect the run-up on gently sloped (dissipative) beaches. However, an equivalent vertical run-up excursion generates very different inundation values when the beach slope of a dissipative beach is modified. The run-up on steep-sloped beaches is influenced by the slope change, but in the transition from run-up to inundation these changes are diminished.

The influence of shoreline variability on inundation is greater for steeper beaches because of the lower magnitude of inundation. This influence, calculated for different beach slopes using the method proposed by Stockdon et al. (2006), is shown in Figure 3.13b. In general, shoreline changes of 10 m with beach slopes lower than 0.04 do not influence the inundation. Focusing on the magnitude of the shoreline changes that take place at Barcelona beaches, it is clear that beach changes related to both the beach planform readjustments and the salient have a potentially significant influence on the inundation for most natural ranges of beach slope. The influence of shoreline variations related to undulation (SU) and mega-

cusps (MC) must be considered when the beach slope becomes higher than 0.04. Finally, the shoreline variability caused by beach cusp dynamics is a secondary factor for inundation on most beaches (Figure 3.13b).

3.6 Conclusions

La Barceloneta I, Somorrostro and Nova Icaria are characterized by alongshore heterogeneous inundation which is in general higher in the southwestern zone than in the northeastern zone because of the orientation of the beaches with respect to the wave direction approach. With the new morphological configuration, the inundation alongshore La Barceloneta II changed, increasing from the southwestern section (La Barceloneta II-S) to the salient, and then decreased at the northeastern section (La Barceloneta II-N). Besides, the morphological features shape the inundation, leading to non-uniformity alongshore. The magnitude of the inundation is different between these beaches, with the highest values at La Barceloneta II (71 m), followed by Nova Icaria (54 m) and finally Somorrostro (37 m). Beach inundation depends largely on the beach slope (inundation increases with decreasing slope).

Shoreline changes during storms were disaggregated in beach planform changes (defined by a hyperbolic fit) and morphological features changes (estimated from the residuals of the hyperbolic fit). It was thus possible to estimate the mobility of beach cusps, megacusps, a salient and a shoreline undulation. The largest shoreline variations were caused by beach planform readjustments and salient modifications (maximum shoreline displacement >20 m). Megacusps and shoreline undulation gave maximum variability of about 10 m, while the shoreline variation associated with beach cusp was lower than 2 m.

The observed inundation results from the combined effect of hydrodynamics on the beach and the shoreline displacement caused by the storm. The landward shoreline displacement caused by beach planform readjustment is the foremost influence on inundation at Barcelona beaches. The planform and salient shoreline changes can cause 50% of the maximum inundation measured, followed by the megacusps and the shoreline undulation which also often cause around 25% of the maximum inundation and finally, the beach cusp influence is negligible and

can be disregarded.

Shoreline changes during storm conditions make a large contribution to the inundation value on Barcelona beaches. From a more general perspective, shoreline variability during storms should be considered especially on steep beaches, whereas on gently sloped (dissipative) beaches the inundation is greater and the shoreline contribution smaller. However, the inundation in dissipative beaches is highly sensitive to changes in the beach slope and these morphological changes should be also taken into account for a more accurate prediction of the inundation processes.

Chapter 4

STORM-SURGE INUNDATION ALONG A MULTIBARRED BEACH

Edited and extended version of
A. Sancho-García, B.G. Ruessink and
J. Guillén. 2011. Storm-surge inundation
along a multibarred beach. Journal of
Coastal Research SI 64, 1911-1915.

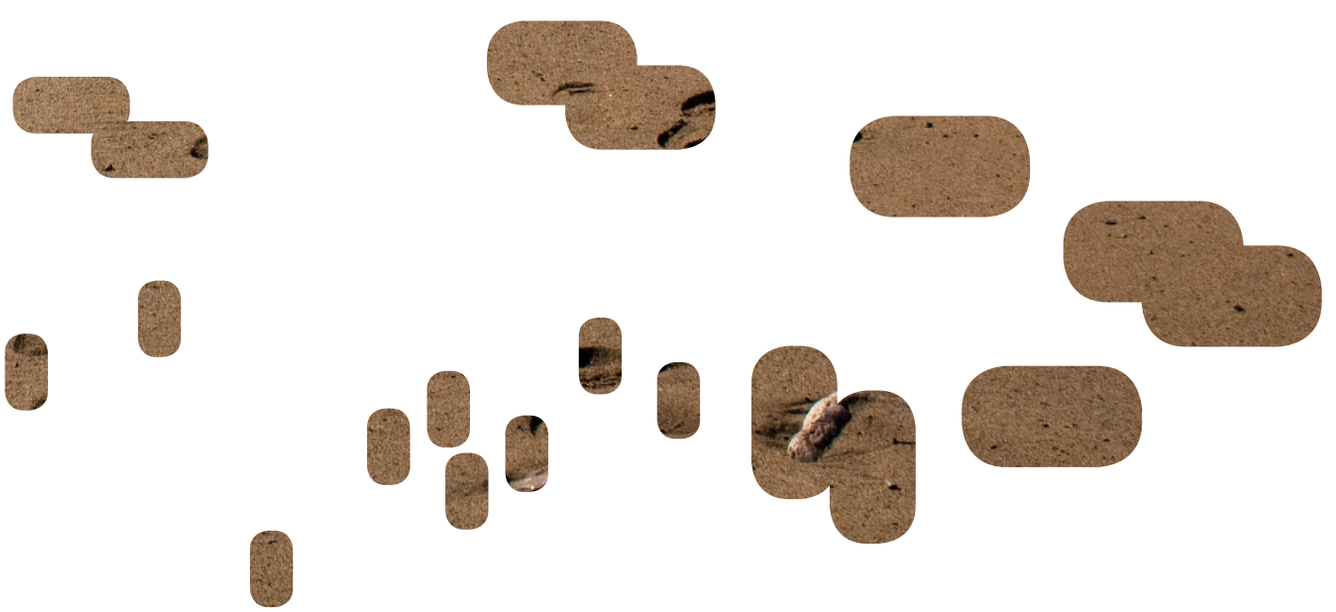

4.1 Introduction

A considerable portion of the world's population lives in coastal areas and is exposed to natural hazards, such as coastal erosion and flooding, that are produced by sediment starvation, storms, tsunamis, and sea-level rise (Ferreira et al., 2006). The water level increases considerably during storms because of the storm surge and the wave runup resulting from setup and swash (Stockdon et al., 2006). A storm surge is generated by extreme wind stress acting on shallow continental shelf seas and can lead to severe coastal inundation. A well-known example is the storm surge of 31 January to 1 February 1953, which caused considerable damage and loss of life in the Netherlands and the United Kingdom (Wolf and Flather, 2005; Brown et al., 2007) when dikes and seawalls were breached. Therefore, suitable coastal management should understand and quantitatively predict the processes controlling coastal inundation.

Coastal inundation is an instantaneous process and quantitative measures of it are scarce; however, video monitoring techniques now provide frequent and accurate measurements of coastal inundation (Kroon et al., 2007; Sancho-Garcia et al., 2008). Furthermore, previous studies have demonstrated that inundation is influenced by alongshore variability related to beach morphology (Masselink et al., 1997; Ruggiero et al., 2004; Bryan and Coco, 2010), although the effect of submerged morphology (*sandbars*) on inundation is still poorly understood (Stephens et al., 2011).

The main aim of this chapter is to quantify the inundation affecting a microtidal, sandy multibarred beach (Noordwijk, the Netherlands) during severe storms between 1998 and 2005 using video monitoring techniques and to analyze the effects of nearshore subtidal sandbars on inundation during a storm in October 1998 using the XBeach model (Roelvink et al., 2009). It also examines the prediction capability of a simple inundation parameter comprising a runup expression, the offshore wave conditions, the surge level and the beach foreshore slope, and demonstrates that inundation at this beach is governed primarily by the storm surge level.

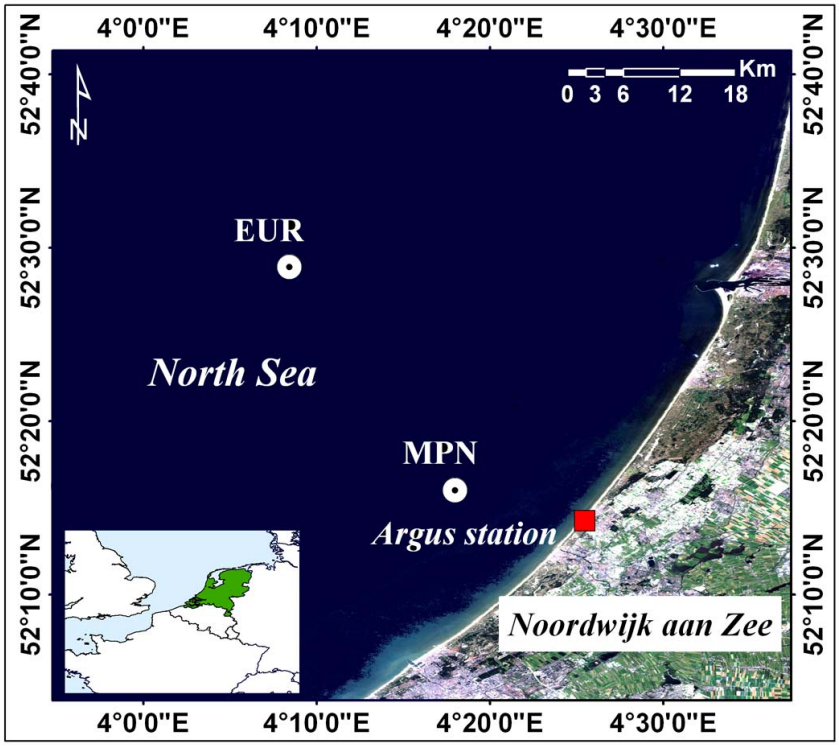

Figure 4.1: Study area with the hydrodynamic data collection, Meetpoint Noordwijk (MPN) and Europlatform (EUR), and with the position of the Argus station (red square). The image used is a product of IMAGE2000. Intellectual property rights IMAGE2000 of JRC, based on Landsat 7 ETM+ © ESA, distributed by Eurimage; ortho-correction EU15 © Metria, ortho-correction other countries GISAT; mosaic production GISAT.

4.2 Field site description

Noordwijk is located on the central Dutch coast, oriented 28^{o} from the north and facing the semi-enclosed North Sea (Figure 4.1). It is a sandy, wave-dominated coast with a beach and nearshore zone that consists of a single intertidal slip-face ridge and two subtidal bars (van Enckevort and Ruessink, 2003a). Occasionally, a second intertidal bar may form on a pre-existing bar during low-energy wave conditions (Quartel et al., 2007). The median grain size (D50) of sediments is 250 μm on the beach, 150μm from the beach to a seaward distance of 600 m (water depth - 4 to -5 m) and 300 μm to a seaward distance of 800 m (Ojeda et al., 2008). The waves, mainly incident from a southwestern to northwestern direction, have an average offshore root-mean-square (rms) wave height (H_{rms}) of 0.7 m and a corresponding peak period (T_p) of 6 s. The tide at

Noordwijk is semi-diurnal and microtidal. The mean tidal range is 1.8 m and 1.4 m during spring and neap tide, respectively.

During the study period, from February to March 1998, a 1.7 Mm^3 nourishment was placed at a depth of 5 to 8 m over an approximately 3-km-wide (alongshore) area roughly 900 m from the shore. The shoreface nourishment was implemented as a hump over the seaward side of the outer subtidal bar (Ojeda et al., 2008; Quera, 2010).

Event	Initial date	$\mathrm{H}_{rms_{mean}}$ (m)	$\mathrm{H}_{rms_{max}}$ (m)	$\mathrm{T}_{p_{mean}}$ (s)	Mean Direction (^{o})	$\eta_{\mathrm{surge_{mean}}}$ (m)	$\eta_{\mathrm{surge_{max}}}$ (m)	Duration (h)
1	27/10/1998	2.3	3.4	7.8	272 (W)	0.7	1.3	98
2	16/02/1999	2.4	3.5	8.3	310 (NW)	0.8	1.2	49
3	21/02/1999	2.2	3.2	8.0	305 (NW)	0.7	1.1	64
4	07/09/2001	2.1	2.7	7.8	326 (NW)	0.6	0.8	88
5	22/02/2002	2.4	3.2	8.0	294 (WNW)	0.7	1.2	45
6	05/10/2003	2.2	3.4	8.0	295 (WNW)	0.5	1.1	69
7	15/12/2005	2.7	3.3	8.6	333 (NNW)	0.7	1.2	69

Table 4.1: Characterization of storm events

4.3 Methods

4.3.1 Video observations

Storm events between 1999 and 2005 were selected using hourly records of offshore wave and water level collected at Meetpost Noordwijk (MPN in Figure 4.1), which is located 9.5 km offshore at 18 m water depth. Gaps in the wave data series were filled with data from Europlatform (EUR in Figure 4.1) located 21 km offshore at 30 m water depth. The storm events were selected as periods of at least 30 hours during which H_{rms} exceeded 2 m and the surge level (η_{surge}, defined as the difference between measured and astronomical water levels, $\eta_{\mathrm{meas}} - \eta_{\mathrm{pred}}$) was greater than 0.5 m. The threshold for the start and the end of each storm was a H_{rms} less than 1.5 m and a positive surge level. The study focuses on the seven largest storms (Table 4.1).

Beach inundation for each storm event was obtained hourly by means of an Argus video system (Holman and Stanley, 2007). The beach and the nearshore zone of Noordwijk have been video-monitored since 1995. This Argus video

system is mounted on the roof of a hotel at a height of 62 m above mean sea level, and consists of five cameras that together view the coast over 6 km in the alongshore direction, and 1·5 km in the cross-shore direction. Images are in the visible range of light and the sampling is done every daylight hour during a ten-minute period (two pictures per second). The 10-minute average time Argus images were geometrically transformed to obtain a rectified plan view of the beach and the nearshore zone. The region of interest covered 900 m in the alongshore direction with the camera position on the left side and 300 m in the cross-shore direction. The pixel size of the rectified images was 1 x 1 m.

Event	Beach slope			
	β_{int}	β_{sup}	Regression (n° waterlines)	
			R^2	rmse (m)
1	0.022	0.047	0.83 (21)	11.03
2	0.019	0.040	0.91 (87)	8.77
3	0.019	0.040	0.91 (87)	8.77
4	0.015	0.039	0.91 (97)	11.20
5	0.016	0.041	0.93 (126)	11.11
6	0.016	0.044	0.94 (83)	9.43
7	0.016	0.046	0.95 (69)	8.14

Table 4.2: Values of the intertidal (β_{int}) and supratidal (β_{sup}) beach slope for each storm event. Accuracy of the theoretical waterline induced by the astronomical tide only; in brackets, the number of waterlines used in the linear regression.

The hourly waterline position was extracted from each plan view by the automated alongshore tracking of the intensity maxima across the waterline (Pape et al., 2010). These high intensities are generated by the swash-induced foam. In total, the data set comprise 184 waterlines. The beach inundation is defined as the distance between the observed instantaneous waterline and the theoretical waterline position induced by the astronomical tide only. Thus, in order to obtain the inundation, the theoretical position of the waterline related to the astronomical tide had to be estimated. The waterline was extracted from the overall image dataset during low-energy conditions (H_{rms} <0.7 m and $\eta_{\text{surge}}\pm$ 3 cm) and with an astronomical tide around $\pm$ 5 cm of $\pm$ 1, $\pm$ 0.75, $\pm$ 0.5 and $\pm$ 0.25 m. A linear regression between the alongshore-averaged position of each waterline and the corresponding astronomical tide was computed for each year considering a constant beach slope. The slope of this linear regression was the intertidal beach slope

(β_{int}) (Table 4.2). Finally, beach inundation (4.2f) was calculated as the distance between the waterline (wl in Figure, 4.2d) and the theoretical waterline position considering only the astronomical tide (wl_{tide} in Figure, 4.2e) alongshore-normal beach profiles defined every meter. Figure 4.2 shows an example of this methodology followed for calculating the inundation at one beach profile for Event 7.

4.3.2 Inundation parameterization

The hourly observed inundation at each profile was compared with an inundation parameter, I_p, defined as:

$$\mathrm{I_p} = \frac{\beta\sqrt{\mathrm{H_0 L_0}} + \eta_{\mathrm{surge}}}{\beta} \tag{4.1}$$

which includes the beach slope (β), a runup expression (adapted from Stockdon et al. (2006)), $\beta\sqrt{H_0 L_0}$, where $\mathrm{H_0}$ and $\mathrm{L_0}$ are the deep-water wave height and wavelength respectively, and the surge level (η_{surge}).

The beach profile is represented as two lines with different slopes, so two different beach slopes (β) were defined in order to apply the inundation parameter, I_p: the intertidal beach slope, (β_{int}), calculated previously and the supratidal beach slope (β_{sup}) estimated from annual beach topographic surveys. The limit for considering and using the supratidal or intertidal beach slope was a water level of $+$ 0.9 m NAP ($=$ Dutch ordinance level, $\approx$ mean sea level) because it is the mean maximum water level of the waterlines considering only the astronomical tide.
Intertidal beach slope values were typically 1:60, characteristic of a dissipative beach, with little interannual variability (Table 4.2). The supratidal beach was steeper, typically 1:25 (Table 4.2).

4.3.3 XBeach model

From the selected storms, the storm event of October 1998 was modeled in order to analyze the influence of the sandbars on the inundation. This storm had a long duration, the wave fronts approached the shoreline with a low wave angle, which improves the 1D approximation to the real situation, and some morphological changes occurring during the storm were related to the intertidal bars.

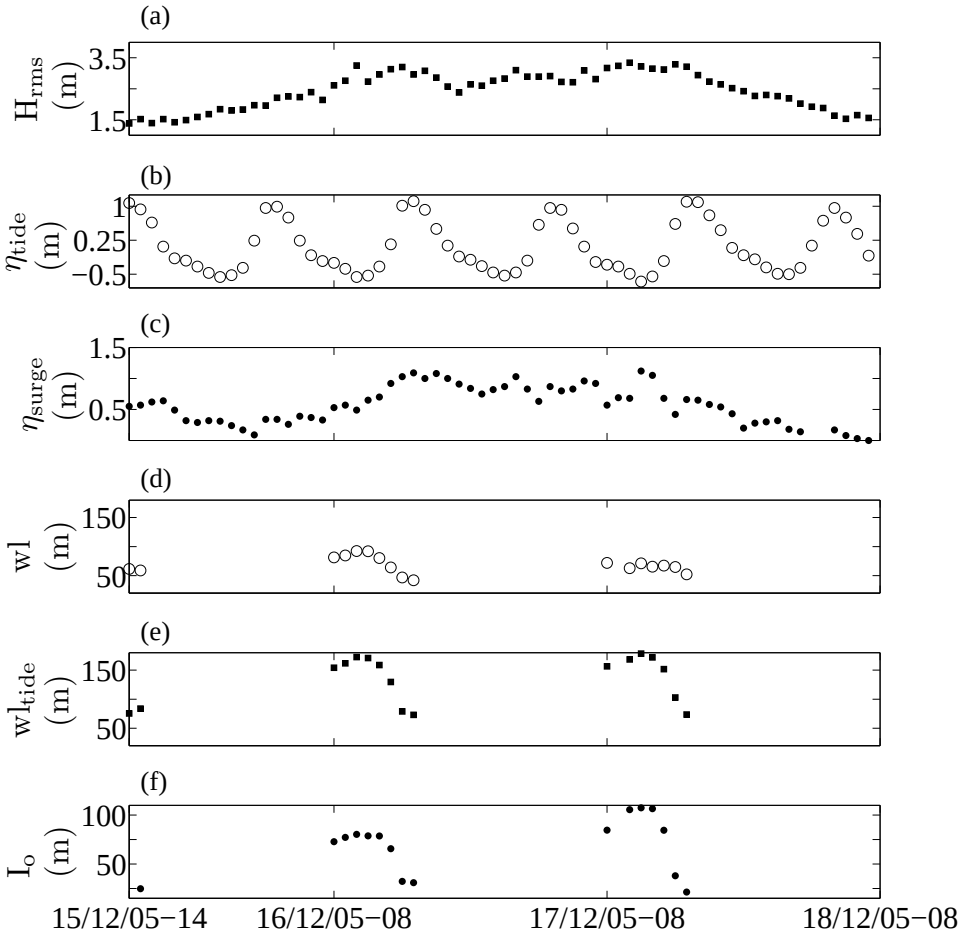

Figure 4.2: Hydrodynamic conditions and inundation at one profile (y = -400 m) for Event 7. (a) Astronomical tide level, η_{tide}; (b) offshore root-mean-square wave height, H_{rms}; (c) surge level, η_{surge}; (d) cross-shore position of the waterline, wl; (e) theoretical cross-shore position of the waterline considering only the astronomical tide, wl_{tide}; (f) inundation, I_o. Note that cross-shore distance is positive going offshore, so a decrease to 0 in (d) and (e) indicates that the waterline is located further landward.

The 2DH model XBeach solves coupled equations for cross-shore and longshore hydrodynamics and morphodynamics on the time scale of wave groups, including the generation of infragravity waves (Roelvink et al., 2009). To test the influence of the sandbars on the inundation, 1D-simulations of this storm were made using six different beach profiles of Noordwijk (Figure 4.3). Two of these profiles were extracted from a Noordwijk bathymetry carried out in 1999 and 2005 (BP335 (1999) and BP335 (2005), respectively), while the remainder correspond to a bathymetry done in August 1998, a few months before the storm event of

October 1998. The beach profiles selected had a wider range of submerged morphology because of the different location and the morphology of the inner and the outer bars. The barless profile is based on the beach profile BP245 (Figure 4.3), smoothing the area where the sandbars were located. In all simulations, the beach profile was 5 km long, the grid resolution increased to the shore from 100, 50, 10 to 3 m and was referenced to the Dutch vertical ordnance datum (NAP). As the interest is in the hydrodynamics, the bathymetry was not allowed to evolve during the simulation.

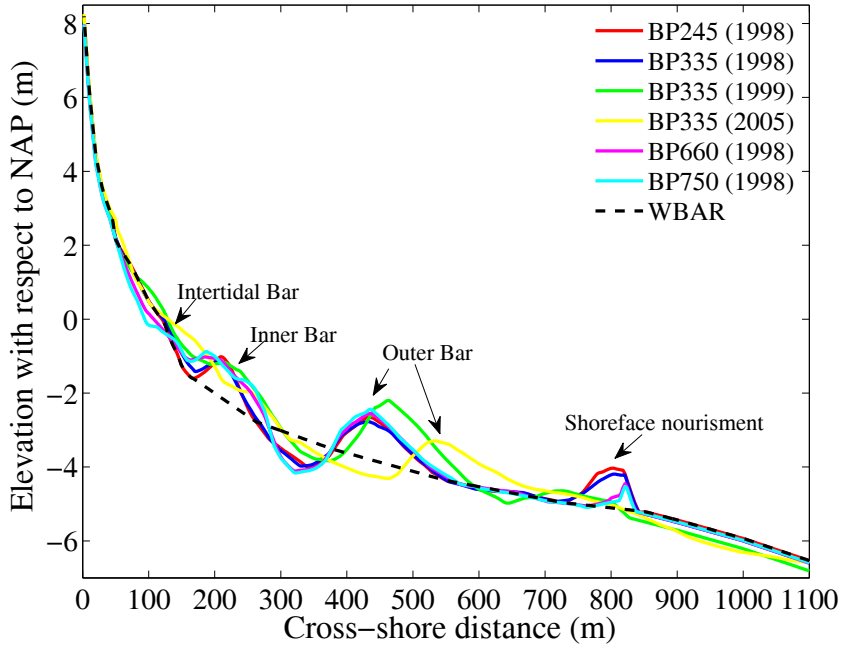

Figure 4.3: Cross-shore profiles of Noordwijk used in the XBeach simulations, indicating the intertidal bar, the two subtidal bars and the shoreface nourishment. For design reasons, only the most onshore zone of the beach profiles is illustrated. The barred profile nomenclature contains the Argus location of each profile and in brackets the year of the beach profile survey.

For each barred profile, three control points were selected (outer bar crest, inner bar crest and trough) in order to check the the water level and the wave height during the simulation. It should be noted that the control points in the barless profile were selected at the same location as in the barred profile BP245 on which it was based. The parameter settings are common for all the simulations, except for the location of the control points, and they are shown in Table 4.3. Using the option *runup gauge* in the XBeach model, the water level at the waterline was obtained every second. In order to obtain the inundation and to compare the results with the observations, for each hour of simulation (3600 s), the 98th percentile was

obtained from the 1-second time series of the water level (η_{wl}). When this water level had been obtained, η_{wl} included the contribution of the *setup* (η_{setup}), *tide* (η_{tide}), *surge* (η_{surge}) and the high peaks of the *swash* (η_{swash}).

$$\eta_{\mathrm{wl}} = \eta_{\mathrm{setup}} + \eta_{\mathrm{swash}} + \eta_{\mathrm{tide}} + \eta_{\mathrm{surge}} \tag{4.2}$$

Parameter	Setting	Parameter	Setting
Grid input		***Tide***	
nx	517	zs0file	surge.dat
ny	0	tideloc	1
xori	-5000.00	***Sediments***	
yori	0.00	D50	0.00025
alfa	0.00	D90	0.000375
depfile	bathy.dep	rhos	2650
vardx	1	sedtrans	0
xfile	x.grd	por	0.4
yfile	y.grd	CFL	0.7
posdwn	-1	***Morphology***	
thetamin	-90	morphology	0
thetamax	90	swave	1
dtheta	180	lwave	1
Waves		rugdepth	0.01
instat	4	***Time steps***	
bcfile	boundarylst.dat	tstart	1200
delta	0.0	tint	100
epsi	0	tintp	1
break	3	tintm	3600
gamma	0.55	taper	100
alpha	1.	tstop	364800
n	10	***Output***	
roller	1	nglobalvar	5
beta	0.1	H	
rfb	0	zb	
wci	0	zs	
Physical constants		ue	
rho	1025	E	
g	9.81	nmeanvar	3
Boundaries		H	
front	0	E	
back	1	zs	
Flow		npointvar	3
nuh	0.1	H	
nuhfac	1	hh	
carspan	0	zs	
hmin	0.05	npoints	3
eps	0.01	-170 0	
umin	0.0	-209 0	
C	65	nrugauge	1
scheme	upwind1	-300.0 0	
gammax	2		

Table 4.3: XBeach parameter settings for the simulations.

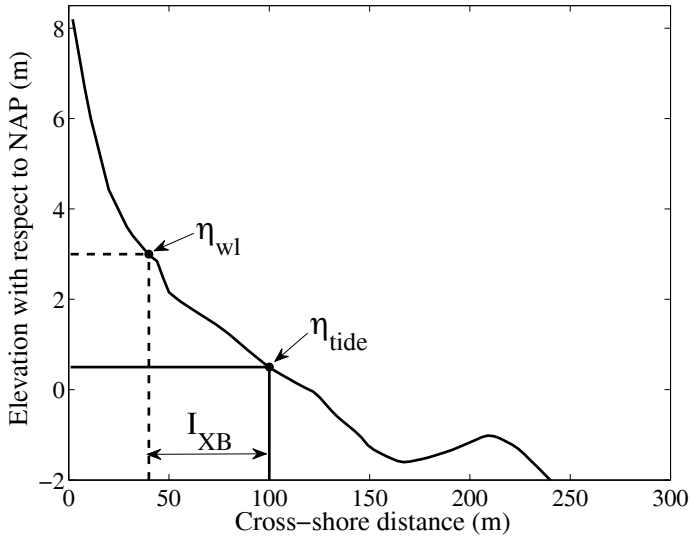

Figure 4.4: Example of the methodology used to calculate the modeled inundation (I_{XB}). η_{wl} is the water level at the waterline and η_{tide} is the astronomical tide level.

Finally, the horizontal inundation, (I_{XB}), was obtained following a similar procedure to that with the video observations. The modeled inundation is defined as the horizontal distance between the location of the water level, η_{wl}, and the location of the corresponding astronomical tide (see Figure 4.4).

4.4 Results and discussion

4.4.1 Inundation observed

The seven storms selected were characterized by wave directions from west to north-northwest, surge levels from 0.5 to 1.3 m and wave heights from 1.5 to 3.5 m. The inundation was smallest during Events 1 and 4 (maximum alongshore-averaged observed inundation $\bar{\mathrm{I}}_o \approx 90$ m, Figure 4.5a,d) and largest during Events 3 and 6 (maximum $\bar{\mathrm{I}}_o \approx 105$ m, Figure 4.5c,f). In general, the inundation was alongshore non-uniform before the peak of each storm, except for Event 3, and alongshore uniform during and after the peak of the storm. This alongshore non-uniform inundation resulted from alongshore non-uniformity in the intertidal bars that was present before the storm. As can be seen in Figure 4.6, the alongshore shapes of the intertidal bar existing some days before the beginning of Event 1 and the waterlines before the peak of storm had the same alongshore variation. After the peak of the storm, both were uniform. Owing

to the long storm duration (>30h), large H_{rms} ($\geq$2m) and large positive surge levels (η_{surge} $\geq$0.5m), the intertidal bars are likely to be destroyed during each storm, as previously observed (Quartel et al., 2007), causing the inundation to become more uniform alongshore. For this reason, Events 2 and 3, which were two consecutive northwest storms separated by approximately three days only, differed in behavior. The time span between Events 2 and 3 was too short for intertidal sandbars to form and hence the inundation during Event 3 was far more uniform prior to its peak than it was during Event 2.

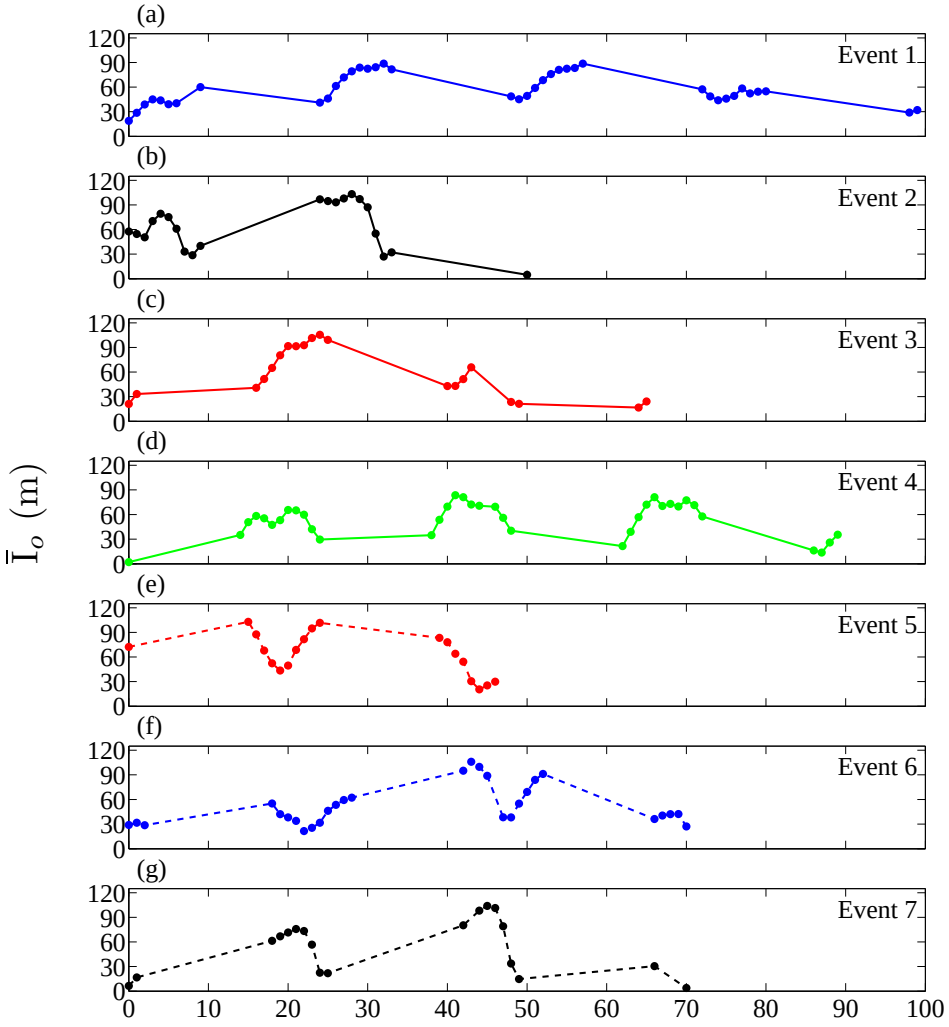

Figure 4.5: Temporal evolution of the alongshore-averaged observed inundation ($\bar{I}_o$) in each storm event: (a) Event 1; (b) Event 2; (c) Event 3; (d) Event 4; (e) Event 5; (f) Event 6; (g) Event 7.

The averaged inundation observed for the i-th beach profile ($\mathrm{I}_{o_{i,j}}$) in each storm event (j) is shown in Figure 4.7. Generally, the inundation decreased from the southern profiles (i =-900) towards the southern profiles (i =-100). Event 3 showed the most homogeneous inundation alongshore (as explained above), while the NNW Event 7 exhibited a different alongshore behavior of the inundation, the southern profiles showing the least inundation and the northern profiles the greatest inundation. This change in the general alongshore pattern in the inundation is probably linked to the proximity of the inner bar to the shoreline. In Event 7, the proximity of the inner bar to the shoreline increased from the northern section to the southern section of Noordwijk.

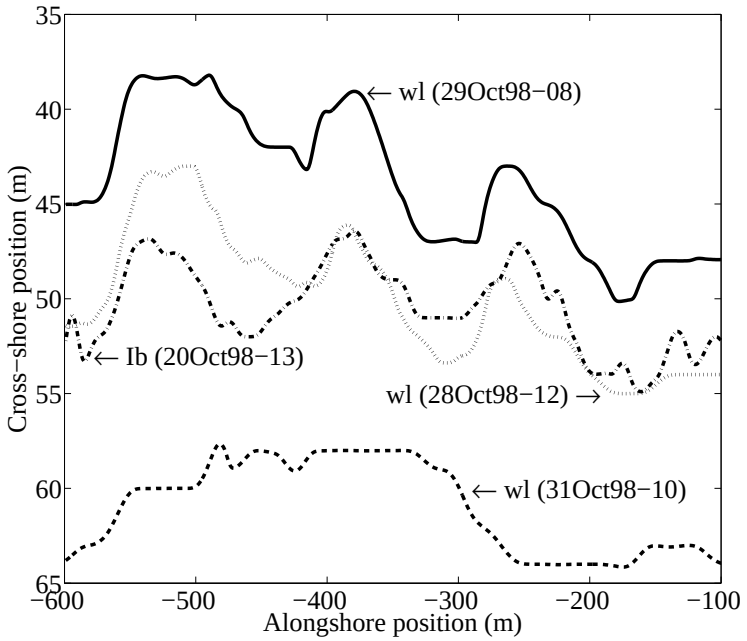

Figure 4.6: Waterlines and intertidal bar line during Event 1 (October, 1998).

The temporal evolution of the alongshore-averaged observed inundation for each storm event ($\bar{\mathrm{I}}_o$) is shown in Figure 4.5. The temporal evolution of $\bar{\mathrm{I}}_o$ during a storm followed a similar pattern which depended on the astronomical tide. For similar surge levels and wave heights, the inundation values were lower during high tide than low tide. For instance, during Event 7 the $\bar{\mathrm{I}}_o$ was 20 m and 103 m at high and low tide, respectively (Figures 4.5g and 4.8). Brown et al. (2007) suggested that the coastal inundation can be severe during storm surge events, particularly when they coincide with a high tide and result in overtopping and breaching. However, overtopping and/or breaching did not occur during the

storms studied. According to the results during high tide conditions, inundation was less than during low tide. An explanation for this would be that during these conditions the waterline is located in the supratidal zone of the beach, where the slope is twice as high as the intertidal beach slope and therefore less inundation could occur.

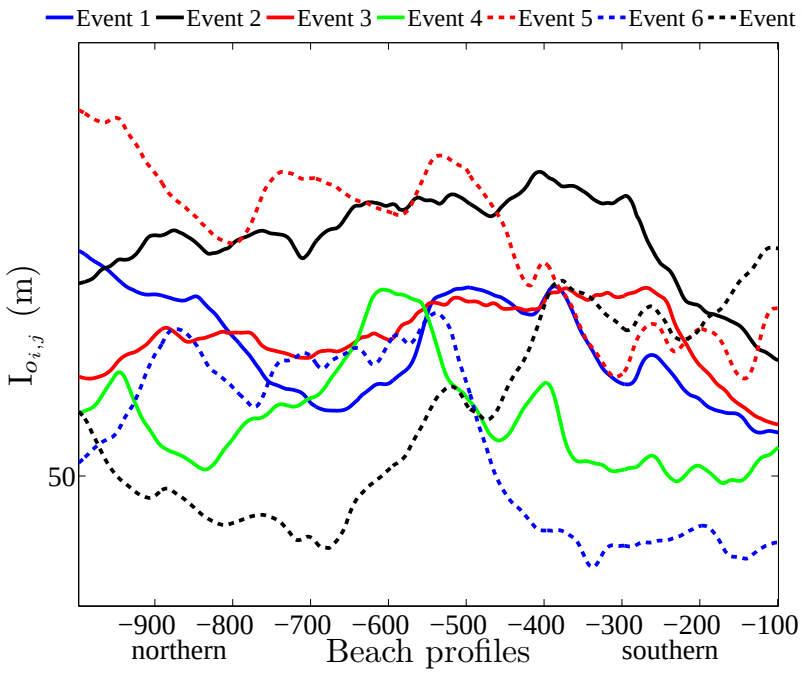

Figure 4.7: Average inundation observed for each beach profile in each storm event ($I_{o_{i,j}}$).

4.4.2 Inundation parameter

The inundation predicted using Equation (4.1) slightly underpredicted the observed inundation. The correlation coefficient squared (R^2) between the alongshore-averaged observed inundation ($\bar{I}_o$) and the predicted inundation (I_p) considering all the events amounted to 0.77 and the root-mean-square difference between observations and predictions (rmse) was 11.70 m (Figure 4.9). In more detail, Event 3 resulted in the highest correlation, R^2 = 0.91 (rmse = 8.84 m), and Event 4 in the lowest, R^2 = 0.65 (rmse = 12.36) (Table 4.4). Event 4 was characterized by a constant northwest wave direction and wave heights and surge level values were approximately constant during the event, but it produced the lowest correlation. The reason for this is not well understood but it could be a combination of the high incidence wave angle and the lower surge levels and wave heights.

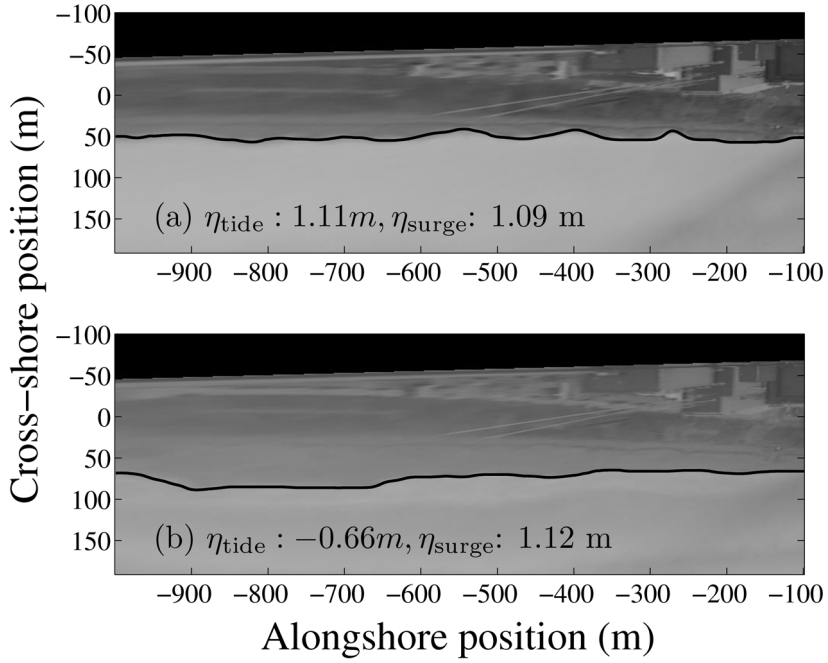

Figure 4.8: Inundation for Event 7 at high tide (a) and at low tide (b). Positions are given in Argus coordinates.

Event	$\bar{\mathrm{I}}_o$ vs. I_p					
	$\beta(\mathrm{H_0L_0})^{0.5} + \eta_{\text{surge}}$		η_{surge}		$\beta(\mathrm{H_0L_0})^{0.5}$	
	R^2	rmse (m)	R^2	rmse (m)	R^2	rmse (m)
1	0.90	5.97	0.54	13.15	0.39	14.86
2	0.87	9.56	0.90	8.32	0.39	20.39
3	0.91	8.84	0.92	8.67	0.39	23.43
4	0.65	12.36	0.58	13.47	0.24	18.18
5	0.86	9.53	0.84	10.44	0.35	20.83
6	0.67	14.29	0.39	19.23	0.45	18.32
7	0.69	17.88	0.79	14.96	0.14	30.06

Table 4.4: Accuracy of the inundation parameter, I_p, including terms in Equation (4.1).

Finally, the R^2 and the rmse between the observed inundation (I_o) and the predicted inundation (I_p) along Noordwijk beach showed similar values in all storm events except for Events 4, 5 and 6. The most drastic change in the correlation coefficient along the beach was observed in Event 6, in which the R^2 decreased from 0.75 ($\mathrm{rmse} \approx 12$ m) to 0.45 ($\mathrm{rmse} \approx 17$ m) along a distance of approximately 350 m (Figure 4.10). The inundation parameter (4.1) considers the same intertidal (β_{int}) and supratidal (β_{sup}) beach slope along the beach but different in

each storm event. In Event 6, for lower water levels (lower surge values and low tide), the inundation was considerably higher for the northern beach profiles than for the southern ones. Under these conditions Equation (4.1) considers only β_{int}, which is mainly controlled by the inner bar. From the images, the inner bar is located more onshore in the northern profiles than in the southern profiles and for this reason β_{int} should be lower in the northern profiles. However, the use of a constant beach slope alongshore means that this effect is not considered in I_p, which explains the alongshore differences in R^2 and rmse in Event 6.

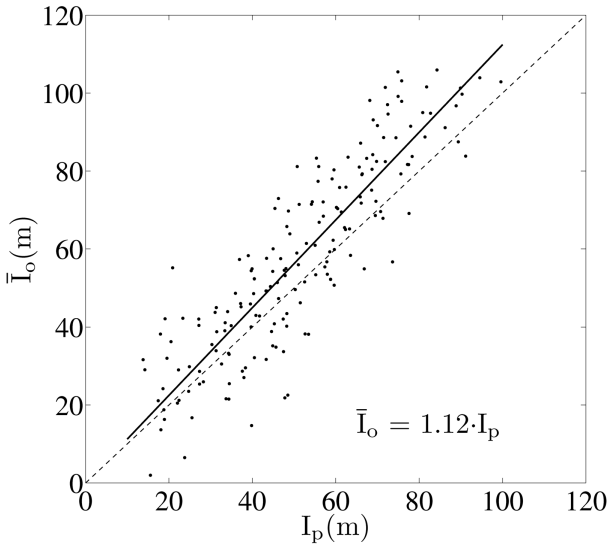

Figure 4.9: Inundation parameter (I_p) versus alongshore-averaged observed inundation ($\bar{\mathrm{I}}_o$). Solid line represents the best fit to the data and dashed line is a 1:1 line

In order to evaluate the contribution of the wave runup and the surge processes in the inundation at Noordwijk, both terms were independently correlated with the alongshore-averaged inundation considering all the storm events (Table 4.4). Considering only the surge level term, the correlation was R^2 = 0.62 ($\mathrm{rmse} \approx 14$ m), whereas considering only the runup term, the correlation decreased to R^2 = 0.31 ($\mathrm{rmse} \approx 20$ m). This suggests that events depended mainly on surge levels. Analyzing event by event, the correlation in most events was more or less equal (Events 2, 3, 4, 5), though it was worse for Events 1 and 6 and better for Event 7 (R^2 = 0.79, $\mathrm{rmse} \approx 15$ m) when only the surge level was considered (Table 4.4). Event 7 is characterized by a north-northwestern wave direction, which is the direction from which the largest waves arrive (Wolf and Flather, 2005; Quera, 2010). In the North Sea, winds from these directions produce large surge and this

will therefore explain the better correlation when the inundation parameter only includes the surge level.

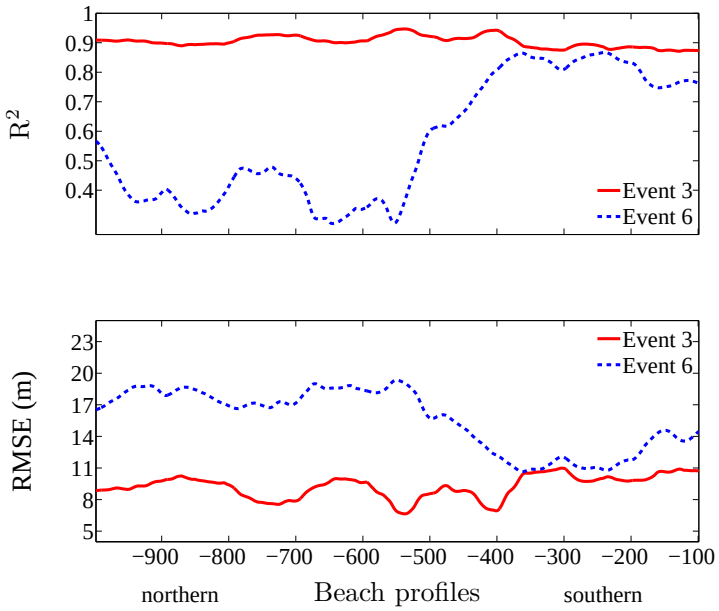

Figure 4.10: Correlation-coefficient squared (R^2) and root-mean-square difference (RMSE) between the observed inundation (I_o) and the predicted inundation (I_p) for each beach profile in Events 3 and 6.

4.4.3 Inundation modeled

The wave height and the water level of the storm of October 1998 were well reproduced at the offshore boundary of each beach profile, except for a few hours at the peak of the storm in which H_{rms} was slightly lower than the H_{rms} input (Figure 4.11). The modeled root mean square wave height at the three control points (the location of these control point was at the outer bar crest and inner bar crest and trough) for the barred and the barless profiles is shown in Figure 4.12. It is noted that in the barless profile the control points were selected at the same location as in the barred profile BP245 (1998) on which it was based. The H_{rms} at the three control points depended on the depth of the bar crest and trough. Thus, the deeper (shallower) the bar crest/trough was, the higher (lower) the H_{rms} was. The maximum H_{rms} was found at the control points of the barless profile (WBAR). The maximum difference in the H_{rms} between the barless and the barred profiles was 0.5 m. Among the barred profiles, the highest and the lowest H_{rms} at the outer bar crest was found in the beach profile which had the deepest (BP335 (2005)) and shallowest (BP335 (1999)) outer bar crests, respectively

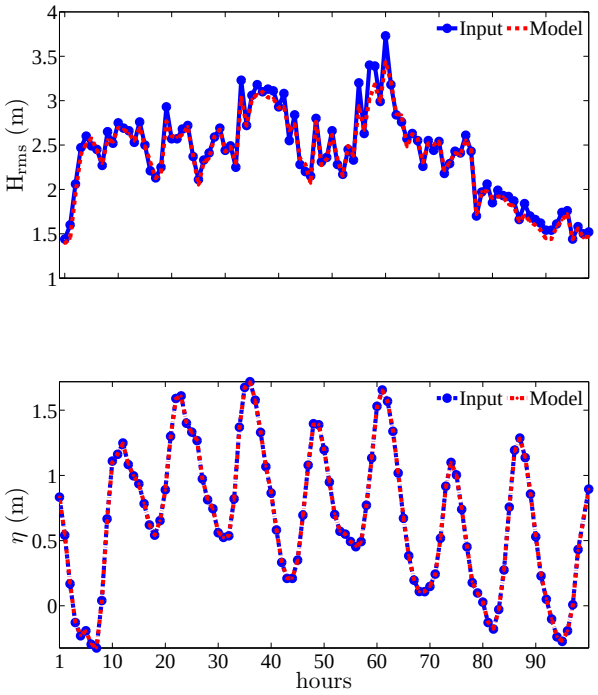

Figure 4.11: Time series of the input and modeled offshore root-mean-square wave height,H_{rms}
(top) and water level, η, (bottom) for the storm of October 1998.

(Figure 4.12a). At the inner bar crest and trough the highest H_{rms} was observed in the beach profile with the worst-developed inner bar (BP335 (2005)) (Figure 4.12b and c) and the lowest H_{rms} was observed at the beach profile with the widest inner bar and the shallowest bar trough (BP750 (1998)). The differences in H_{rms} in the barred profiles, without considering the beach profile BP335 (2005), were lower ($\approx$0.10 m).

The water levels at the three control points were higher for the barred profiles than for the barless profile, although the differences were small ($\approx$10 cm). The water level obtained at these controls points is composed of the surge and the astronomical tide (both terms are constant in all beach profiles), and also the wave setup. Because the wave setup is usually generated during energy dissipation over the bars (Stephens et al., 2011), at the control points of the barred profiles the wave setup should be higher, explaining the slightly higher water levels values at the barred profiles than at the barless profile. The modeled water level at the waterline (η_{wl}) varied between approximately 0.18 and 3 m with respect to the NAP and the maximum water level was found at the peak of the storm (Figure 4.13a). Quite the opposite, η_{wl} was higher at the barless profile than at the barred

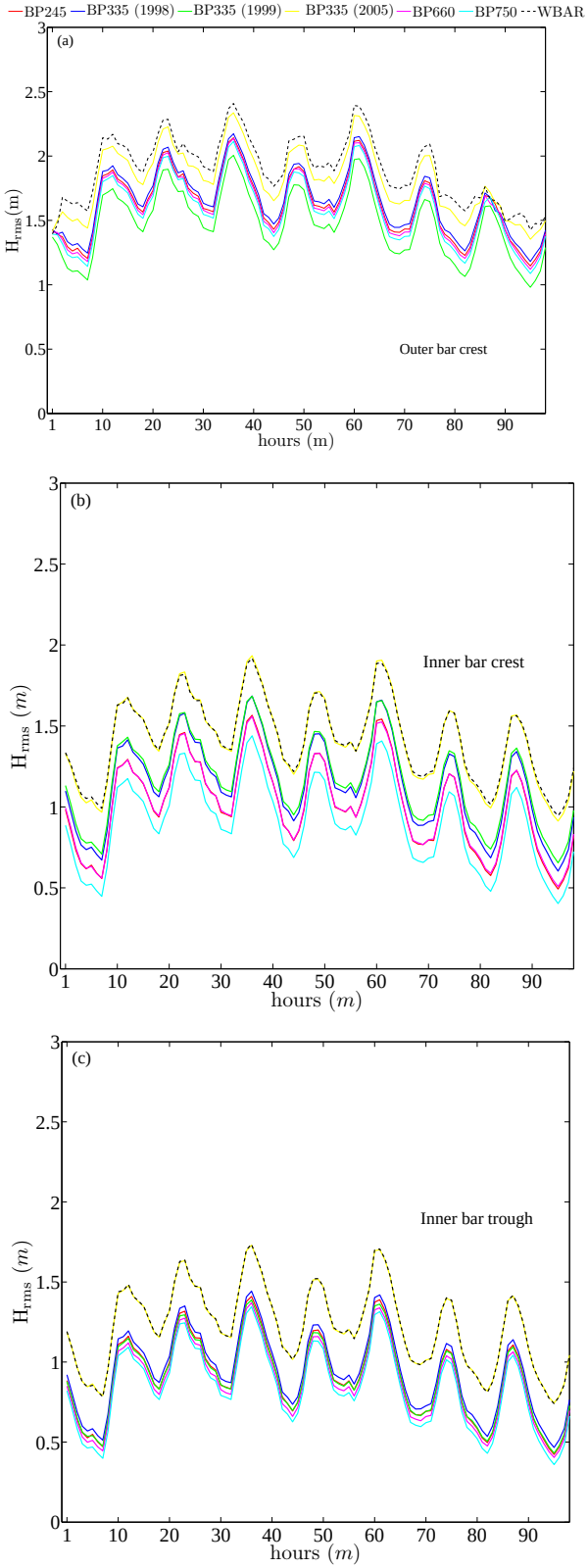

Figure 4.12: Averaged 3600-s time series of the modeled offshore root mean square wave height, H_{rms}, at different locations of the barred profiles and barless profile: (a) outer bar crest; (b) inner bar crest; (c) inner bar trough.

profiles but the differences were small (less than 20 cm). The lower water level in the barred profiles is probably due to the higher wave dissipation in these profiles than in the barless profile. At the peak of the storm (H_{rms} = 3.73 m, T_p = 9.49 s) the highest differences in η_{wl} between the barred profiles and the barless profile (WBAR) were found and ranged from 8 cm (BP750 (1998)) to 44 cm (BP245 (1998)) (Figure 4.13b).

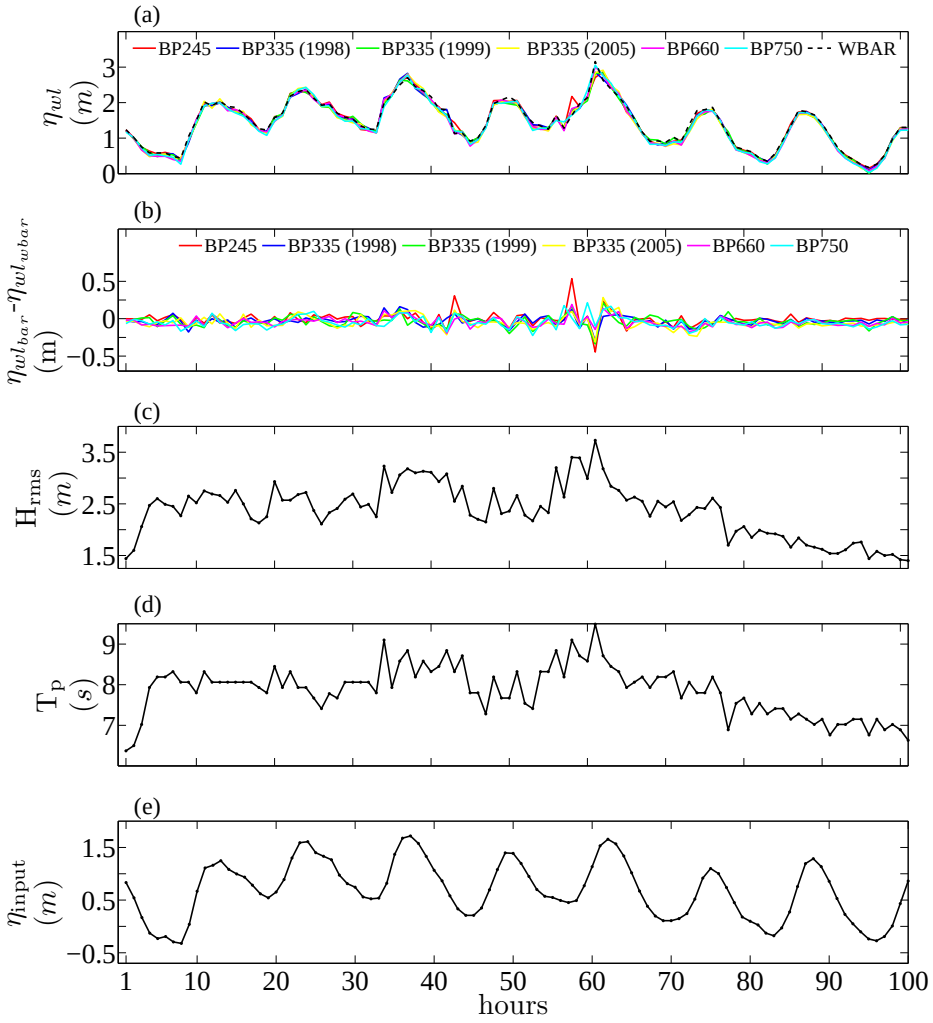

Figure 4.13: Hydrodynamic conditions of the storm of October 1998 and the modeled water level at waterline. (a) Modeled water level at the waterline time-series, η_{wl}, for each beach profile; (b) difference of the water level at the waterline between the barred profiles ($\eta_{wl_{bar}}$) and the barless profile ($\eta_{wl_{wbar}}$); (c) input offshore root-mean-square wave height, H_{rms}, time-series; (d) input peak period, T_p, time-series ; (e) input water level time-series, η_{input};

The inundation modeled after eliminating the astronomical tide (I_{XB}) varied between 9 and 105 m (Figure 4.14). The maximum inundation values were ob-

served in the beach profile with a well-developed intertidal bar, a slightly developed inner bar and the deepest outer bar (BP335 (2005)), while the minimum inundation values were observed in the beach profile with the widest inner bar close to the shoreline (BP750 (1998)). Intermediate inundation values were observed in the barless profile (WBAR) and in the barred profiles with the narrowest inner bar but with the highest bar crest (BP245 (1998) and BP335 (1998)). The magnitude of the inundation depended on the astronomical tide, in particular for the barred profiles with a well-developed intertidal bar and with a wide inner bar close to the shoreline (BP335 (2005), BP660 (1998) and BP750 (1998), respectively). In these profiles, the inundation was considerably higher at low tide than at high tide. Among all the beach profiles analyzed, at high tide the highest (54 m) and the lowest (9 m) inundation observed was in the beach profiles with the furthest and the closest inner bar to the shore, respectively (BP335 (1999) and BP750 (1998)). At low tide the highest (105 m) and the lowest (12 m) inundation observed was in the beach profiles with a well-developed intertidal bar and a slightly developed inner bar (BP335 (2005)) and the beach profile with the most seaward inner bar (BP335 (1999)), respectively.

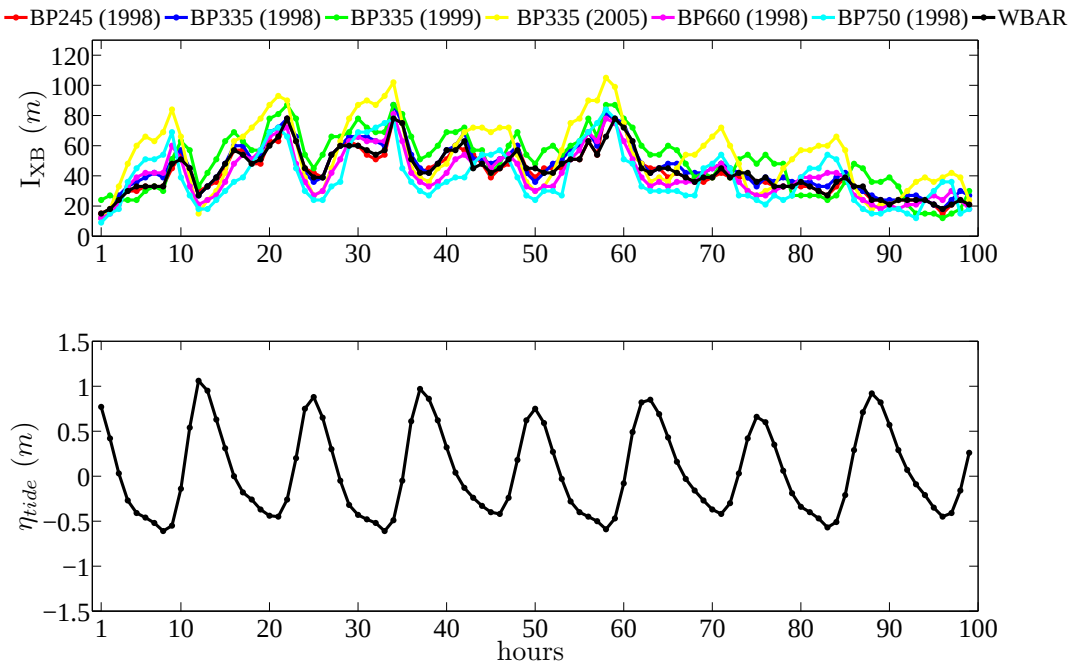

Figure 4.14: Top, temporal evolution of the inundation modeled (I_{XB}) of the storm of October 1998 for the different beach profiles. Bottom, time-series of the astronomical tide (η_{tide}) during the same storm.

The I_{XB} was similar for the barred profiles with the narrowest inner bar but with the highest bar crest (BP245 (1998) and BP335 (1998)) and for the barless profile (WBAR). It is noteworthy that these Noordwijk profiles only differed from the WBAR profile by the sandbars. The barless profile was equal to BP245 from -2 m to 8 m depth. As inundation, after removing the astronomical tide, depends on the shape of the beach profile, these similar inundation values for BP245 (1998), BP335 (1998) and WBAR are to be expected.

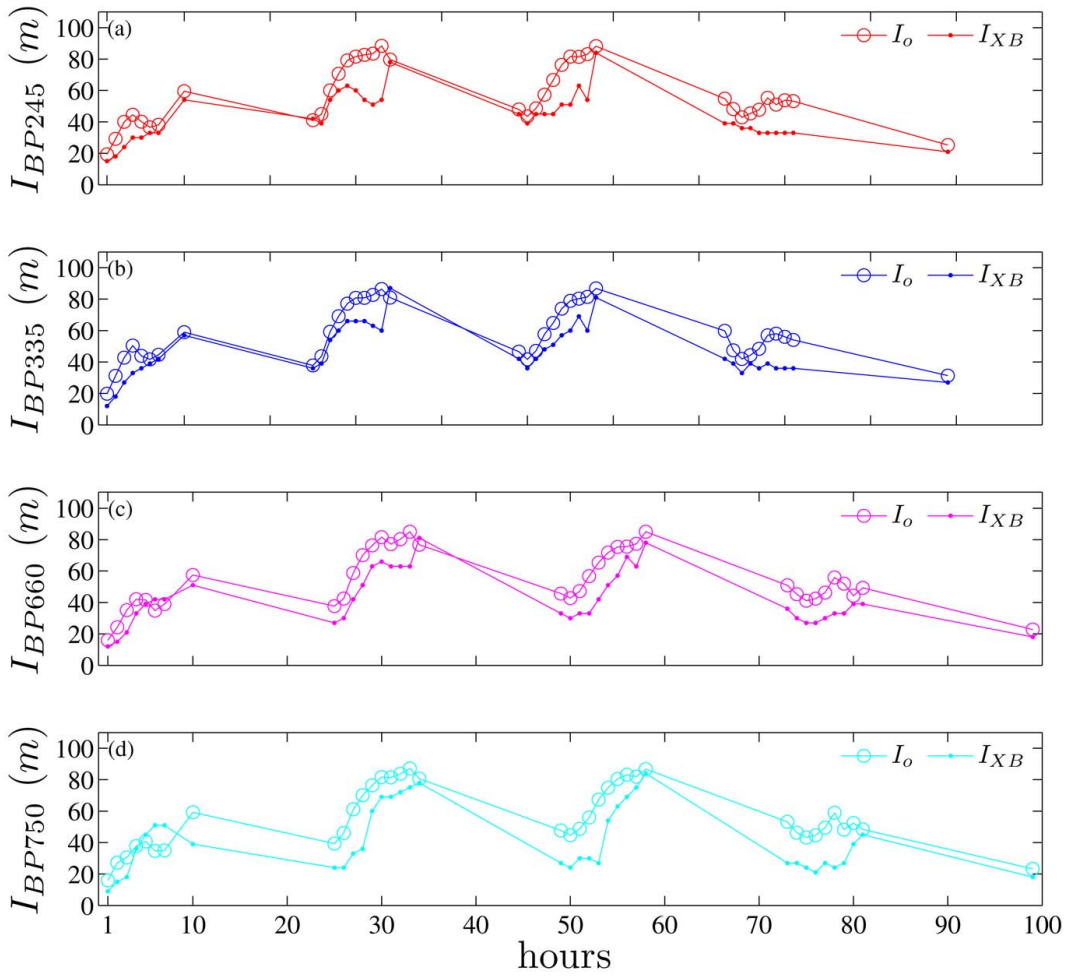

Figure 4.15: Modeled (I_{XB}) and observed (I_o) inundation during the storm of October 1998. (a) Inundation at the beach profile BP245 (1998) (I_{BP245}); (b) Inundation at beach profile BP335 (1998) (I_{BP335}); (c) Inundation at beach profile BP660 (1998) (I_{BP660}); (d) Inundation at beach profile BP750 (1998) (I_{BP750}).

The differences in the inundation between the barred beach profiles highlighted the importance of the proximity of the inner bar to the shore and, especially, the existence of an intertidal bar if the inner bar is located further offshore. Hence,

beach profiles with a wide inner bar close to the shore (BP660 (1998) and BP750 (1998)) exhibited similar inundation behavior to the beach profile characterized by a more seaward inner bar and a very well-developed intertidal bar (BP335 (2005)). If the morphological changes during this storm were considered, the inundation behavior might be different because of the reset of the intertidal bars under certain storm conditions. On the other hand, in the beach profile characterized by the absence of an intertidal bar and a deeper inner bar inundation was higher than in the other barred profiles (BP335 (1999)).

The comparison between the modeled inundation ($\mathrm{I_{XB}}$) and the observed inundation ($\mathrm{I_o}$) for the Noordwijk beach profiles showed that XBeach underestimated the inundation (Figure 4.15) except during a few hours at the beginning of the storm, in which the inundation was overestimated (between 7 and 17 m depending on the beach profile). The differences between $\mathrm{I_o}$ and $\mathrm{I_{XB}}$ were lower at the beginning of the storm than during the highest-energy conditions of the storm (maximum difference, $\approx 30m$, was observed at BP750 (1998)). The best correlation between $\mathrm{I_o}$ and $\mathrm{I_{XB}}$ was found for beach profile BP335 (1998) (Table 4.5). The reasons for the differences between the observed and modeled inundation could be that the bathymetry used in the simulations corresponds to some months before (during the summer season), that the morphology did not vary during the simulations, and that the 1D simulations disregarded the alongshore variability effects. When the bathymetry was done, the inner bar had an irregular shape (van Enckevort and Ruessink, 2003b), whereas previous to the storm it had a crescent shape. Additionally, the storm caused the straightening of the inner bar during the most energetic conditions, and three days later it evolved to a crescent shape. Therefore, the discrepancies between the observed inundation and the inundation obtained from the XBeach model emphasize the importance of the three-dimensional features of the bars.

Beach profile	m	$\mathrm{R^2}$	RMSE (m)
BP245 (1998)	1.29	0.72	10.07
BP335 (1998)	1.21	0.79	8.11
BP660 (1998)	1.25	0.77	8.94
BP750 (1998)	1.24	0.38	15.57

Table 4.5: Accuracy of the inundation modeled using the XBeach

4.5 Conclusions

A methodology for calculating the inundation during storms in a sandy multiple-bar microtidal beach using video observations has been developed and applied to the seven severest storms affecting Noordwijk beach in the Netherlands during the period 1998-2005. The inundation subtracting the astronomical tide effects varied between 22 and 105 m and was non-uniform alongshore prior to the peak of a storm because of alongshore variations in the intertidal sandbars. During the peak of the storm, most of the intertidal sandbars disappeared and the inundation then became more uniform alongshore.

The inundation was higher at low tide than at high tide for similar surge levels because of the change in slope of the beach profile. During high tide, the inundation took place in the upper part of the beach profile, where the beach slope is twice as high as on the intertidal beach slope, so the inundation was lower.

The inundation at Noordwijk beach during the storm surge of October 1998 was modeled using XBeach, considering six barred beach profiles and a synthetic beach profile without sandbars. The inundation was only affected by the morphology close to the shoreline, that is by the intertidal bars or by the inner bar if it is wide and closer to shoreline. The outer bar does not seem to influence the inundation behavior.

The XBeach model underestimates the inundation disregarding the astronomical tide at Noordwijk because the morphological changes are not considered in the simulation. Further 2D simulations using a time-varying morphology, different hydrodynamics conditions, and three-dimensional features of the bars are now needed to understand better the role of sandbars on inundation and to confirm that inundation is underestimated if the morphological changes during the storm are not considered.

Finally, the simple inundation parameter, I_p, which includes a runup expression and the surge level, estimated the observations reasonably well and indicated that the surge level is the main factor influencing the magnitude of the inundation at these beaches.

Chapter 5

BEACH INUNDATION PREDICTION DURING STORMS AT A TIDELESS EMBAYED BEACH

Edited version of A. Sancho-García, J. Guillén and G. Simarro. Beach inundation prediction during storms at a tideless embayed beach. Submitted to Coastal Engineering.

5.1 Introduction

Coastal regions are frequently subject to inundation produced by storms. Storm-induced inundation is due to the sum of astronomical tide, surge level and wave runup. The surge levels are dependent on changes in the atmospheric pressure (*e.g.*, low pressure systems) (Ciavola et al., 2011) and are largely affected by the bathymetric characteristics of the continental shelf (width and depth) (del Rio et al., 2012). In the tideless Mediterranean sea, surge levels as a whole are likely to be much lower because of the much greater water depth (Wolf, 2009), so wave runup may be the main process controlling beach inundation during storms (Bosom and Jimenez, 2011).

Wave runup is defined as the time-varying location of the waterline about still water level. It can be decomposed into *setup*, a steady elevation of mean water level, and *swash*, fluctuations about the setup level (Guza and Thornton, 1982). Further, the swash signal has two different energy components: the *infragravity* component, which dominates the swash signal on dissipative beaches (Ruessink et al., 1998; Ruggiero et al., 2004; Stockdon et al., 2006), and the *incident* component, which dominates the swash signal on reflective beaches (Stockdon et al., 2006).

Proposed runup formulas have been based on laboratory experiments (Hunt, 1959; Battjes, 1974; Mase, 1989; Roberts et al., 2010), on model computations (Guza and Feddersen, 2012) and on field studies (Guza and Thornton, 1982; Holman and Sallenger, 1985; Holman, 1986; Nielsen and Hanslow, 1991; Douglas, 1992; Ruessink et al., 1998; Ruggiero et al., 2001, 2004; Stockdon et al., 2006; Salmon et al., 2007; Bryan et al., 2009; Vousdoukas et al., 2009; Guedes et al., 2011; Senechal et al., 2011; Mather et al., 2011; Vousdoukas et al., 2012). Most of the field studies were accomplished on natural, sandy, open oceanic macrotidal beaches affected by the surge level, and their morphological states ranged from reflective to dissipative. The studies are site-specific, with the exception of the one by Stockdon et al. (2006), which includes beaches located in different coastal environments. All the above-mentioned studies disregard the wave direction.

Few of the above studies focus on embayed beaches. The studies by Salmon et al. (2007), Bryan et al. (2009) and Guedes et al. (2011) were carried out on

the same natural, microtidal embayed beach located in New Zealand; the study by Vousdoukas et al. (2009) was carried out on three narrow and microtidal sediment-starved pocket beaches of Lesbos Island (NE Aegean Sea, Greece); and the study by Mather et al. (2011) was carried out on several natural embayed beaches of South Africa with a wave climate influenced by tropical cyclones. However, to our knowledge, no runup study has been done on artificial and tideless embayed beaches characterized by large protection structures (*e.g.*, dikes and breakwaters), where wave transformation processes such as diffraction can be important.

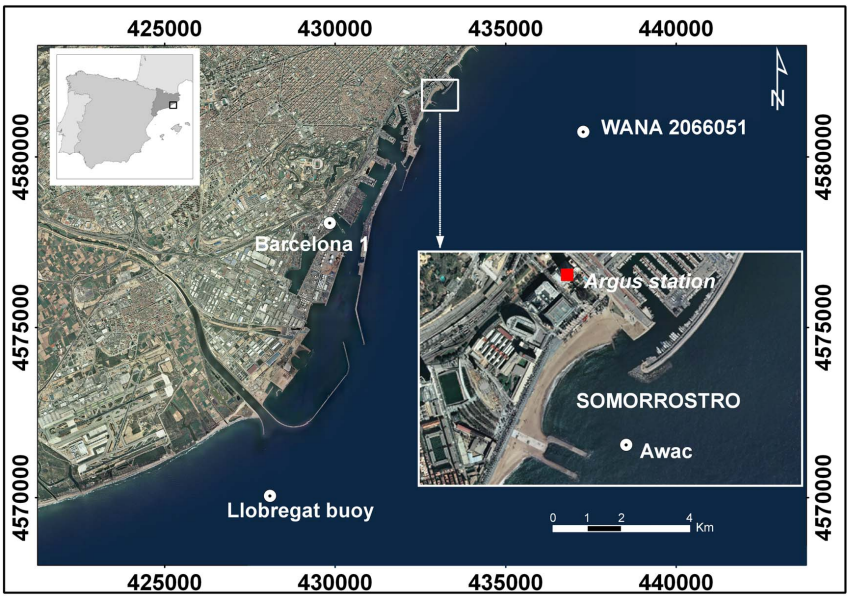

Figure 5.1: Study area: Argus station (red square), 'Barcelona 1 tidal gauge, Llobregat deep-water buoy, WANA node 206601 and AWAC local wave sensor. The orthophotos are copyright of the ICC, and are available at www.icc.cat.

The aim of this chapter was to evaluate the runup formulation of Stockdon et al. (2006) (hereinafter Stockdon's formulation), using different wave heights as input for predicting coastal inundation during energetic storm conditions at Somorrostro, an artificial, tideless and steep embayed beach in Barcelona (Spain). Besides using deep water conditions as proposed by Stockdon et al. (2006), we also consider using the wave conditions near the shore to account for wave transformation processes. The data set employed for our purpose comprised eight years of video observations (from 2001 to 2008) and 20 selected storms with different wave directions. The wave height data set was composed of wave measurements

in deep waters, the wave measurements at a water depth of 10 m, the wave conditions at the latter location as propagated from deep waters using the Coastal Modeling System (hereafter SMC from the Spanish "Sistema Modelado Costero") by Gonzalez et al. (2007), and the wave breaking height given by SMC.

5.2 Field site

Somorrostro beach is located in the city of Barcelona, on the southern coast of Catalonia, Spain, in the western Mediterranean Sea (Figure 5.1). Barcelona has a coastline 13 km long, containing the city harbor in the southernmost part, three marinas and 3 km of beaches. Barcelona's beaches are artificial and were created as a part of the urban renewal that took place in the zone for the 1992 Olympic Games. This study focuses on Somorrostro beach, a non-barred beach bounded to the north by the Olympic Marina and to the south by a double dike. The beach is 400 m long and is oriented N32E. The tidal range is less than 20 cm and waves are the main stirring mechanism controlling coastal evolution (Ojeda et al., 2008). The beach has a steep slope (β_f): on average $\beta_f \simeq 0.080$, increasing slightly from south to north.

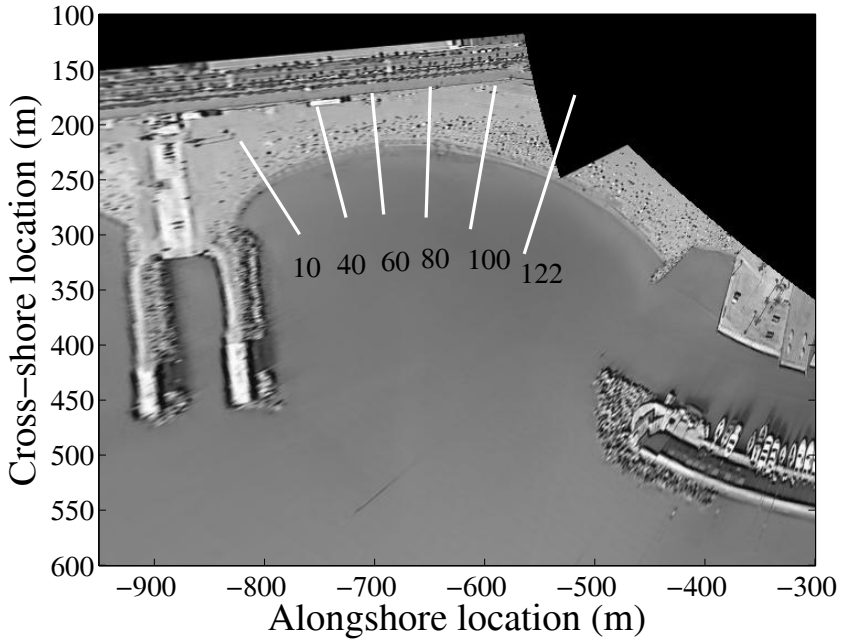

Figure 5.2: Argus plan view with the locations and the numbering of the control profiles.

5.3 Material and methods

5.3.1 Wave and tidal data

The runup parameterization was evaluated using three different wave heights: 1) deep water measurements from the Llobregat buoy (www.xiom.cat, denoted here with subindex "0"); 2) local wave measurements (denoted with "1"); and 3) local wave computations propagating the Llobregat buoy conditions shorewards using the SMC (denoted with "2" and "b", as detailed below).

The Llobregat buoy (see Figure 5.1) is located at a depth of 45 m and has provided wave height since 2001 and wave direction and peak period since 2004, recording data every hour. Interruptions in the buoy time series and the lack of the wave direction before 2004 were filled in using data from the WANA model (node 2066051, Figure 5.1), which provides directional wave information every three hours. The WANA data has been computed by the Spanish National Institute of Meteorology using the HIRLAM and WAM numerical models since 1991 (Spanish Port Authority, www.puertos.es). Wave height data from the WANA model were calibrated through linear regression using the buoy measurements from October 2001 to December 2008 ($r-$squared = 0.70). Before 2004 the wave peak period (T_p) was obtained using a calibration between the wave significant period ($\mathrm{T}_{1/3}$) and the wave peak period for the period 2004-2008 ($r-$squared = 0.62). The wave direction data were not calibrated because a very poor relationship was found.

All the storm events between 2001 and 2008 with maximum significant wave height (H_0) above 3 m at the Llobregat buoy and wave directions from NE to S were selected for the study (Table 5.1). A threshold of 1 m for each storm event was used to establish the initial and final days. Some additional events (13, 15 and 16 in Table 5.1) were selected for a better examination of the influence of wave transformation processes on beach inundation predictability.

Local wave measurements were provided from a Nortek AWAC acoustic doppler current profiler (hereinafter denoted as AWAC) from the Coastal Ocean Observatory (COO) situated at 10 m depth near the exit of the Olympic Marina (Figure 5.1). The wave measurements (significant wave height, H_1, and peak

period, T_{p1}) were available from May 2005, although some interruptions occurred during this time (*e.g.*, during Event 20). The wave direction (θ_1) was available from March 2007. The AWAC also provides the pressure of the water column.

Event	initial date	$\mathrm{H}_{0,\max}\,(\mathrm{m})$	$\mathrm{T}_{p,\mathrm{H}_{0,\max}}\,(\mathrm{s})$	$\theta_{\mathrm{mean}}\,(^\circ)$	data available
1	13/12/2001	3.16	9.83	67	H_0
2	03/01/2002	3.34	10.20	111	H_0
3	11/04/2002	3.15	10.44	108	H_0
4	06/05/2002	3.79	11.01	114	H_0
5	13/10/2003	4.11	9.96	105	H_0
6	28/10/2003	4.09	9.71	178	H_0
7	07/12/2003	3.15	8.98	98	H_0
8	20/02/2004	3.25	7.70	120	H_0
9	27/03/2004	3.39	9.10	105	H_0
10	15/04/2004	3.27	10.00	119	H_0
11	01/12/2005	3.81	10.00	197	H_0, H_1
12	09/12/2005	2.12	6.20	97	H_0, H_1
13	27/01/2006	3.01	10.00	96	H_0, H_1
14	18/03/2006	2.35	9.10	97	H_0, H_1
15	03/05/2006	2.39	9.10	115	H_0, H_1
16	27/03/2007	3.26	7.70	93	H_0
17	20/10/2007	3.09	8.30	79	H_0
18	15/12/2007	3.50	10.00	88	H_0, H_1
19	08/05/2008	2.77	8.30	136	H_0, H_1, H_2, H_b
20	25/12/2008	4.65	12.50	94	H_0, H_2, H_b

Table 5.1: Characteristics of the storm events analyzed.

The wave transformation processes from the Llobregat buoy to Somorrostro beach were modeled for several hours of Events 19 and 20 using the SMC. The simulations presented here were carried out with the *Oluca-SP* package, based on spectral analysis. This model includes the effect of shoaling, refraction, energy dissipation (bottom friction and wave breaking), diffraction and wave-current interaction (Gonzalez et al., 2007). The same bathymetry and grid were used for both events, with a horizontal resolution of 10 m. Two different wave heights were recorded from SMC: the wave height at the location of the AWAC (H_2) and the breaking wave height for six control beach profiles in Figure 5.2 (H_b), but in this case only for Event 19, for which, through the wave height gradient, the model showed that the waves were breaking at depths below 3 m. Therefore, H_b

is an approximation of the significant breaking wave height.

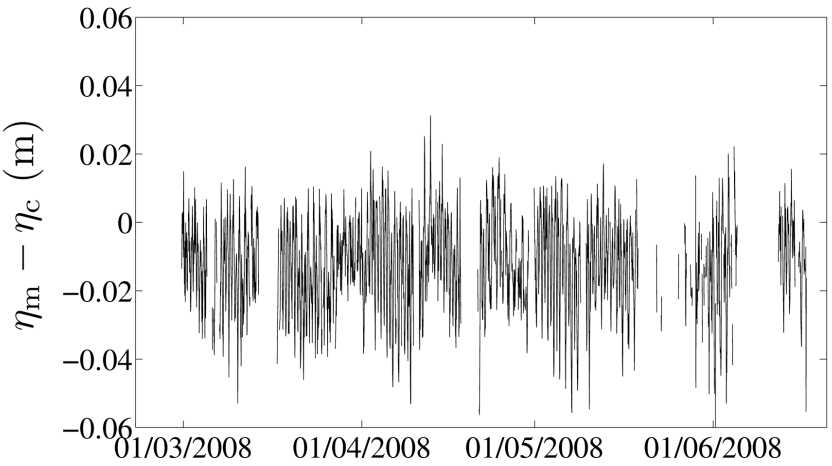

Figure 5.3: Difference ($\eta_{\mathrm{m}} - \eta_{\mathrm{c}}$) between tide measurements from the Barcelona 1 tide gauge (η_{m}) and the tidal variations calculated using the AWAC measurements and the meteorological data (η_{c}).

Some authors (Vousdoukas et al. (2012) among others) have suggested that the runup prediction capability improves when the shore-normal wind speed component and the tidal elevation are included in the parameterization. Here we consider the astronomical and surge tides, therefore including wind effects. The total tide, η, a combination of astronomical and surge tides, was obtained in two different ways. First, tide measurements were obtained from the *Barcelona 1* tide gauge deployed at the Barcelona harbor (Spanish Port Authority www.puertos.es, Figure 5.1), recording from January 1992 to November 2008 with a few interruptions. In December 2008, this gauge was replaced and no calibrated tidal measurements were available thereafter. Second, the tidal variations were estimated using the pressure from the AWAC and the atmospheric pressure from a meteorological station close to Somorrostro (COO). The two results showed very good agreement (Figure 5.3), with $r-$squared = 0.98 and a root mean square error $(\mathrm{RMSE}) = 13\,\mathrm{cm}$. For simplicity, only the observations from the tide gauge were used, and it should be noted that for Event 20 the tidal measurements were unavailable from both systems.

5.3.2 Observed beach inundation

An Argus Video system (Holman and Stanley, 2007) located atop a building close to the Olympic Marina (Figure 5.1) at a height of around 142 m has been

deployed since 2001 (COO). The Argus station is composed of five cameras pointing at the Barcelona beaches and offering a 180° view of the coast. The images are in the visible range of light and the sampling is done every daylight hour during a ten-minute period (1 picture per second).

The waterline position was obtained hourly from the ten-minute time-exposure (timex) images using the Intertidal Beach Mapper software (IBM, included in the Argus Runtime Environment). During the peak of the storms, some problems were often found in the waterline detection owing to the bad visibility caused by the presence of fog, clouds or rain. Hence, in these moments, and whenever there was a lack of contrast between sand and water, the waterline positions were mapped manually from the images. The image coordinates were transformed to real coordinates following the usual procedures (Holland et al., 1997). In total, our data set comprises 795 waterlines. Because we were using time-averaged images, the obtained waterline position should have captured the effects of sea level (surge and astronomical tides), setup and the mean position of the fluctuations associated with the swash.

The inundation is defined here as the horizontal distance between the waterline position and the initial reference shoreline (IRS) for each event. Each IRS corresponds to a few days before the storm event, when the wave height was less than 0.5 m and the water level was approximately zero. The temporal evolution of the inundation at Somorrostro was measured following 122 profiles along the beach every 2 m; six of them, the "control profiles" (CP, profiles 10, 40, 60, 80, 100 and 122) are shown in Figure 5.2. The profile direction at each point was defined as perpendicular to a reference shoreline (the average of the overall IRS).

5.3.3 Wave runup formulation

Out of the different runup equations in the literature, the formulation by Stockdon et al. (2006) is used here because it was proposed to consider runup observations from beaches with different morphological states. This formulation, which represents the elevation of extreme runup peaks given by the 2% excee-

dence value, considers deep water conditions and reads:

$$\mathrm{R}_{2\%} = 1.10\,(\mathrm{H}_0\mathrm{L}_0)^{0.5}\left(0.35\beta_f + \frac{(0.563{\beta_f}^2 + 0.004)^{0.5}}{2}\right), \qquad (5.1)$$

where H_0 is the deep water significant wave height and L_0 the wavelength corresponding to the peak period (T_p). In deep waters the dispersion relationship is

$$\mathrm{L}_0 = \frac{g\mathrm{T}_p^2}{2\pi}, \qquad (5.2)$$

where $g = 9.8\mathrm{m/s}^2$ is the gravity. In Equation (5.1), β_f is the foreshore beach slope. Following Ruessink et al. (1998), the foreshore slope was defined in a region between the maximum and minimum cross-shore location which can reach the runup (maximum and minimum inundation observed). Sixteen topographic d-GPS surveys were available from 2004 during calm conditions (wave height of less than 0.5 m). An average foreshore slope was calculated for each beach profile using all the available topographic data.

At beaches such as the one under consideration, the influence of the coastal structures on the wave propagation process is essential. For this reason, the runup was also computed with the above expression but using, instead of deep water conditions (H_0 and L_0), the conditions measured with the AWAC (H_1 and L_1) and those computed by propagating deep water conditions to the AWAC position (H_2 and L_2). Above, the values of L_1 and L_2 are computed by iteratively solving the dispersion relationship.

Finally, to further evaluate the potential influence of the local wave transformation processes on the inundation, it was checked in the control profiles whether the runup correlated well directly with the wave height at breaking (H_b).

5.3.4 Comparison of observed and predicted inundation

The inundation observed at Somorrostro is due to the sum of the wave runup (R), astronomical tide (η_{tide}) and surge tide (η_{surge}). The observed inundation (IO)

was compared with the computed inundation (IC)

$$\mathrm{IC} = \frac{\mathrm{R} + \eta_{\mathrm{tide}} + \eta_{\mathrm{surge}}}{\beta_f}, \tag{5.3}$$

where the runup R was parameterized as described in the above paragraphs.

Unlike other studies in which only one cross-shore transect is considered, the alongshore variability was analyzed, and the runup parameterization was evaluated for each beach profile taking into consideration that the foreshore slope and the wave conditions (in the case of H_b) vary alongshore.

We define the difference in the inundation as $\Delta = \mathrm{IC} - \mathrm{IO}$, where IC is the inundation computed using Equation (5.3) and IO is the observed inundation. For the i-th profile, the mean difference considering the observation for the j-th storm will be denoted here as $\Delta_{i,j}$, while the mean difference for the 795 observations corresponding to all the storms will be $\Delta_{i,\,\mathrm{all}}$. In addition to the difference Δ, we used averaged observed inundations ($\mathrm{IO}_{i,j}$ and $\mathrm{IO}_{i,\mathrm{all}}$) similarly.

It should be noted that the morphological changes that occurred during some events caused detectable inaccuracies. During some eastern storms (Events 13, 18 and 20), the observations were considerably higher than the estimations after the peak of the storm for the southwestern beach profiles (contrary to the general trend). This finding is explained by the fact that these storms (especially Event 20) eroded Somorrostro beach considerably, giving higher measured inundation of the beach and producing inaccuracies in the inundation estimations. On the other hand, for some other events (*e.g.*, Event 6) the shoreline accreted after the peak of the storm, resulting in negative inundations. These inundation values were not taken into account.

Finally, it should be pointed out that Stockdon's formulation corresponds to the 2% runup exceedance and must therefore overpredict our observed inundation because we are using time-averaged images (timex) to measure a mean beach inundation (*i.e.*, mean wave runup). The expression by Nielsen and Hanslow (1991)

for the mean wave runup is:

$$\overline{\mathrm{R}} = \begin{cases} 0.98 \cdot 0.05\sqrt{\mathrm{H_{rms}L_0}} & \text{if } \beta_f < 0.1, \\ 0.98 \cdot 0.6\beta_f\sqrt{\mathrm{H_{rms}L_0}} & \text{if } \beta_f \geqslant 0.1. \end{cases} \tag{5.4}$$

where H_{rms} is the offshore root mean square wave height.

Nielsen and Hanslow (1991) also gave an expression for $\mathrm{R}_{2\%}$ which gives approximately twice the mean runup expression ($\mathrm{R}_{2\%} \approx 2\overline{\mathrm{R}}$). However, the aim of this chapter is to evaluate the variability associated with the wave processes, so we used Stockdon's formulation, which takes into account beaches with different morphological states, even though the observations correspond to the 2% runup exceedance.

5.4 Results

The alongshore distribution of the inundation at Somorrostro followed a non-uniform pattern. As a general trend, the northeastern area was less inundated because it is more protected from the most frequent and energetic storms (E-NE) and also because the beach slope is higher in that part of the beach. This general pattern changed, for example, for Event 11 (SSW), in which the northeastern area was more inundated than the southwestern area (the maximum inundation values for this storm, 12 m, were found in the northeastern area) because the southwestern area is the one most protected from storms, with a S and SSW direction. The maximum inundation values were observed in Event 20 (E), reaching values of up to 38 m.

5.4.1 Evaluation of the runup formulas using a deep water wave height H_0

The distribution of the time-averaged differences, $\Delta_{i,\mathrm{all}}$, for all the profiles, i, is shown in Figure 5.4a using Stockdon's formulation with the deep water conditions (*i.e.*, H_0 and L_0). As expected, this approach overestimates the inundation for all Somorrostro beach profiles on average. The differences are not uniform alongshore: the maximum for the first profile, where mean inundation was the lowest ($\mathrm{IO}_{1,\,\mathrm{all}} = 4.80\,\mathrm{m}$, Figure 5.4c), was $\Delta_{1,\,\mathrm{all}} = 12.42\mathrm{m}$. The minimum

difference was in the 23^{rd} profile ($\Delta_{23,\,\mathrm{all}} = 8.00\,\mathrm{m}$), where the mean inundation was the highest ($\mathrm{IO}_{1,\,\mathrm{all}} = 9.10\,\mathrm{m}$). The central beach profiles exhibited uniform differences ($\Delta_{i,\,\mathrm{all}} \approx 9\,\mathrm{m}$).

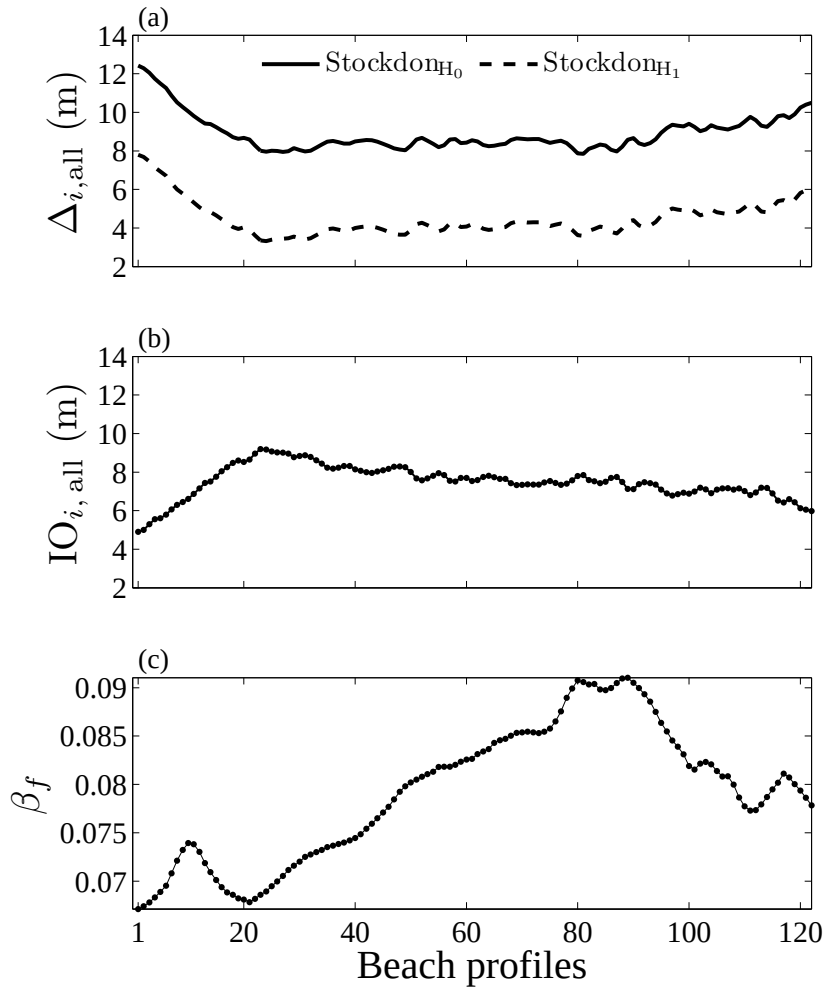

Figure 5.4: (a) Mean differences, $\Delta_{i,\,\mathrm{all}}$, for the formulation of Stockdon et al. (2006) using H_0 and H_1; (b) average inundation observed, $\mathrm{IO}_{i,\,\mathrm{all}}$ for each beach profile; (c) foreshore beach slope, β_f, for each beach profile.

When the data were analyzed by events, the lowest differences between the observations and the estimations were found in the eastern Event 9 ($\Delta_{i,9}$ from 2 to 9 m, $\mathrm{IO}_{i,9}$ being from 7 to 12 m), while the highest differences were found in the southern events (Events 6, 11, and 15). The general trend, as shown in Figure 5.5, was for southern and southwestern events to show greater differences, whereas southeastern and eastern events showed smaller differences (though still overestimating the inundation). For the sake of clarity, Figure 5.5 only considers the storm events in which H_1 are available and displays the results for the six

control profiles.

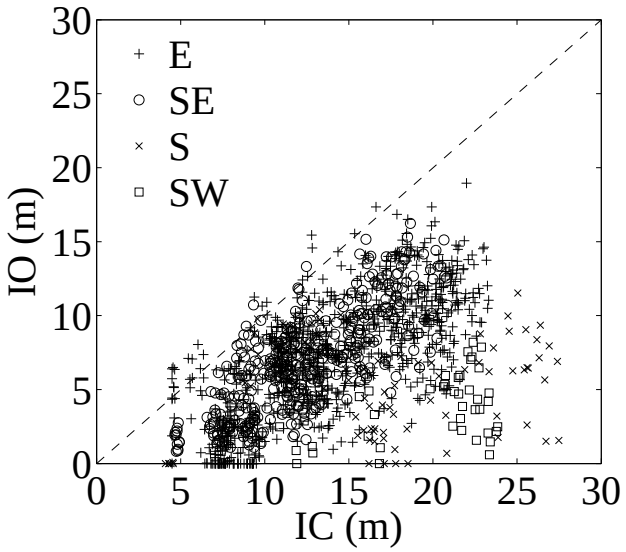

Figure 5.5: Observed (IO) and computed (IC) inundations in the six control profiles for the events in which H_1 is available (see Table 5.1), using deep water conditions.

Finally, the temporal evolution of the predicted inundation and the observations during the storms followed different patterns depending on the angle of wave incidence. As a general trend, for the events in which the waves approached normal to the shore (*i.e.*, SE), the differences between the observations and the estimations were similar throughout the events, being slightly greater at the peak of the storm. For wave incidences nearly normal to the shore (*e.g.*, ESE) the differences between the estimations and the observations were lower before than after the peak of the storm, whereas for more oblique angles of wave incidence (ENE, E and SSW) the differences between observations and estimations were higher before than after the peak of the storm. These trends are illustrated in Figure 5.6 for three different storms.

5.4.2 Evaluation of the runup formulas using a local wave height H_1 and H_2

The difference between the observed and the computed inundation dropped when H_0 and L_0 were replaced by the local wave height measurements from the AWAC (H_1 and L_1) in the runup expression (5.1), although the inundation

was still overestimated (Figure 5.4a). From Figure 5.4a, the mean differences diminished by approximately 5 m.

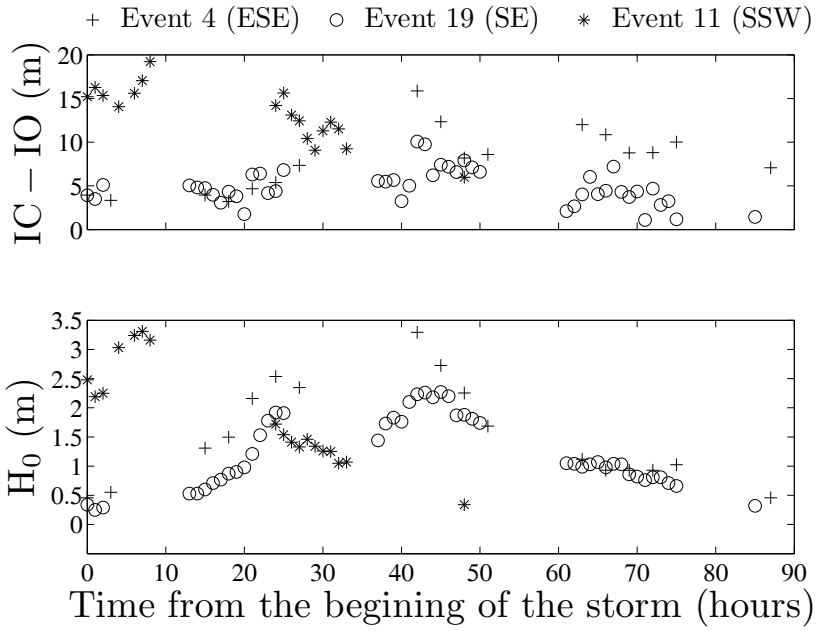

Figure 5.6: Differences between the observed (IO) and the computed inundation (IC) during storms with different wave approaches (values for the control beach profile i = 100). Top, differences between the observations and the computations (IC − IO) for the control beach profile i = 100 in Events 4, 11 and 19. Bottom, temporal evolution of the deep-water wave height (H_0) for these events.

The drop in the differences between the observations and the computations when H_1 was used proved to be particularly important for southern and south-western events (see Figure 5.7), which showed the greatest differences for deep water conditions (Figure 5.5). For instance, the differences decreased by between 8 and 10 m for Event 11 (SSW), and by around 4 m for Event 19 (SE), while the mean differences decreased by only 2 to 3 m for the eastern Events 12, 13, 14, 15, and 18.

The above-mentioned different temporal evolution patterns within the storms depending on the wave incidence angle (Figure 5.6) were not observed when H_1 and L_1 were used (not shown). As a general trend, the observations were then similar to the estimations after the peak of the storm. For Events 13, 18 and 19 the observations were slightly higher after the peak (*i.e.*, IO $>$ IC).

Whenever direct measurements of the local wave height (H_1) are unavailable, the use of a modeled local wave height (H_2) has proven to give good results. In our case the correlation of H_1 and H_2 has $\mathrm{R}^2 = 0.97$ and $\mathrm{RMSE} = 0.05\,\mathrm{m}$. The results computed using Stockdon's formulation with H_1 or H_2 for Event 19 (this is the only event for which both H_1 and H_2 are available) were consequently similar: the differences ranged from 0.12 to 5 m for H_1 and from -0.37 to 5.3 for H_2. For Event 20 (for which H_1 was not available) the inundation for H_2 clearly underestimated the inundation at the southwestern end of the beach ($\Delta_{i,20} \approx -8$ m for profiles $i = 1, \ldots, 20$), while at the northeastern end of the beach the predicted inundation was slightly higher than the observed inundation (differences of around 1 m).

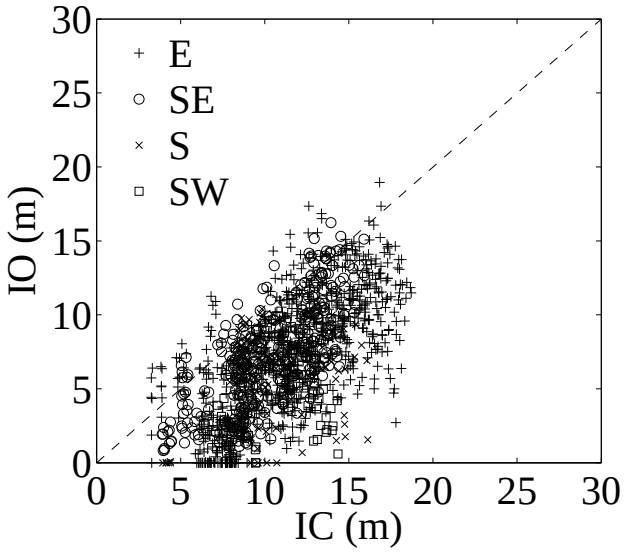

Figure 5.7: Observed (IO) and computed (IC) inundations using conditions at $h = 10\,\mathrm{m}$ for the six control profiles.

5.5 Discussion

A new engineering approach for stabilizing eroding coastlines used in the last few decades consists in creating headland-bay beaches in combination with artificial nourishments (Hsu and Evans, 1989; Klein et al., 2003). Since wave runup motions deliver much of the energy responsible for beach erosion (Sallenger, 2000; Ruggiero et al., 2001) and define the area that can be flooded, their predictability has become increasingly important for effective design of artificial embayed beaches. In addition, Mather et al. (2011) found anomalous runup obser-

vations (inaccurate runup prediction) near a man-made structure of an embayed beach.

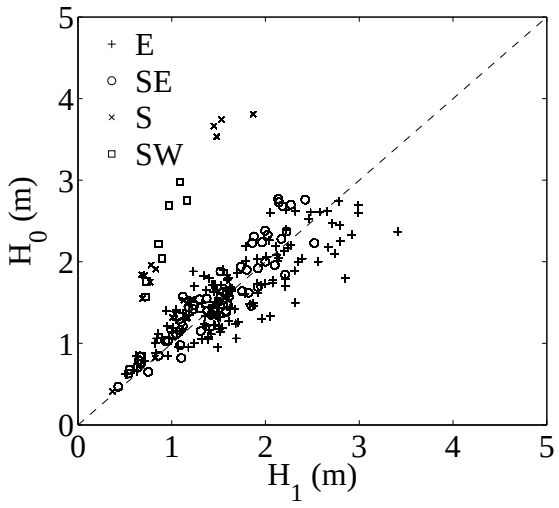

Figure 5.8: Comparison of H_0 and H_1 for different wave angles.

Owing to the wave processes (*i.e.*, refraction and frictional dissipation across the shelf mainly), Stockdon et al. (2006) suggested that the runup prediction using deep water buoy measurements may result in significantly higher results than those obtained using a wave height measured at a local (closer to the shore) buoy. Our results using H_1 (wave height measurements at 10 m depth) seem to confirm the above statement. The differences between the inundation predicted using H_1 and the observations were smaller, but the inundation was still overpredicted. Nonetheless, H_0 (deep water measurements) were generally higher than H_1 (local wave measurements). Most important, this is particularly so for the southern and southwestern events (Figure 5.8), in which refraction and difraction effects are important, and the effects on the computed inundations are clearly shown in Figures 5.5 and 5.7.

Table 5.2 presents the linear regression analysis between H_0 and H_1 (including storm events and also the rest of the data available) from 2005 to 2011. The table presents the results split into a finer wave direction discrimination: ENE, E, ESE, SE, SSE, S and SSW. From the table, the directions S and SSW are those in which H_0 is significantly higher than H_1, as already detected in Figure 5.8 for the storm events. We point out that direction ENE, for which there were no storm events with measured H_1, also gives greater differences in Table 5.2. For

	m,	R^2	RMSE (m)
all	1.16	0.67	0.26
ENE	1.21	0.63	0.31
E	1.10	0.79	0.23
ESE	1.07	0.86	0.18
SE	1.09	0.86	0.18
SSE	1.13	0.59	0.17
S	1.36	0.62	0.18
SSW	1.68	0.61	0.26

Table 5.2: Linear regresssion $\mathrm{H}_0 = m\mathrm{H}_1$ (through the origin) grouped by wave directions for the period 2005 to 2011 (not only storm events but all the recorded data). If $m > 1$, as is the case, H_0 is generally larger than H_1.

the complete data set used to build Table 5.2, H_0 was more than 0.5 m higher than H_1 in 11% of the cases for ENE directions, and in 17% of the cases for SSW directions, while for the E and S directions this difference was only observed in $\sim 4\%$ and for ESE, SE and SSE only in $\sim 1\%$. Therefore, ENE, S and SSW are the wave directions in which the differences between H_0 and H_1 are greatest and, consequently, in which the use of H_0 in Stockdon's formulation must give the highests differences. These directions are the ones approaching Somorrostro most obliquely.

The temporal evolution of the predicted and observed inundation for the storms with nearly shore-normal wave incidence (ESE) showed that the differences increased after the peak of the storm. For these events, the wave directions changed to southern after the peak of the storm. As the waves approached Somorrostro more obliquely, this would explain the greater differences. The decrease in the differences (Δ) after the peak of the storm events with oblique wave angles (NE, E and SSW) is explained by the morphological changes that took place. Using H_1 in Stockdon's formulation, we did not observe the different evolution pattern depending on the wave direction approach because the wave processes were already included.

The beach inundation variability associated with the wave transformation processes from deep water conditions is quantified in Table 5.3 as the mean (Δ_{all}) and the standard deviation (σ_{all}) of the differences between observations and computation of the inundation using H_0 and H_1 in Stockdon's formulation, considering

all the observations for the control beach profiles grouped by wave directions. For waves that are shore-normal or mostly shore-normal, the beach inundation computation is independent of the wave height used in the runup expression and Stockdon's formulation is suitable; however, for waves approaching obliquely to the shore, the use of a deep water wave height, H_0, will produce greater discrepancies in the beach inundation prediction.

	H_0		H_1	
	Δ_{all} (m)	σ_{all} (m)	Δ_{all} (m)	σ_{all} (m)
E	6.7	0.3	4.4	0.3
SE	5.5	0.4	3.2	0.5
S	10.0	1.1	4.3	1.0
SW	15.1	0.5	7.6	0.6

Table 5.3: Mean differences and standard deviation between inundation computed using H_0 and H_1 and inundation observed in the control beach profiles grouped by wave directions for the storm events in which data were available for both wave heights.

.

Embayed beaches have an asymmetric planform characterized by a strongly curved zone (in our case for the profiles $i = 1, \ldots, 20$), a gently curved center ($i = 21, \ldots, 80$) and a relative straight section ($i = 80, \ldots, 122$). Diffraction and the refraction patterns associated with the prevailing waves determine the beach planform shape (Short and Masselink, 1999). The inundation at an embayed beach is thus linked to the beach planform shape. In our case, we usually found the greatest differences between the estimations and the observations at the southwestern end of Somorrostro, which is in the curved zone shadowed by the double dike, and also at the very northeastern end, which is affected by the Olympic Marina (Figure 5.4). The foreshore slope, which is related to the planform, is already taken into account in Expressions (5.1) and (5.3). The fact that the inundation differences are related to the planform suggests that the foreshore slope is not sufficient to characterize the inundation, *i.e.*, that the influence of the planform (which is also affected by the wave direction) goes beyond the foreshore slope.

The influence of the embayed beach planform should be better captured by the breaking wave height, H_b (Figure 5.9), since this wave height includes more details of the wave processes (*i.e.*, diffraction and refraction). Roberts et al. (2010), after laboratory studies using a movable bed, concluded that the wave

runup on a non-scarped beach was approximately equal to the significant breaking wave height (*i.e.*, $\mathrm{R} \simeq \mathrm{H}_b$).

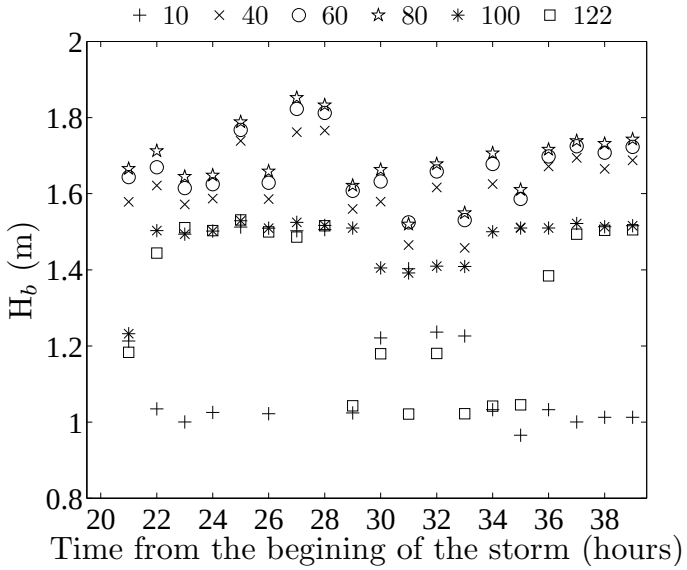

Figure 5.9: H_b during some hours of Event 19 in the six control beach profiles (for design reasons not all the hours are shown).

Figure 5.10a shows the comparison of the observed inundation and the computed inundation in the six control profiles for Event 19 through expression (5.3) if the runup is directly assumed to be H_b. The results obtained in this way (Figure 5.10a) are similar to those obtained using Stockdon's formulation with H_0. $\mathrm{R} = \mathrm{H}_b$ overpredicts the inundation because the assumption of Roberts et al. (2010) ($\mathrm{R} = \mathrm{H}_b$) is for maximum runup. For this particular event, it is noteworthy that $\mathrm{R} = 0.61\mathrm{H}_b$ is the best choice for fitting the observed inundation (Figure 5.10b). The inundation computed using $\mathrm{R} = 0.61\mathrm{H}_b$ is referred to as $\mathrm{IC}_{b,\mathrm{cal}}$ hereafter. Interestingly, the relation between the expressions of the mean runup ($\overline{\mathrm{R}}$) and the 2% runup ($\mathrm{R}_{2\%}$) of Nielsen and Hanslow (1991) is $\overline{\mathrm{R}} \approx 0.5\mathrm{R}_{2\%}$, as occurs now with H_b (noting that $0.61 \sim 0.50$).

The observed inundation (IO) and that computed using the different wave heights (IC_0, IC_1, IC_b and $\mathrm{IC}_{b,\mathrm{cal}}$) in Event 19 for the control beach profiles is summarized in Figure 5.11. From the figure, the inundation variability along the embayed beach is better captured when the breaking wave height is directly assumed to be proportional to the runup. On the other hand, when the inundation is

calculated using Stockdon's formulation with either H_0 or H_1, this characteristic inundation behavior of embayed beaches is not reproduced.

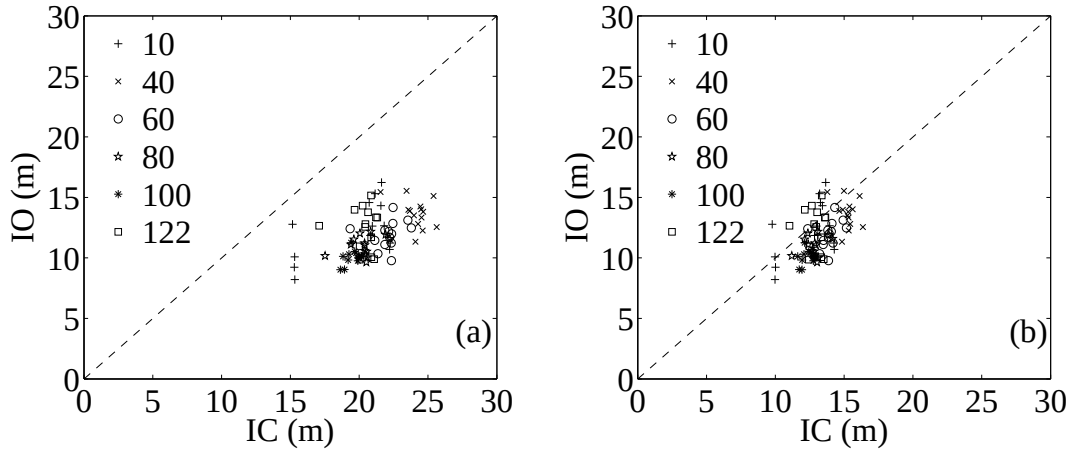

Figure 5.10: (a) Observed (IO) and computed (IC) inundations using $\mathrm{R} = \mathrm{H}_b$ for the six control profiles; (b) Observed (IO) and computed (IC) inundations using $\mathrm{R} = 0.61\mathrm{H}_b$ for the six control profiles.

5.6 Conclusions

Inundation computations at a tideless embayed beach using different wave heights (H_0, H_1, H_2) have been compared with observations. In general, the inundations computed using Stockdon's formulation with deep water conditions are higher than the observed ones (between 8 and 12 m). The difference between the computed inundation and the observations when the deep water wave height is replaced by a local wave height, H_1, in the formulation of Stockdon et al. (2006) is approximately 5 m. This finding suggests that the use of the local wave height in Stockdon's formulation provides an intermediate wave runup between the mean observed and the 2% runup exceedance ($\mathrm{R}_{2\%}$) calculated in Stockdon et al. (2006).

For engineering purposes, to define the flooded area at an embayed beach, the use of Stockdon's formulation with deep water wave measurements seems suitable since it gives results on the safe side irrespective of the wave direction. However, this formulation can give considerable differences for waves approaching obliquely to the shore and better results (still on the safe side) can be obtained using a local wave height that will take into account, to some extent, the influence of wave propagation processes on the inundation. Moreover, in the

case of unavailable local wave measurements, the use of a modeled wave height, H_2, is suitable. The SMC model has been shown to suitably reproduce the wave transformation processes from deep to local water depths for a problem in which diffraction and refraction effects are great.

The distribution of the differences is heterogeneous along the beach, but follows the beach planform shape, being higher in the most curved zone, where the diffraction processes are greater. The foreshore slope is related to the beach planform shape (which is affected by the wave direction), but is not sufficient to characterize the inundation throughout the runup. Therefore, the alongshore variability of the inundation cannot be captured using either H_0 or H_1. In our case, the differences between the computation and the observations are not further diminished when the wave runup is assumed to be equal to H_b because it is for maximum runup values. Nonetheless, the inundation computed using H_b as the runup reproduces the alongshore variability of the inundation. To adjust the estimations using H_b to the mean inundation observed at Somorrostro, it must be assumed that $R = 0.61H_b$.

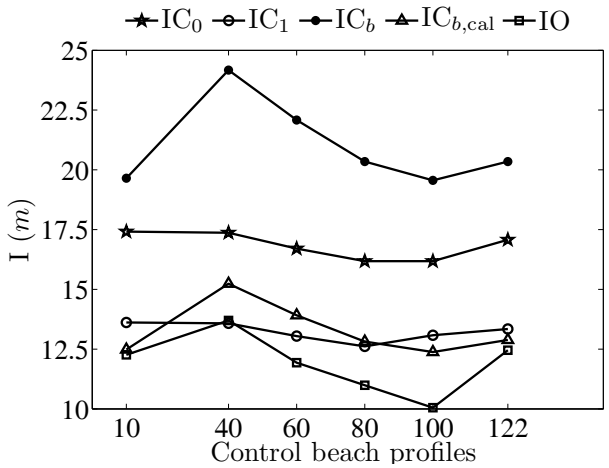

Figure 5.11: Mean observed (IO) and computed inundation for Event 19 using H_0 and H_1 in the formulation of Stockdon et al. (2006) (IC_0 and IC_1), computed inundation using the assumption of Roberts et al. (2010) (IC_b) and using the expression of Roberts et al. (2010) but calibrated for Somorrostro ($IC_{b,cal}$) in the control beach profiles.

Chapter 6

CONCLUSIONS

6.1 Specific answers to the original research questions

The general objective of the research presented in this thesis was to provide more insight into beach inundation processes at embayed and open beaches and to determine how morphological changes could interfere with these processes. To this end, video measurements of beach inundation and the characteristic morphological changes were carried out at three artificial, tideless embayed beaches located in Barcelona, Spain (NW Mediterranean) and on an open, microtidal multibarred beach located in Noordwijk, the Netherlands (North Sea). The most important findings of this research are summarized by answering the research questions that were formulated in the introduction.

1. **What are the shoreline changes at tideless embayed beaches during storms?**

   A preliminary step for evaluating how shoreline changes can affect beach inundation at embayed beaches during storms is to analyze the shoreline variability associated with natural processes.

   This thesis has presented a new methodological approach for analyzing beach rotation which eliminates the morphological effects (*e.g.*, those related to the formation, changes in shape or migration of megacusps) and improves the choice of the pivotal point. This methodological contribution was developed for Barcelona beaches but can be useful for other embayed beaches.

   The shoreline changes at embayed beaches were divided into morphological features and beach planform changes. The morphological features analyzed at steep embayed beaches are beach cusps, megacusps, shoreline undulations and a salient. On the other hand, the characteristic beach planform change of embayed beaches is beach rotation, which occurs when there is an opposite behavior (erosion/accretion) of similar magnitude in the two sections of the beach separated by a pivotal point. In addition to beach rotation, other beach planform changes studied are landward/seaward displacements and changes

in beach orientation.

2. **How do protection works affect shoreline reshaping and hydrodynamics during storms at embayed beaches?**

   Shoreline changes induced by human activities on the beach also affect beach inundation at embayed beaches during storms. Many beaches around the world are affected by protection works such as beach nourishment and construction of coastal structures. These works are aimed at reducing wave energy on the beach, thus modifying the wave-induced current system and the morphological configuration, in order to reduce erosion and stabilize the beach. To achieve these goals, the embayed beach of La Barceloneta was nourished and two breakwaters (one submerged and one detached) were built.

   At embayed beaches without coastal structures the wave-induced current system is composed of a homogeneous alongshore current whose direction depends on the wave direction approach. When a detached breakwater is built in the middle of an embayed beach, the most obvious shoreline change is the transformation into two embayed beaches separated by a salient, which in some cases is created artificially.

   At La Barceloneta beach, in addition to the detached breakwater, the construction of a submerged breakwater normal to the northern double-dike transformed the wave-induced current system into a more complex system. As a result, the wave-induced current system at each section of the beach has a differential current pattern: the dominant alongshore currents at the two beaches are in opposite directions, both running towards the salient.

   The combination of the detached and the submerged breakwater increases the variability of shoreline responses and modifies the beach rotation process. Thus, under similar storm conditions the shoreline change at each embayed beach could be different or even opposite (e.g. general erosion at one beach and general accretion at the other beach). Furthermore, the beach rotation is only clockwise in the southern section, whereas in the northern

section it is only counter-clockwise.

Finally, the submerged breakwater can drastically enhance the shoreline erosion at the embayed beach in its lee under waves approaching the shore normal to the submerged breakwater.

3. **What are the differences in beach inundation behavior between embayed beaches and open multibarred beaches?**

   In this thesis the beach inundation behavior has been analyzed at three tideless steep embayed beaches located in Barcelona (NW Mediterranean) and at an open, microtidal, multibarred beach located in Noordwijk (North Sea).

   The maximum inundation observed (105 m) was at Noordwijk. At open microtidal beaches the magnitude of the inundation is mainly influenced by the surge level and the inundation is alongshore uniform to the wave direction approach.

   At the embayed beaches of Barcelona the highest values were observed at La Barceloneta II (71 m), followed by Nova Icaria (54 m), La Barceloneta I (38 m) and finally Somorrostro (37 m). The beach inundation at these beaches is controlled by the wave runup rather than the surge tide and the alongshore distribution of the inundation is heterogeneous, depending strongly on the wave direction approach.

4. **How do morphological features and the beach planform modify beach inundation?**

   The effects of the previous beach morphological configuration and changes induced during the storm are presented for two scenarios.

   (a) **When the morphological features developed before the beginning of the storm.** In general, the influence of morphological features on inundation is directly proportional to the magnitude of the morphologies.

In addition, the morphological features located on the beach face shape the inundation at the beginning of the storm, leading to non-uniformity alongshore.

- *Embayed beaches:* the inundation values are higher in the bay than at the horn of the beach cusps, although the differences are small (around 2-3 m). Megacusps reduce the inundation when they are present before the beginning of the storm (e.g. at Barcelona beaches the maximum decrease in inundation was around 10 m). The differences in the inundation values between the cusp and the bay of the shoreline undulation are approximately 10 m. The presence of the salient modifies the inundation along the beach according to its amplitude (several tens of meters). However, when waves overtop the detached breakwater during energetic storm conditions the salient is completely inundated and its influence on the inundation is almost negligible.

- *Open and multibarred beaches:* The beach profile of multibarred beaches is characterized by two types of beach slope: the intertidal (gentle) and the supratidal (steep) slope. Therefore, the magnitude of beach inundation depends on the astronomical tide, being lower during high tide than low tide.
  The influence of the morphology of the submerged sandbars on inundation decreases with water depth. The influence of the inner bars increases with their proximity to the intertidal zone, whereas the outer bars do not seem to influence inundation. In general, the presence of inner bars near the intertidal zone modifies the slope (gently) and favors inundation during low tide.
  Finally, the alongshore shapes of intertidal bars cause alongshore non-uniformity of the inundation before the peak of the storm.

(b) **When the morphological features are formed or evolve during the storm or the morphological configuration of the beach is changed during the storm.**

- *Embayed beaches:* under high-energy conditions beach cusps are destroyed, so their influence can be disregarded. However, when the

megacusps are formed during the storm they can decrease the inundation by almost 10 m (normal ranges of influence vary between 3 and 7 m). If these features migrate alongshore, the inundation increases (maximum observed 14 m) at its previous location. The influence of shoreline undulation is similar to that of megacusps. Both morphological features cause inundation variability of around 25% of the maximum inundation observed. Finally, the salient is the morphological feature that had the greatest influence on beach inundation at the embayed beaches studied. Morphological changes associated with the salient can account for more than half of the inundation.

The beach planform changes during the storm add a new factor to be considered: when the beach planform changes are landward, the inundation is higher, whereas when the beach planform changes are seaward, the inundation is lower or there is no inundation. As the beach rotation includes an opposite movement landward/seaward of similar magnitude in the two sections of the beach separated by a pivotal point, the effect on the inundation is different at each section of the beach. Beach planform changes are the main influence on these embayed beaches and can reach more than half of the maximum inundation observed.

- *Open and multibarred beaches:* The main morphological change affecting beach inundation observed was the disappearance of the intertidal sandbars during the peak of the storm. As a consequence of this, the inundation became more uniform alongshore and the intertidal zone flattened, increasing the inundation on the beach after the peak of the storm.

5. **Should shoreline changes be included in inundation prediction?**

   As stated above, if the shoreline changes are not considered, errors in beach inundation prediction can occur. Furthermore, shoreline variability during storms at embayed beaches can be of the same order of magnitude (meters to tens of meters) as the inundation. From a general perspective, the inundation

is more influenced by shoreline changes at steep beaches because of the lower magnitude of inundation in comparison with gently sloped beaches.

Focusing on the magnitude of the shoreline changes that take place at embayed beaches such as those of Barcelona, it is clear that beach changes related to both the beach planform readjustments and the salient have a potentially significant influence on inundation for most natural ranges of beach slope. Shoreline variations related to undulations and megacusps represent more than 25% of the maximum inundation when the beach slope is higher than 0.04. Finally, the influence of beach cusp variability on inundation is very small and can be disregarded.

At open and multibarred beaches with gently slopes ($\beta < 0.04$), the magnitude of the inundation is very sensitive to the change of slope. Consequently, beach slope variability should be considered in the prediction and the understanding of inundation processes at multibarred beaches. The beach profile at Noordwijk is characterized by two types of beach slope: the intertidal and the supratidal beach slope. Hence, the inundation at multibarred and open beaches can be reasonably well predicted using a simple runup equation (see Equation 4.1) but two different beach slopes must be considered for an accurate prediction of beach inundation.

On the other hand, the influence of shoreline changes is low because the magnitude of the beach inundation (tens to hundreds of meters) is larger than the shoreline modifications during the storm. However, when the morphological changes produce a change in the intertidal beach slope, they should be taken into account. For example, the disappearance of intertidal bars after the peak of the storm decreases the beach slope and therefore increases the inundation. Finally, the influence on the inundation of inner and outer bars seems to be subordinate to the intertidal zone.

6. **Are the wave runup formulations suitable for predicting beach inundation at embayed beaches?**

In this thesis, the beach inundation prediction at embayed beaches has been evaluated using the formulation of Stockdon et al. (2006), considering deep-

water measurements and local wave measurements and computations, and the formulation of Roberts et al. (2010). For engineering purposes, to define the flooded area at an embayed beach, the use of Stockdon's formulation with deep-water wave measurements seems suitable since it gives results on the safe side irrespective of the wave direction. However, this formulation can give considerable differences for waves approaching obliquely to the shore, and better results (still on the safe side) can be obtained using a local wave height that will, to some extent, take into account the influence of wave propagation processes on inundation.

However, the alongshore variability of the inundation at embayed beaches cannot be captured using either deep water or local wave measurements in Stockdon's formulation. The foreshore slope, which is included in Stockdon's formulation, is related to the beach planform shape (which is affected by the wave direction) but is not sufficient to characterize the inundation throughout the runup. The alongshore variability of the inundation is better captured when the wave runup is assumed to be proportional to breaking wave height (H_b): Roberts et al. (2010) proposed that wave runup is equal to H_b and this assumption will correspond to a maximum inundation estimation. To fit video observations of the beach inundation with the prediction, the wave runup must be assumed as $\mathrm{R} = 0.61\mathrm{H}_b$ corresponding to a mean beach inundation.

6.2 Further research

This thesis has provided greater insight into beach inundation on tideless embayed beaches and open, microtidal multibarred beaches and how they can be affected by shoreline changes. However, beach inundation is site-specific and observations in different coastal systems are necessary in order to thoroughly understand the process.

The methodology for measuring beach inundation followed in this thesis consists in extracting the waterline from the timex images during the storm. This methodology identifies the morphological patterns and quantifies the beach

inundation alongshore without depending on topographic surveys. The study of beach inundation during storms using this methodology — combined with wave runup measurements from several timestacks along the beach, local and deep-water wave measurements, local water level measurements, and topographic surveys before and after the storm — will provide additional information for improving inundation prediction, such as the exact contribution of runup, surge and astronomical tides.

The influence of submerged sandbars on inundation is not totally understood and further research is needed. For example, a complete study of their influence will consist in the modelling of energetic storms with different wave conditions and surge levels at a multibarred beach on which the 3D features of the submerged sandbars evolve during the storm. Results could be validated with video measurements of the beach inundation. The XBeach model and the new video monitoring system installed recently at the multibarred and tideless beach close to Barcelona (Castelldefels beach), which also belongs to the Coastal Ocean Observatory (COO, http://coo.icm.csic.es/), meet all the conditions for accomplishing this study.

Finally, coastal inundation during storms is one of the most important hazards affecting coastal areas. The global mean sea level is expected to rise throughout the 21st century and coastal inundation will therefore increase in proportion to the slope of the coastal area. The results provided by this thesis, and in particular the information on how morphological changes influence inundation, can be introduced in predictive tools for establishing set-back lines, generating coastal hazard maps, developing warning systems and highlighting critical situations that might result in severe coastal erosion or infrastructural damage.

Bibliography

Aagaard, T. and Holm, J. (1989). Digitization of wave run-up using video records. *Journal of Coastal Research*, 5(3):547–551.

Ahrens, J. P. and Seelig, W. N. (1996). Wave runup on beaches. In *Proceedings 25th International Conference on Coastal Engineering, American Society Civil Engineers*, volume 1, pages 981–993.

Anthony, E. J., Gardel, A., Dolique, F., and Guiral, D. (2002). Short-term changes in the plan shape of a sandy beach in response to sheltering by a nearshore mud bank, Cayenne, French Guiana. *Earth Surface Processes and Landforms*, 27(8):857–866.

Archetti, R. and Romagnoli, C. (2011). Analysis of the effects of different storm events on shoreline dynamics of an artificially embayed beach. *Earth Surface Processes and Landforms*, 36(11):1449–1463.

Archetti, R. and Zanuttigh, B. (2010). Integrated monitoring of the hydro-morphodynamics of a beach protected by low crested detached breakwaters. *Coastal Engineering*, 57(10):879–891.

Ariza, E., Jimenez, J. A., and Sarda, R. (2008). A critical assessment of beach management on the Catalan coast. *Ocean & Coastal Management*, 51(2):141–160.

Bailey, D. G. and Shand, R. D. (1994). Determining wave run-up using automated video analysis. In *Proceedings 2nd NZ Conference on Image and Vision Computing*, pages 2.11.1–2.11.8.

Battjes, J. A. (1971). Runup distributions of waves breaking on slopes. *Journal of waterways, harbours and coastal engineering division*, 97(1):99–114.

Battjes, J. A. (1974). *Computations of set-up, longshore currents, run-up overtopping due to wind-generated waves*. PhD thesis, Delft.

Benavente, J., del Rio, L., Gracia, F. J., and Martinez-del Pozo, J. A. (2006). Coastal flooding hazard related to storms and coastal evolution in Valdelagrana spit (Cadiz Bay Natural Park, SW Spain). *Continental Shelf Research*, 26:1061–1076.

Bosom, E. and Jimenez, J. A. (2011). Probabilistic coastal vulnerability assessment to storms at regional scale - application to catalan beaches (NW Mediterranean). *Natural Hazards and Earth System Sciences*, 11(2):475–484.

Bricio, L., Negro, V., and Diez, J. J. (2008). Geometric detached breakwater indicators on the Spanish northeast coastline. *Journal of Coastal Research*, 24(5):1289–1303.

Brown, J. D., Spencer, T., and Moeller, I. (2007). Modeling storm surge flooding of an urban area with particular reference to modeling uncertainties: A case study of Canvey Island, United Kingdom. *Water Resources Research*, 43(6):W06402.

Bryan, K. R. and Coco, G. (2010). Observations of nonlinear runup patterns on plane and rhythmic beach morphology. *Journal of Geophysical Research-oceans*, 115:C09017.

Bryan, K. R., Salmon, S. A., and Coco, G. (2009). Measuring storm run-up on intermediate beaches using video. In *31th International Conference on Coastal Engineering*, pages 854–864.

Ciavola, P., Ferreira, O., Haerens, P., Van Koningsveld, M., Armaroli, C., and Lequeux, Q. (2011). Storm impacts along European coastlines. Part 1: The joint effort of the MICORE and ConHaz Projects. *Environmental Science & Policy*, 14(7):912–923.

Condon, A. J. and Sheng, Y. P. (2012). Evaluation of coastal inundation hazard for present and future climates. *Natural Hazards*, 62(2):345–373.

Cooper, J. A. G., Jackson, D. W. T., Navas, F., McKenna, J., and Malvarez, G. (2004). Identifying storm impacts on an embayed, high-energy coastline: examples from western Ireland. *Marine Geology*, 210:261–280.

de Alegria-Arzaburu, A. R. and Masselink, G. (2010). Storm response and beach rotation on a gravel beach, Slapton Sands, UK. *Marine Geology*, 278(1-4):77–99.

del Rio, L., Plomaritis, T. A., Benavente, J., Valladares, M., and Ribera., P. (2012). Establishing storm thresholds for the Spanish Gulf of Cadiz coast. *Geomophology*, 143-144:13–23.

Dodd, N., Stoker, A. M., Calvete, D., and Sriariyawat, A. (2008). On beach cusp formation. *Journal of Fluid Mechanics*, 597:145–169.

Douglas, S. (1992). Estimating extreme values of run-up on beaches. *Journal of waterways, harbours and ocean engineering*, 118(2):220–224.

Emanuel, K. (2005). Increasing destructiveness of tropical cyclones over the past 30 years. *Nature*, 436:686–688.

Ferreira, O., Garcia, T., Matias, A., Taborda, R., and Dias, J. A. (2006). An integrated method for the determination of set-back lines for coastal erosion hazards on sandy shores. *Continental Shelf Research*, 26:1030–1044.

Garnier, R., Ortega-Sanchez, M., Losada, M. A., Falques, A., and Dodd, N. (2010). Beach cusps and inner surf zone processes: growth or destruction? A case study of Trafalgar Beach (Cadiz, Spain). *Scientia Marina*, 74(3):539–553.

Gonzalez, M., Medina, R., Gonzalez-Ondina, J., Osorio, A., Mendez, F. J., and Garcia, E. (2007). An integrated coastal modeling system for analyzing beach processes and beach restoration projects, SMC. *Computers & Geosciences*, 33(7):916–931.

Gourlay, M. R. (1992). Wave set-up, wave run-up and beach water table: Interaction between surf zone hydraulics and groundwater hydraulics. *Coastal Engineering*, 17:93–144.

Guedes, R. M. C., Bryan, K. R., Coco, G., and Holman, R. A. (2011). The effects of tides on swash statistics on an intermediate beach. *Journal of Geophysical Research-oceans*, 116:C04008.

Guillen, J., Garcia-Olivares, A., Ojeda, E., Osorio, A., Chic, O., and Gonzalez, R. (2008). Long-term quantification of beach users using video monitoring. *Journal of Coastal Research*, 24(6):1612–1619.

Guza, R. T. and Feddersen, F. (2012). Effect of wave frequency and directional spread on shoreline runup. *Geophysical Research Letters*, 39:L11607.

Guza, R. T. and Thornton, E. B. (1982). Swash oscillations on a natural beach. *Journal of Geophysical Research-oceans and Atmospheres*, 87(NC1):483–491.

Hanson, H., Brampton, A., Capobianco, M., Dette, H. H., Hamm, L., Laustrup, C., Lechuga, A., and Spanhoff, R. (2002). Beach nourishment projects, practices, and objectives - a European overview. *Coastal Engineering*, 47(2):81–111.

Holland, K. T., Holman, R. A., Lippmann, T. C., Stanley, J., and Plant, N. (1997). Practical use of video imagery in nearshore oceanographic field studies. *IEEE Journal of Oceanic Engineering*, 22(1):81–92.

Holland, K. T., Raubenheimer, B., Guza, R. T., and Holman, R. A. (1995). Runup kinematics on a natural beach. *Journal of Geophysical Research*, 100(3):4985–4993.

Holman, R. A. (1981). Infragravity energy in the surf zone. *Journal of Geophysical Research-oceans and Atmospheres*, 86(NC7):6442–6450.

Holman, R. A. (1986). Extreme values statistics for wave run-up on a natural beach. *Coastal Engineering*, 9:527–544.

Holman, R. A. and Guza, R. T. (1984). Measuring run-up on a natural beach. *Coastal Engineering*, 8:129–140.

Holman, R. A. and Sallenger, A. H. (1985). Setup and swash on a natural beach. *Journal of Geophysical Research*, 90:945–953.

Holman, R. A. and Stanley, J. (2007). The history and technical capabilities of Argus. *Coastal Engineering*, 54:477–491.

Hsu, J. R. C. and Evans, C. (1989). Parabolic bay shapes and applications. *Proceedings of the Institution of Civil Engineers Part 2-research and Theory*, 87:557–570.

Hsu, J. R. C., Yu, M. J., Lee, F. C., and Benedet, L. (2010). Static bay beach concept for scientists and engineers: A review. *Coastal Engineering*, 57(2):76–91.

Hunt, I. A. (1959). Design of sewalls and breakwaters. *Journal of waterways and harbours division. Proceedings of the American Society of civil Engineers*, 85:123–152.

Ilic, S., Chadwick, A. J., and Fleming, C. (2005). Investigation of detached breakwaters. Part 1 - hydrodynamics. In *Proceedings of the Institution of Civil Engineers: Maritime Engineering*, volume 158, pages 91–102. Thomas Telford Publishing.

Ilic, S., van der Westhuysen, A. J., Roelvink, J. A., and Chadwick, A. J. (2007). Multidirectional wave transformation around detached breakwaters. *Coastal Engineering*, 54(10):775–789.

Klein, A. H. F., Benedet, L., and Schumacher, D. H. (2002). Short-term beach rotation processes in distinct headland bay beach systems. *Journal of Coastal Research*, 18(3):442–458.

Klein, A. H. F., Ferreira, O., Dias, J. M. A., Tessler, M. G., Silveira, L. F., Benedet, L., de Menezes, J. T., and de Abreu, J. G. N. (2010). Morphodynamics of structurally controlled headland-bay beaches in southeastern Brazil: A review. *Coastal Engineering*, 57(2):98–111.

Klein, A. H. F., Vargas, A., Raabe, A. L. A., and Hsu, J. R. C. (2003). Visual assessment of bayed beach stability with computer software. *Computers & Geosciences*, 29(10):1249–1257.

Kobayashi, N. (1999). Wave runup and overtopping on beaches and coastal structures. *Advances In Coastal and Ocean Engineering*, 5:95–154.

Kron, W. (2008). Coasts: The riskiest places on earth. In *32th Proceedings of the International Conference on Coastal Engineering*, pages 3–21.

Kroon, A., Davidson, M. A., Aarninkhof, S. J., Archetti, R., Armaroli, C., Gonzalez, M., Medri, S., Osorio, A., Aagaard, T., Holman, R. A., and Spanhoff, R. (2007). Application of remote sensing video systems to coastaline management problems. *Coastal Engineering*, 54:493–505.

Krumbein, W. (1944). Shore processes and beach characteristics. Technical Report vol 3, Beach Erosion Board, U.S. Army Corps of Engineers.

Lausman, R., Klein, A. H. F., and Stive, M. (2006). Uncertainty in the application of parabolic bay shape equation: A case of study. Master's thesis, Delft University of Technology (DUT).

Marra, J., Allen, T., Easterling, D., Fauver, S., Karl, T., Levinson, D., Marcy, D., Payne, J., Pietrafesa, L., Shea, E., and Vaughan, L. (2007). An integrating architecture for coastal inundation and erosion program planning and product development. *Marine Technology Society Journal*, 41(1):62–75.

Martino, E., Moreno, L. J., and Kraus, N. C. (2005). Uncertainties in design guidance for headland-bay beaches. In *Proceedings of 5th International Conference on Coastal dynamics 2005, ASCE*.

Martins, C. C., de Mahiquesh, M. M., and Dias, J. M. A. (2010). Daily morphological changes determined by high-energy events on an embayed beach: a qualitative model. *Earth Surface Processes and Landforms*, 35(4):487–495.

Mase, H. (1989). Random wave runup height on gentle slope. *Journal of Waterways, Harbours and Ocean Engineering*, 5(5):649–661.

Masselink, G., Hegge, B. J., and Pattiaratchi, C. B. (1997). Beach cusp morphodynamics. *Earth Surface Processes and Landforms*, 22(12):1139–1155.

Masselink, G. and Pattiaratchi, C. B. (1998). Morphological evolution of beach cusps and associated swash circulation patterns. *Marine Geology*, 146(1-4):93–113.

Mather, A., Stretch, D., and Garland, G. (2011). Predicting extreme wave run-up on natural beaches for coastal planning and management. *Coastal Engineering Journal*, 53(2):87–109.

McCall, R. T., Van Thiel de Vries, J. S. M., Plant, N. G., Van Dongeren, A. R., Roelvink, J. A., Thompson, D. M., and Reniers, A. J. H. M. (2010). Two-dimensional time dependent hurricane overwash and erosion modeling at Santa Rosa Island. *Coastal Engineering*, 57(7):668–683.

Mimura, N., Yasuhara, K., Kawagoe, S., Yokoki, H., and Kazama, S. (2011). Damage from the great East Japan earthquake and tsunami - a quick report. *Mitigation and Adaptation Strategies For Global Change*, 16(7):803–818.

Moreno, L. J. and Kraus, N. C. (1999). Equilibrium shape of headland-bay beaches for engineering design. In *Coastal Sediments '99, ASCE*, pages 860–875.

Nicholls, R. J. (2004). Coastal flooding and wetland loss in the 21st century: changes under the SRES climate and socio-economic scenarios. *Global Environmental Change-human and Policy Dimensions*, 14(1):69–86.

Nicholls, R. J. and Cazenave, A. (2010). Sea-level rise and its impact on coastal zones. *Science*, 328(5985):1517–1520.

Nielsen, P. and Hanslow, D. J. (1991). Wave runup distributions on natural beaches. *Journal of Coastal Research*, 7(4):1139–1152.

Ojeda, E. and Guillen, J. (2008). Shoreline dynamics and beach rotation of artificial embayed beaches. *Marine Geology*, 253:51–62.

Ojeda, E., Guillen, J., and Ribas, F. (2006). Bar and shoreline coupling in artificial embayed beaches. In *30th International Conference on Coastal Engineering*, pages 2714–2725.

Ojeda, E., Guillen, J., and Ribas, F. (2010). The morphodynamic responses of artificial embayed beaches to storm events. *Advances in Geosciencies*, 26:99–103.

Ojeda, E., Ribas, F., and Guillen, J. (2011). Dynamics of single-barred embayed beaches. *Marine Geology*, 280:76–90.

Ojeda, E., Ruessink, B. G., and Guillen, J. (2008). Morphodynamic response of a two-barred beach to a shoreface nourishment. *Coastal Engineering*, 55(12):1185–1196.

Oliveira, F. S. B. F. and Barreiro, O. M. (2010). Application of empirical models to bay-shaped beaches in portugal. *Coastal Engineering*, 57(2):124–131.

Pape, L., Plant, N. G., and Ruessink, B. G. (2010). On cross-shore migration and equilibrium states of nearshore sandbars. *Journal of Geophysical Research-earth Surface*, 115:F03008.

Patro, S., Chatterjee, C., Mohanty, S., Singh, R., and Raghuwanshi, N. S. (2009). Flood inundation modeling using MIKE FLOOD and remote sensing data. *Journal of the Indian Society of Remote Sensing*, 37(1):107–118.

Quartel, S., Ruessink, B. G., and Kroon, A. (2007). Daily to seasonal cross-shore behaviour of quasi-persistent intertidal beach morphology. *Earth Surface Processes and Landforms*, 32(9):1293–1307.

Quera, Q. (2010). Evaluation of the nourishments and the Dutch coast protection policy for the Noordwijk coast (The Netherlands). Master's thesis, Utrecht University.

Ranasinghe, R., Larson, M., and Savioli, J. (2010). Shoreline response to a single shore-parallel submerged breakwater. *Coastal Engineering*, 57(11-12):1006–1017.

Ranasinghe, R., Symonds, G., Black, K., and Holman, R. A. (2004). Morphodynamics of intermediate beaches: a video imaging and numerical modelling study. *Coastal Engineering*, 51(7):629–655.

Ranasinghe, R. and Turner, I. L. (2006). Shoreline response to submerged structures: A review. *Coastal Engineering*, 53(1):65–79.

Roberts, T. M., Wang, P., and Kraus, N. C. (2010). Limits of wave runup and corresponding beach-profile change from large-scale laboratory data. *Journal of Coastal Research*, 26(1):184–198.

Roelvink, D., Reniers, A., van Dongeren, A. V., Van Thiel de Vries, J. S. M., McCall, R. T., and Lescinski, J. (2009). Modelling storm impacts on beaches, dunes and barrier islands. *Coastal Engineering*, 56(11-12):1133–1152.

Ruessink, B. G., Kleimhans, M. G., and van del Beukel, P. G. L. (1998). Observations of swash under highly dissipative conditions. *Journal of Geophysical Research*, 103(2):3111–3118.

Ruggiero, P., Holman, R. A., and Beach, R. A. (2004). Wave run-up on a high-energy dissipative beach. *Journal of Geophysical Research*, 109:407–419.

Ruggiero, P., Komar, P. D., McDougal, W. G., Marra, J. J., and Beach, R. A. (2001). Wave runup, extreme water levels and the erosion of properties backing beaches. *Journal of Coastal Research*, 17(2):407–419.

Sallenger, A. H. (2000). Storm impact scale for barrier islands. *Journal of Coastal Research*, 16(3):890–895.

Salmon, S., Bryan, K. R., and Coco, G. (2007). The use of video systems to measure run-up on beaches. *Journal of Coastal Research SI*, 50:211–215.

Sancho-Garcia, A., Guillen, J., Ojeda, E., and Piccardo, D. (2008). Inundacion de las playas de barcelona durante temporales. *Geo-Temas*, 10:583–586.

Sanjaume, E. and Pardo-Pascual, J. E. (2005). Erosion by human impact on the Valencian coastline (E of Spain). *Journal of Coastal Research SI*, 49:76–82.

Senechal, N., Giovani, C., Bryan, K. R., and Holman, R. A. (2011). Wave runup during extrem storms conditions. *Journal of Geophysical Research*, 116:C07032.

Short, A. D. and Masselink, G. (1999). *Handbook of Beach and Shoreface Morphodynamics*, chapter Embayed and structurally controlled beaches, pages 230–249. Willey.

Stephens, S. A., Coco, G., and Bryan, K. R. (2011). Numerical simulations of wave setup over barred beach profiles: Implications for predictability. *Journal of Waterway Port Coastal and Ocean Engineering-asce*, 137(4):175–181.

Stockdon, H. F., Holman, R. A., Howd, P. A., and Sallenger Jr, A. H. (2006). Empirical parameterization of setup, swash and runup. *Coastal Engineering*, 53:573–588.

Thomas, T., Phillips, M. R., Williams, A. T., and Jenkins, R. E. (2011). Medium timescale beach rotation; gale climate and offshore island influences. *Geomorphology*, 135(1-2):97–107.

Turner, I. L. (2006). Discriminating modes of shoreline response to offshore-detached structures. *Journal of Waterway Port Coastal and Ocean Engineering-ASCE*, 132(3):180–191.

van Enckevort, I. M. J. and Ruessink, B. G. (2003a). Video observations of nearshore bar behaviour. Part 1 alongshore uniform variability. *Continental Shelf Research*, 23:501–512.

van Enckevort, I. M. J. and Ruessink, B. G. (2003b). Video observations of nearshore bar behaviour. Part 2 alongshore non-uniform variability. *Coastal Engineering*, 23:513–532.

Vousdoukas, M. I., Velegrakis, A. F., Dimou, K., Zervakis, V., and Conley, D. C. (2009). Wave run-up observations in microtidal, sediment-starved pocket beaches of the Eastern Mediterranean. *Journal of Marine Systems*, 78:S37–S47.

Vousdoukas, M. I., Wziatek, D., and Almeida, L. P. (2012). Coastal vulnerability assessment based on video wave run-up observations at a mesotidal, steep-sloped beach. *Ocean Dynamics*, 62(1):123–137.

Walton, T. L. (1992). Interim guidance for prediction of wave run-up on beaches. *Ocean Engineering*, 19(2):199–207.

Wolf, J. (2009). Coastal flooding: impacts of coupled wave-surge-tide models. *Natural Hazards*, 49(2):241–260.

Wolf, J. and Flather, R. A. (2005). Modelling waves and surges during the 1953 storm. *Philosophical Transactions of the Royal Society A-mathematical Physical and Engineering Sciences*, 363(1831):1359–1375.

Wright, L. D. and Short, A. D. (1984). Morphodynamic variability of surf zones and beaches - a synthesis. *Marine Geology*, 56(1-4):93–118.

Yasso, W. E. (1965). Plan geometry of headland bay beaches. *Journal of Geology*, 73:702–714.

Zhang, K. Q., Douglas, B. C., and Leatherman, S. P. (2004). Global warming and coastal erosion. *Climatic Change*, 64(1-2):41–58.

Research activity

Peer-reviewed

J.A. Jiménez, **A. Sancho-García**, E. Bosom, H.I. Valdemoro and J. Guillén. Storm-induced damages along the Catalan coast (NW Mediterranean) during the period 1958-2008. 2012. *Geomorphology*, 143 (SI), 24-33. DOI: 10.1016/j.geomorph.2011.07.

Submitted papers

A. Sancho-García and J. Guillén. Beach inundation prediction during storms at a tideless embayed beach. *Submitted to Coastal Engineering*

A. Sancho-García, J. Guillén and E. Ojeda. Shoreline reshaping of an embayed beach during storms after protections works. *Submitted to Geo-Marine Letters*

A. Sancho-García and J. Guillén. Beach inundation and shoreline variability during storms. *Submitted to Marine Geology*

International conference papers

A. Sancho-García, B.G. Ruessink and J. Guillén. Storm surge inundation along a multibarred beach. 2011. *Journal of Coastal Research*, 64 (SI), 1911-1915. DOI: 10.1016/j.geomorph.2011.07.

A. Sancho-García and J. Guillén. Run-up along embayed beaches during storms (Barcelona, NW Mediterranean). 2010. *Rapp. Comm. Int. Mer Medit*,

39, 796.

A. Sancho-García, J. Guillén and E. Ojeda. Consequences of a detached breakwater on the morphological response to storms of La Barceloneta beach (Barcelona, Spain). 2009. *4th International Short Conference on Applied Coastal Research*, 347-352.

International Conferences

July 2012. 33th International Conference on Coastal Engineering. Santanter, Spain. **A. Sancho-García**, J. Guillén, G. Simarro, R. Medina and V. Canovas. "Beach inundation prediction using different wave heights as inputs".

May 2011. 11th International Coastal Symposium. Szczecin, Poland. **A. Sancho-García**, B.G. Ruessink and J. Guillén. "Storm-surge inundation along a multibarred beach.".

June 2010. 32th International Conference on Coastal Engineering. Shanghai, China. J.A. Jiménez, **A. Sancho-García**, E. Bosom, H.I. Valdemoro and J. Guillén. "Validation of vulnerability assessment to storms at the Catalan coast (NW Mediterranean) during the last 50 years".

May 2010. 39th CIESM congress. Venice, Italy. **A. Sancho-García** and J.Guillén. "Run-up along embayed beaches during storms (Barcelona, NW Mediterranean)".

September 2009. 27th Meeting of the International Association of Sedimentologists. Alghero, Island of Sardinia, Italy. F. Rizzetto, J. Guillén, L. Tosi, J. Jimenéz, V. Gracia, **A. Sancho** and P. Teatini. "Multidisciplinary approach to study coastal changes: Carried out in the Barcelona and Venice areas (Spain and Italy, respectively)".

June 2009. 4th SCACR. International Short Conference on Applied Coastal Reserach. Barcelona, Spain. **A. Sancho-García**, J. Guillén and E. Ojeda. "Consequences of a detached breakwater on the morphological response to storms of

La Barceloneta beach (Barcelona. Spain)".

National Conferences

July 2012. VIII Congreso Geológico de España. Oviedo, Spain. **A. Sancho-García**, J. Guillén and B.G., Ruessink. "Effect of the submerged morphology on beach inundation during storms"

September 2011. VI Jornadas de Geomorfología Litoral. Tarragona, Spain. **A. Sancho-García** and J. Guillén. "Diferencias en la respuesta morfológica de una playa a los temporales antes y después de la construcción de un dique exento (playa de la Barceloneta, Barcelona)"

May 2011. XI Jornadas de Puertos y Costas. Las Palmas de Gran Canaria, Spain. **A. Sancho-García**, B.G. Ruessink and J. Guillén. "Observación y Predicción de la Inundación en Playas Multibarradas (Noordwijk, Holanda)".

May 2009. X Jornadas de Puertos y Costas. Santander, Spain. **A. Sancho-García**, J. Guillén, and E. Ojeda. "Observaciones sistemáticas de la inundación provocada durante temporales en playas encajadas".

Short stays in Spain and foreign institutions

February 2011. Stay in the Environmental Hydraulics Institute "IH Cantabria", Cantabria University. Parque Científico y Tecnológico de Cantabria, C/ Isabel Torres 15, 39011, Santander, Spain. *Supervisor:* Dr. Raúl Medina.

From April to June 2010. Stay in the Department of Physical Geography, Faculty of Geosciencies, Institute for Marine and Atmospheric Research, Utrecht University. P.O. Box 80.115, 3508 TC Utrecht, The Netherlands. *Supervisor:* Dr. B.G. Ruessink.

Veles e vents

Veles e vents han mos desigs complir
faent camins dubtosos per la mar:
mestre i ponent contra d'ells veig armar;
xaloc, llevant, los deuen subvenir,
ab llurs amics lo grec e lo migjorn,
fent humils precs al vent tramuntanal
que en son bufar los sia parcial
e que tots cinc complesquen mon retorn.

Bullirà el mar com la cassola en forn,
mudant color e l'estat natural,
e mostrarà voler tota res mal
que sobre si atur un punt al jorn.
Grans e pocs peixs a recors correran
e cercaran amagatalls secrets:
fugint al mar, on són nudrits e fets,
per gran remei en terra eixiran.

Los pelegrins tots ensems votaran
e prometran molts dons de cera fets,
la gran paor traurà al llum los secrets
que al confés descuberts no seran,
e en lo perill no em caureu de l'esment,
ans votaré al Déu qui ens ha lligats
de no minvar mes fermes voluntats
e que tots temps me sereu de present.

Jo tem la mort per no ser-vos absent,
perquè amor per mort és anul·lats,
mas jo no creu que mon voler sobrats
pusca esser per tal departiment.

Jo só gelós de vostre escàs voler
que, jo morint, no meta mi en oblit.
Sol est pensar me tol del món delit,
car, nós vivint, no creu se pusca fer:
aprés ma mort, d'amar perdau poder
e sia tost en ira convertit.

E jo forçat d'aquest món ser eixit,
tot lo meu mal serà vós no veer.
Oh Déu! per què terme no hi ha en amor,
car prop d'aquell jo em trobara tot sol?
Vostre voler sabera quant me vol,
tement, fiant de tot l'avenidor!

Jo son aquell pus extrem amador
aprés d'aquell a qui Déu vida tol:
puix jo son viu, mon cor no mostra dol
tant com la mort, per sa extrema dolor.
A bé o mal d'amor jo só dispost,
mas per mon fat fortuna cas no em porta:
tot esvetlat, ab desbarrada porta
me trobarà, faent humil respost.

Jo desig ço que em porà ser gran cost
i aquest esper de molts mals m'aconhorta;
a mi no plau ma vida ser estorta
d'un cas molt fer, qual prec Déu sia tost.

Lladoncs les gents no els calrà donar fe
al que amor fora mi obrarà:
lo seu poder en acte es mostrarà
e los meus dits ab los fets provaré.

Amor, de vós, jo en sent més que no en sé,
de què la part pitjor me'n romandrà,
e de vós sap lo qui sens vós està.
A joc de daus vos acompararé

Ausiàs March, segle XV